Collective Coordinate Description of Kink-Antikink Interaction

by

Ishmael Takyi

Thesis presented in partial fulfilment of the requirements for the degree of Master of Science in Physics in the Faculty of Science at Stellenbosch University

Department of Physics,
Merensky Building, Merriman Ave.
Stellenbosch University,
Private Bag X1, Matieland, 7602, South Africa.

Supervisor: Prof. Herbert Weigel

December 2015

Declaration

By submitting this thesis electronically, I declare that the entirety of the work contained therein is my own, original work, that I am the sole author thereof (save to the extent explicitly otherwise stated), that reproduction and publication thereof by Stellenbosch University will not infringe any third party rights and that I have not previously in its entirety or in part submitted it for obtaining any qualification.

Date: December 2015 .....

Abstract

Collective Coordinate Description of Kink-Antikink Interaction

I. Takyi

Department of Physics,
Merensky Building, Merriman Ave.
Stellenbosch University,
Private Bag X1, Matieland, 7602, South Africa.

Thesis: MSc (Theoretical Physics)

December 2015

In this thesis we explore resonance solutions in one space and one time dimensions in the non-linear non-integrable ϕ^4 and ϕ^6 models. These resonances occur when the relative velocity between the kink and antikink falls below a specific critical velocity. It has been claimed that the presence of an internal vibrational mode is a necessary condition for the existence of these solutions. However, this mode is part of the solutions in the small amplitude formulation only in the ϕ^4 model. Based on this, we investigate whether the availability of such a mode in the (reduced) collective coordinate ansätze will explain the resonance solutions regardless of whether or not it is a solution within the small amplitude approximation. We extend previous collective coordinate ansätze to three independent functions. Except for special scenarios this circumvents the problem seen in earlier studies that the coordinates are ill-defined when the kink-antikink separation tends to zero. We quantitatively compare the numerical results of the ordinary differential equations obtained from these ansätze to that of the partial differential equations in both the ϕ^4 and ϕ^6 models.

Uittreksel

Kollektiewe Koördineer Beskrywing van Kink-Antikink Interaksie

I. Takyi

Department Fisika,
Merenskygebou, Merrimanlaan
Stellenbosch Universiteit,
Privaatsak X1, Matieland, 7602, Suid-Afrika.

Tesis: MSc (Teoretiese Fisika)

Desember 2015

In hierdie tesis ondersoek ons die resonansie oplossings in een ruimte en een tyd dimensie van die nie-lineere nie-integreebare ϕ^4 en ϕ^6 modelle; wat voorkom wanneer die relativistiese snelheid tussen die kink en antikink val onder 'n sekere kritiese waarde. Dit is 'n standaard veronderstelling dat die teenwoordigheid van 'n interne vibrasie mode 'n noodsaaklike kondisie vir die bestaan van hierdie vibrasie oplossings is nietemin is die oplossings ook deel van die lae amplitude formulering van die ϕ^4 model. Gebaseer op hierdie idiee ondersoek ons of die beskikbaarheid van hierdie mode in die (gereduseerde) kollektiewe koordinaat ansätze die resonansie sal verduidelik ongeag of dit 'n oplossing in die klein amplitude benadering is. Ons oorweegook 'n kollektiewe koordinaat ansätze met drie vryheids grade in so 'n manier dat die evolusie van die resonansie veranderlike wat onstaan goed gedefinieer is. Ons vergelyk die numeriese resultate van die gewone differensiaal vergelykings wat volg met die volledige stel gedeeltelike differensiaal vergelykings beide nie ϕ^4 en ϕ^6 modelle.

Acknowledgements

I am grateful to the Almighty God who is the source of my inspiration and strength and without whom this project would not have been accomplished.

I use this opportunity to express my sincere appreciation to my supervisor, Professor Herbert Weigel for his constructive criticism, encouragement and enthusiasm he exhibited in carrying out this project and editing my funny sentences. I am highly indebted to African Institute for Mathematical Science (AIMS) and the University of Stellenbosch for providing financial support for this dissertation.

And finally I am pleased to thank my mother and Elizabeth Opoku for their encouragement in all my endeavours especially in carrying out this project.

Contents

List of Figures

List of Tables

Chapter 1

Introduction

This thesis centers on obtaining information about the collective coordinate (reduced) finite-dimensional description of kink-antikink scattering in classical non-linear field theories, in particular the non-integrable ϕ^4 and ϕ^6 models in one space and one time dimension. The kink solutions from these models generally have finite energy with a localised, non-dispersive energy density and which, in effect, resemble extended particles. This interesting phenomenon of the kink solutions is typical to solutions of non-linear wave-equations and has motivated the notion of solitary waves. As we will discuss in the next section solitary waves have profound applications in many areas of physics, not only particle physics.

1.1 Non-Linear Solitary Waves

In 1834 J. Scott Russell [1] discovered a long permanent pattern of waves on the Edinburgh-Glasgow canal. He called these waves " the great waves of translation " (later became known as solitary waves). To understand the interesting phenomenon of these waves, Russell did extensive experiments in a laboratory wave tank. He observed that indeed these solitary waves are long, shallow, and of a permanent form. His discovery raised a lot of controversy and discussion as to how such waves have a permanent form. This was later resolved by Korteweg and de Vries [2]. They studied the non-linear evolution equation

$$u_t + 6uu_x + u_{xx} = 0, \tag{1.1.1}$$

where the subscripts denote partial derivatives with respect to time (t) and spatial (x) coordinates, respectively. They discovered that solutions of this equation indeed have a permanent form and move undistorted. In 1965 Zabusky and Kruskal [3] did further studies of the Korteweg-de Vries equation and found another important feature of certain solitary waves: after their interaction they maintain their shape and move undistorted. They called these waves solitons.

To distinguish between these two categories of waves we consider the propagation of a wave modelled by a one-dimensional d'Alembert equation

$$\phi_{tt} - \phi_{xx} = 0. \tag{1.1.2}$$

The subscripts xx, tt represent the second-order differentiation with respect to x and t, respectively, and $\phi(x,t)$ is a real scalar field in $1+1$ dimension. The solutions of (1.1.2) are expressed in terms of the characteristic variables $(x \pm t)$ as

$$\phi(x,t) = g(x+t) \quad \text{or} \quad \phi(x,t) = f(x-t), \tag{1.1.3}$$

where g and f are arbitrary differentiable functions. Important features of these solutions are discussed by Rajaraman [4]:

(I) If $g(x-t)$ is a localised function say

$$g(x-t) = \int \mathrm{d}k \left[a(k)\cos(kx-\omega t) + b(k)\sin(kx-\omega t)\right],$$

then we can construct a localised wave packet with their plane wave components travelling with uniform velocity $c = \dfrac{\omega}{k} = 1$ such that its shape does not dissipate.

(II) Also if $f(x-t)$ and $g(x+t)$ are two localised wave packets, then

$$h(x,t) = f(x-t) + g(x+t),$$

is also a solution of (1.1.2) since the differential field equation is linear. At large negative time $(t \to -\infty)$ the two wave packets of $h(x,t)$ are well separated. In the course of time they approach each other undistorted, interact with each other and separate again retaining their shapes and velocities at large positive time $(t \to \infty)$.

Adding even linear terms to the equation (1.1.2) destroys those features. As an example, the Klein-Gordon equation is linear and its complete set of solutions constitute the plane waves, $\cos(kx \pm \omega t)$ and $\sin(kx \pm \omega t)$, with a dispersion relation

$$\omega^2 = k^2 + m^2. \tag{1.1.4}$$

It determines $\omega(k)$ for given k, where k is the wave number and ω is the frequency. The condition (1.1.4) depicts that waves of different wave number propagate with different velocities

$$c = \frac{\omega}{k} = \sqrt{\left(\frac{m}{k}\right)^2 + 1}. \tag{1.1.5}$$

This is characteristic for a dispersive wave and in effect destroys the features described above.

It can be shown numerically that, adding a non-linear term, for example ϕ^3, to the Klein-Gordon equation as in

$$\phi_{tt} - \phi_{xx} - \phi + \phi^3 = 0, \tag{1.1.6}$$

yields a dispersive wave solution for the non-linear part (involving ϕ^3). Interestingly enough, the combined effects of the dispersive and non-linear terms in the above equation balance each other in such a way that their solutions satisfy feature (I). Such solutions are called solitary waves and can exist in one, two or three space dimensions. In some particular cases these solutions also satisfy feature (II) and then they are termed solitons.

A formal definition of these two types of solutions is given in reference [4] based on the energy density that arises from the field equations: a solitary wave of a non-linear field equation is a solution which is localised and non-singular and whose energy density moves undistorted with a constant velocity. Solitons are those solitary waves whose energy density profiles and velocities after any interaction are restored to their original values of the pre-interaction period.

An example of solitary wave is the ϕ^4 model, which is a non-linear extension of the Klein-Gordon field theory that exhibits these solitary waves. They are referred to as kink solitons [4]. The kink solitons from this non-integrable model behave particle-like when subjected to external forces and perturbations [5, 6] and have wide applications in many branches of physics: in cosmology [7, 8] the ϕ^4 kinks describe the fractal structure of the cosmic domain walls [9], in condensed matter physics [10] the ϕ^4 kinks describe domain walls in ferromagnets [11] and ferroelectrics [12]. Another remarkable feature of the kink solution is that its total energy (integrated energy density) is inversely proportional to the coupling constant. Together with other arguments in strong interaction particle physics this has led to the conjecture that baryons are soliton solutions of an effective meson theory [13]. This conjecture is based on considering the number of colors in Quantum Chromodynamics (QCD) as a perturbative expansion parameter. The soliton picture describes baryon properties with remarkable success [14].

As will be discussed later, an interesting feature of the ϕ^4 model is that it possesses an internal shape mode as a time dependent small amplitude fluctuation in the background of the static kink. In the kink-antikink interaction this mode might temporarily store energy and release it at a later stage [15] giving rise to resonance phenomenon in that interaction. The study of this effect amounts to numerically integrating partial differential equations (PDE) for time and space dependent fields that are the equations of motion. The initial conditions are such that in the distant past kink and antikink are well separated and do not interact. Yet they approach each other with a prescribed velocity so that they will interact at some later stage. This relative velocity is the key parameter as the resonances only emerge for certain values thereof. Another important feature of the internal shape mode of the ϕ^4 model is that it allows for oscillations in the width of the kink and in effect causes the so-called kink wobbling [16] in the kink-antikink interaction process.

Interestingly, such resonance solutions have also been observed in the ϕ^6 model [17], but the internal shape mode, which potentially serves as a reservoir to temporarily storage energy in the kink-antikink interactions, is absent in this model. This requires a thorough investigation of the dynamics of the kink-antikink interaction in the ϕ^6 model.

The important role of the shape mode for the kink-antikink interaction in the ϕ^4 model has been concluded from the so-called collective coordinate approximation that we will explain in the next subsection. This approximation has been studied in the past three decades [9, 18, 19, 20, 21, 22]. There are (at least) two reasons why we will re-do and extend this analysis:

(a) a typographical error has propagated through the literature invalidating most of the previous (numerical) results [23] and conclusions drawn thereof

(b) the pure formulation by which the shape mode is introduced in this approximation yields a singularity. This is known as the null-vector problem [24]. To avoid it, the formulation must be extended.

In addition, by applying this approximation to the ϕ^6 model we hope to reveal the origin for the resonance structure in the kink-antikink interaction. We start with the working hypothesis that collective coordinate ansätze with an internal shape mode in either model will explain the resonance type solutions. We shall then investigate whether sizable excitations of the shape mode emerge in either model for resonance type configurations. Of course, we will also compare the solutions from the collective coordinate approximation to those from the PDEs for various relative velocities.

1.1.1 Overview of the Collective Coordinate Approximation

Extensive collective coordinate analysis has been used in references [9, 18, 19, 20]. Those authors assume the field configuration of the colliding kink-antikink

$$\phi(x,t) = \tanh\left(\frac{x+X(t)}{\sqrt{1-v_{in}^2}}\right) - \tanh\left(\frac{x-X(t)}{\sqrt{1-v_{in}^2}}\right) - 1 + A(t)\left[\chi_1^0(x+X(t)) - \chi_1^0(x-X(t))\right], \tag{1.1.7}$$

where χ_1^0 is the internal shape mode. The tanh-functions are the single (anti)kink solutions. The collective coordinate $X(t)$ represents half the distance between the kink and the antikink. The second collective coordinate, $A(t)$ is the amplitude of the internal shape mode in the background of the kink and the antikink. The constant relative velocity v_{in} is chosen for the various field configurations. We stress that (1.1.7) is a solution to the PDE for $X(t) = X_0 \to -\infty$ and $A(t) = 0$. This parametrisation reduces the non-linear PDE (1.1.6) to a set of coupled ODEs with two degrees of freedom. In the earlier work the solutions of the collective coordinate produced remarkable agreement with the solutions of the non-linear PDE system. Above we have already listed criticisms on those studies and also mentioned possible remedies that are at the center of the present project.

There are other applications of collective coordinate approximations. For example references [26, 27] consider the damped ϕ^4 model with an oscillating external force. The corresponding

PDE is

$$\phi_{tt} - \phi_{xx} + \phi^3 - \phi = -\beta\phi_t + \epsilon \sin(\omega t), \tag{1.1.8}$$

where β is the damping coefficient. Furthermore ϵ and ω are the strength and frequency of the external force. The authors of [26, 27] were able to solve the ODE for the collective coordinate parametrisation

$$\phi(x,t) = \tanh\left[\frac{x - X(t)}{\sqrt{2(1-V(t)^2)}}\right] \quad \text{with} \quad V(t) = \dot{X}(t) \tag{1.1.9}$$

up to linear order in ϵ and claimed good agreement of this solution with the one from the PDE. Remarkably these calculations suggested a resonance at half the frequency of the internal shape mode.

In general, collective coordinate approaches reduce (quantum) field theory problems to (quantum) mechanics problems. In the context of the Skyrme soliton model for baryons [30, 31] this is frequently used to generate baryon states and compute observables as matrix elements in the space of the collective coordinates [32].

1.2 Conventions

Unless otherwise stated we will use natural units with $\hbar = c = 1$. The bulk of the notation used in this work follows the features of special relativity. We represent space-time coordinates by the contravariant four-vector

$$x^\mu = (x^0, \vec{x})^\mu, \tag{1.2.1}$$

where x^0 is the time component and $\vec{x} = (x^1, x^2, x^3)$ represents the spatial components. The contravariant four-vector can be transformed to a covariant four-vector x_ν by using the Minkowskian metric tensor

$$g_{\mu\nu} = \begin{pmatrix} 1 & 0 & 0 & 0 \\ 0 & -1 & 0 & 0 \\ 0 & 0 & -1 & 0 \\ 0 & 0 & 0 & -1 \end{pmatrix}_{\mu\nu} \tag{1.2.2}$$

as

$$x_\nu = x^\mu g_{\mu\nu} = (x_0, -\vec{x})_\nu. \tag{1.2.3}$$

It must be noted that a four-vector is defined as any set of four components that transforms as

$$x'^\mu = \sum_{\nu=0}^{3} \Lambda^\mu{}_\nu x^\nu, \tag{1.2.4}$$

where $\Lambda^{\mu}{}_{\nu}$ is the linear Lorentz transformation. For example a Lorentz boost of x^{μ} along the x-axis is parametrized by

$$\Lambda^{\mu}{}_{\nu} = \begin{pmatrix} \gamma & -v\gamma & 0 & 0 \\ -v\gamma & \gamma & 0 & 0 \\ 0 & 0 & 1 & 0 \\ 0 & 0 & 0 & 1 \end{pmatrix}^{\mu}_{\nu}, \tag{1.2.5}$$

with $\gamma = \dfrac{1}{\sqrt{1-v^2}}$. The covariant and contravariant derivative vectors are given as

$$\frac{\partial}{\partial x^{\mu}} = \partial_{\mu} = \left(\partial_t, \vec{\partial}\right)_{\mu}, \tag{1.2.6}$$

and

$$\frac{\partial}{\partial x_{\mu}} = \partial^{\mu} = \left(\partial_t, -\vec{\partial}\right)^{\mu}, \tag{1.2.7}$$

respectively. Furthermore the d'Alembert operator reads

$$\partial_{\mu}\partial^{\mu} = \partial^2 = \partial_t^2 - \vec{\partial}^2. \tag{1.2.8}$$

Above ∂_t and ∂_t^2 represent the first and second derivatives with respect to time. Furthermore $\vec{\partial}$ and $\vec{\partial}^2$ represent the first and second derivatives with respect to space coordinates. In this work, most of the systems we discuss will be in two $(1+1)$ dimensions with the range of the index μ given as $\mu = 0, 1$.

1.3 Lagrange formalism

We consider a dynamical system with its configuration space characterised in terms of some manifold $\Omega = \mathbb{R}^d$, where d is the number of space and time dimensions. For $d = 1$, we have the configuration space of the dynamical system to be the real line. An example of such a system is a point particle moving along an infinite straight line with the configuration described by the positions along the line. If d is very large, then the dynamical system describes a continuous displacement of a quantity in space and time. This physical quantity is a field denoted by $\phi(\vec{x}, t)$. The Lagrange function, L, of this system will be given as the spatial integral of a Lagrangian density which is a function of this field and its first time and spatial derivatives, i.e $\mathcal{L}(\phi, \partial_t\phi, \vec{\partial}\phi)$. The action of the system is defined as

$$S[\phi] = \int_{t_1}^{t_2} L(t)\,\mathrm{d}t = \int_{\Omega} \mathcal{L}(\phi(x), \partial_{\mu}(x))\,\mathrm{d}^4x, \tag{1.3.1}$$

where the integration extends over the space-time manifold Ω with boundary $\partial\Omega$. If we consider an arbitrary variation of the field, $\phi \to \phi + \delta\phi$, subject to the boundary condition $\delta\phi = 0$ on $\partial\Omega$, then the solution of the variational problem $\delta S = 0$ leads to the Euler-Lagrange equation

$$\frac{\partial\mathcal{L}(\phi, \partial_{\mu}\phi)}{\partial\phi(x)} - \partial_{\nu}\frac{\partial\mathcal{L}(\phi, \partial_{\mu}\phi)}{\partial(\partial_{\nu}\phi(x))} = 0 \tag{1.3.2}$$

which is the field equation of motion.

1.3.1 Free Scalar Particle

We consider an isolated free massive particle represented by a real field $\phi = \phi(x,t)$ in one space and one time dimensions. Its Lagrangian density is given by

$$\mathcal{L} = \frac{1}{2}\left(\partial_\mu\phi\partial^\mu\phi - m^2\phi^2(x)\right), \tag{1.3.3}$$

where m is the (positive) mass of the particle. Using the Euler-Lagrange equation (1.3.2), it can easily be shown that this free particle satisfies the Klein-Gordon equation

$$\partial^2\phi(x) + m^2\phi(x) = 0. \tag{1.3.4}$$

The canonical conjugate field momentum of this particle is

$$\pi(x,t) = \frac{\partial\mathcal{L}}{\partial(\dot{\phi}(x,t))} = \dot{\phi}(x,t). \tag{1.3.5}$$

The energy-momentum tensor

$$T^{\mu\nu} = \frac{\partial\mathcal{L}}{\partial(\partial_\mu\phi)}\partial_\nu\phi - g^{\mu\nu}\mathcal{L}, \tag{1.3.6}$$

of this field satisfies the continuity equation, $\partial_\mu T^{\mu\nu} = 0$, and induces the associated conserved charge

$$P^\nu = \int \mathrm{d}^3x\, T^{0\nu}(\vec{x},t). \tag{1.3.7}$$

Its time component represents the field energy and is given as

$$\mathcal{E} \equiv P^0 = \int \mathrm{d}^3x\, T^{00} = \frac{1}{2}\int \mathrm{d}^3x\, \left(\phi_{tt} + \phi_{xx} + m^2\phi^2\right), \tag{1.3.8}$$

where again the subscripts tt and xx represent the second derivatives with respect to the time and space coordinate respectively. The field momentum is

$$P^i = \int \mathrm{d}^3x\, T^{01} = \int \mathrm{d}^3x\, (\phi_t\phi_x), \tag{1.3.9}$$

where the subscripts on ϕ represent first partial differentiation with respect to the indicated coordinates.

The ϕ^4 and ϕ^6 models that we will explore in this project have additional potential terms in the Lagrangian, but the derivative term is always $\frac{1}{2}\partial_\mu\phi\partial^\mu\phi$.

1.4 Outline

This thesis is organised as follows: In chapters 2 and 4, we will introduce the ϕ^4 and ϕ^6 models, respectively, and numerically describe the resonance features of the kink-antikink configuration. In particular, we will describe the internal shape mode of the ϕ^4 model in chapter 2. In chapters 3 and 5, we will adopt the collective coordinate ansätze that reduce the non-linear PDE to a set of coupled ODE with three degrees of freedom in the ϕ^4 and ϕ^6 models. We will furthermore quantitatively compare the numerical solutions to those of the full PDE. We summarise and conclude in chapter 6. Some technical aspects and lengthy formulas are recorded in appendices.

Chapter 2

The ϕ^4 Theory

Here, we introduce the ϕ^4 model, which is a particular interaction potential in the Lagrangian density. The static solutions of the Lagrangian equation represent boson particles which are dissipationless and are referred to as kink solitons (and the antiparticle is referred to as antikink). In section 2.5 we study the collision of the kink-antikink configuration by numerically solving the time-dependent equation of motion (2.2.1) for two distinct initial conditions. In the last section 2.6 we investigate the fluctuation modes around the kink-antikink system. Based on this we give a physical interpretation (using the approach of Campbell *et al.* [33]) for the solutions obtained from the collision of the kink-antikink configuration.

2.1 Introduction

We consider a single scalar field $\phi(x,t)$ in one space (x) and one time (t) dimension whose dynamics is governed by the Lagrangian density

$$\begin{aligned}\mathcal{L} &= \frac{1}{2}\partial_\mu\phi\partial^\mu\phi - U(\phi),\\ &= \frac{1}{2}(\phi_t)^2 - \frac{1}{2}(\phi_x)^2 - U(\phi),\end{aligned} \tag{2.1.1}$$

with $\mu = 0, 1$ and the subscripts x, t represent differentiation with respect to x and t respectively. We assume the scalar potential $U(\phi)$ to be a function of ϕ^2 that satisfies the equation [34, p.111–113]

$$U(\phi) = \nu + \varrho\phi^2 + \lambda\phi^4. \tag{2.1.2}$$

Here ν, ϱ, and λ are real constants with $\lambda > 0$ such that the energy that arises from (2.1.1) is bounded from below. If $\varrho \geq 0$ the potential has a unique minimum and hence has no static solution [4, p.19]. For this reason we assume $\varrho < 0$ and choose

$$\varrho = -2m^2\lambda, \quad \text{and} \quad \nu = \lambda m^4, \tag{2.1.3}$$

where m is a real positive constant. The scalar field potential then attains the compact form

$$U(\phi) = \lambda\left(\phi^2 - m^2\right)^2. \tag{2.1.4}$$

Without loss of generality we can re-scale x, t and ϕ such that $\lambda = \frac{1}{2}$ and $m = 1$. Then equation (2.1.4) becomes

$$U(\phi) = \frac{1}{2}\left(\phi^2 - 1\right)^2, \tag{2.1.5}$$

with two degenerate minima given by $\phi(x,t) = \pm 1$. Choosing the minimum $\phi(x,t) = 1$ and expanding in the shifted field $\phi(x,t) = 1 + \eta(x,t)$ the Lagrangian becomes

$$\mathcal{L} = \frac{1}{2}\partial_\mu \eta \partial^\mu \eta - \frac{1}{2}\left(\eta^4 + 4\eta^2 + 4\eta^3\right). \tag{2.1.6}$$

Comparing this to the Lagrangian density of the Klein-Gordon equation (1.3.3) we have

$$m_\eta^2 = 4, \tag{2.1.7}$$

thus this theory corresponds to a single elementary scalar particle (a boson particle), with mass

$$m_\eta = 2. \tag{2.1.8}$$

This is the mass of the fluctuation mode around the vacuum, that is, the restoring force for the oscillations around $\phi(x,t) = \pm 1$. Though the Lagrangian is invariant under $\phi \leftrightarrow -\phi$, choosing either of the vacuum configuration breaks this symmetry[35, p.369]. This is spontaneous symmetry breaking.

2.2 The Kink and Antikink Solitons of the ϕ^4 Theory

Using equation (1.3.2), the equation of motion for the Lagrange density reads

$$\phi_{tt} - \phi_{xx} = 2\left(\phi - \phi^3\right). \tag{2.2.1}$$

Since we are interested in the static solution, we set the time derivative to zero so that equation (2.2.1) reduces to

$$\frac{\mathrm{d}^2\phi}{\mathrm{d}x^2} = 2\left(\phi^3 - \phi\right). \tag{2.2.2}$$

The kinetic energy part of (2.1.1) is quadratic in time derivatives and hence the stable static (vacuum) solutions of equation (2.2.2) is just the minimum of the scalar potential energy [36, p.7], thus

$$\phi_{vac} = \pm 1.$$

On multiplying both sides of (2.2.2) by $\phi'(x) = \dfrac{\mathrm{d}\phi(x)}{\mathrm{d}x}$ and integrating using the boundary conditions

$$\phi'(-\infty) = 0 \quad \text{and} \quad U\left(\phi(-\infty)\right) = 0,$$

we obtain by the first order differential equation

$$\frac{\mathrm{d}\phi}{\mathrm{d}x} = \pm\left(\phi^2 - 1\right). \tag{2.2.3}$$

Taking the integration constant at any arbitrary point in space to be $x = 0$ with the field value $\phi(0) = 0$, we have

$$x = \pm \int_0^{\phi(x)} \frac{\mathrm{d}\overline{\phi}}{\left(\overline{\phi}^2 - 1\right)} = \pm \operatorname{arctanh}\left(\phi(x)\right).$$

This gives

$$\phi(x) = \pm \tanh x. \tag{2.2.4}$$

These solutions are shown in Figure 2.1. We denote the positive solution of (2.2.4) as $\phi_K(x)$. It is called the kink solution and the negative solution as $\phi_{\bar{K}}(x)$ is called the antikink solution. They are related by the spatial reflection $x \leftrightarrow -x$. These two solutions connect the two vacuum solutions. That is $\phi(x) \to \pm 1$ as $x \to \pm\infty$.

Taking the boost of (2.2.4) with

$$x' = \gamma\left(x - vt\right), \quad \text{and} \quad t' = \gamma\left(t - vx\right),$$

where $\gamma = \dfrac{1}{\sqrt{1 - v^2}}$ is the Lorentz factor, we obtain the moving kink-antikink solution as

$$\phi(x,t) = \pm \tanh\left(\frac{x - vt}{\sqrt{1 - v^2}}\right). \tag{2.2.5}$$

where $|v| < 1$ is the velocity of the kink. It is straightforward to verify that $\phi(x,t)$ is a solution to the wave-equation (2.2.1).

2.3 Energy Density and Energy Functional of the Kink Solution

The energy density of equation (2.1.1) becomes

$$\begin{aligned} T^{00} = \mathcal{E}_4(x,t) &= \frac{1}{2}(\phi_t)^2 + \frac{1}{2}(\phi_x)^2 + U(\phi), \\ &= \frac{1}{2}(\phi_t)^2 + \frac{1}{2}(\phi_x)^2 + \frac{1}{2}\left(\phi^2 - 1\right)^2, \end{aligned} \tag{2.3.1}$$

whose total energy from equation (1.3.8)

$$E[\phi] = \int \mathcal{E}_4(x,t)\,\mathrm{d}x, \tag{2.3.2}$$

is conserved for any solution of equation (2.2.1). For the kink (antikink) solutions the energy density becomes, using equation (2.2.3),

$$\begin{aligned} \mathcal{E}_4(x,t) &= \frac{1}{2}(\phi_x)^2 + U(\phi) = 2U(\phi), \\ &= \left(\tanh^2(x) - 1\right)^2 = \operatorname{sech}^4(x). \end{aligned}$$

This density is also shown in Figure 2.1. The total kink energy becomes

$$\begin{aligned} E[\phi] &= \int_{-\infty}^{\infty} \mathcal{E}_4(x,t)\,\mathrm{d}x, \\ &= \int_{-\infty}^{\infty} \operatorname{sech}^4(x)\ \mathrm{d}x = \frac{4}{3}. \end{aligned}$$

The total energy is referred to as the classical kink mass (M) (by restoring the units (λ, m)):

$$M = \frac{4\sqrt{2}}{3} m^3 \sqrt{\lambda}. \tag{2.3.3}$$

Using equation (2.2.5) we have the energy density of the moving kink as

$$\begin{aligned} \mathcal{E}_4(x,t) &= \left(\frac{v^2}{2\left(1-v^2\right)} + \frac{1}{2}\left(\frac{1}{1-v^2}\right) + \frac{1}{2}\right) \operatorname{sech}^4\left(\frac{x-vt}{\sqrt{1-v^2}}\right), \\ &= \frac{1}{1-v^2} \operatorname{sech}^4\left(\frac{x-vt}{\sqrt{1-v^2}}\right), \end{aligned}$$

which is explicitly time dependent. The total energy in this case becomes

$$\begin{aligned} E[\phi] &= \frac{1}{1-v^2} \int_{-\infty}^{\infty} \operatorname{sech}^4\left(\frac{x-vt}{\sqrt{1-v^2}}\right) \mathrm{d}x \\ &= \frac{1}{1-v^2} \frac{4}{3} \sqrt{1-v^2} = \frac{M}{\sqrt{1-v^2}}. \end{aligned} \tag{2.3.4}$$

Equation (2.3.4) describes the kink as a particle with mass M moving with velocity v, because it is the Einstein mass-energy relation for a particle.

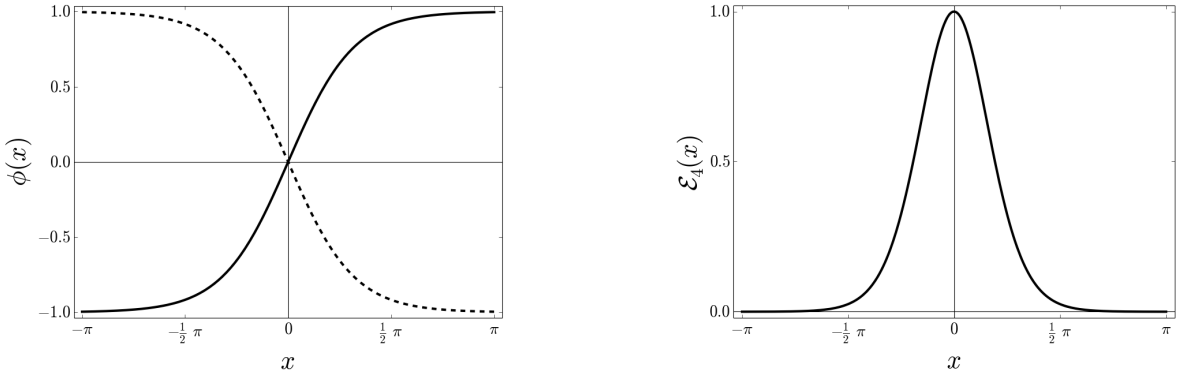

Figure 2.1: Left panel: The kink (solid line) and antikink (dash line) solutions of equation (2.2.4). Right panel: The energy density of the kink solution.

2.4 Translational Invariance

Translating the kink solution (2.2.4) as

$$x \to x + x_0,$$

we obtain

$$\phi(x, x_0) = \tanh(x + x_0), \tag{2.4.1}$$

this corresponds to kink solution centered at $-x_0$. The total energy in this case becomes

$$\begin{aligned} E[\phi] &= \int_{-\infty}^{\infty} \left[\frac{1}{2}(\phi')^2 + U(\phi)\right] \mathrm{d}x = 2\int_{-\infty}^{\infty} U(\phi)\,\mathrm{d}x, \\ &= \int_{-\infty}^{\infty} \operatorname{sech}^4(x + x_0)\ \mathrm{d}x = \frac{4}{3}. \end{aligned} \tag{2.4.2}$$

Thus translating the kink solution does not change the energy of the kink. This effect of the translation causes the existence of the "zero mode" of the kink [7, p.4]. We will use this invariance when analysing the kink-antikink interaction in the next section.

2.5 Kink-Antikink Interaction

We now investigate the interaction of the kink and antikink. We superimpose the solutions of equation (2.2.5) such that they propagate towards each other with relative speed $2v_{in}$. A field configuration of this interaction has been proposed by many authors including [9], [23] and [21], and is given by

$$\begin{aligned} \phi_{K\bar{K}} &= \phi_K(\xi_+) + \phi_{\bar{K}}(\xi_-) - 1, \\ &= \tanh(\xi_+) - \tanh(\xi_-) - 1, \end{aligned} \tag{2.5.1}$$

with

$$\xi_\pm = \frac{x}{\sqrt{1 - v_{in}^2}} \pm X_0 \quad \text{and} \quad \dot{X}_0 = \frac{-v_{in}}{\sqrt{1 - v_{in}^2}}, \tag{2.5.2}$$

where X_0 measures the position of the antikink. We emphasize that for the PDE X_0 is not a function of time, X_0 and its time derivative $\dot{X}_0$ are just initial parameters. At initial time $(t = 0)$, the field configuration of the kink and antikink is given as

$$\begin{aligned} \phi_{K\bar{K}} &= \phi_K(\xi_+) + \phi_{\bar{K}}(\xi_-) - 1, \\ &= \tanh\left(\frac{x}{\sqrt{1 - v_{in}^2}} + X_0\right) - \tanh\left(\frac{x}{\sqrt{1 - v_{in}^2}} - X_0\right) - 1. \end{aligned} \tag{2.5.3}$$

Similarly, the time derivative (of field velocity) at $t = 0$ is:

$$\frac{\partial \phi_{K\bar{K}}}{\partial t} = \dot{X}_0 \operatorname{sech}^2\left(\frac{x}{\sqrt{1 - v_{in}^2}} + X_0\right) + \dot{X}_0 \operatorname{sech}^2\left(\frac{x}{\sqrt{1 - v_{in}^2}} - X_0\right). \tag{2.5.4}$$

We choose the configuration of equation (2.5.3) and (2.5.4) as the initial condition to solve the partial differential equation (2.2.1) numerically (algorithm given in Appendix B.1) by choosing $X_0 \gg 1$ to avoid initial interference and v_{in} such that the kink and antikink propagate towards each other. The initial separation of the kink centers is $2X_0$. The accuracy of our numerical

results is tested by numerically computing the conserved total energy (2.3.2) at all times. It has been numerically observed by [33] and [22] that the shape of the solution strongly depends on whether the initial velocity v_{in} is less or greater than the critical velocity (calculated to be $v_{cr} \approx 0.26$).

We observed two striking results for the initial velocity v_{in} below the critical velocity v_{cr}. In one case the kink and antikink pair collide, reflect, recede to finite separation and return to collide again radiating their energy at every time they collide to form a chaotic bound state as illustrated in Figure 2.2, where we display the solution to the PDE at $x = 0$ as a function of time. This process may repeat several times. In the other case the kink and antikink pair

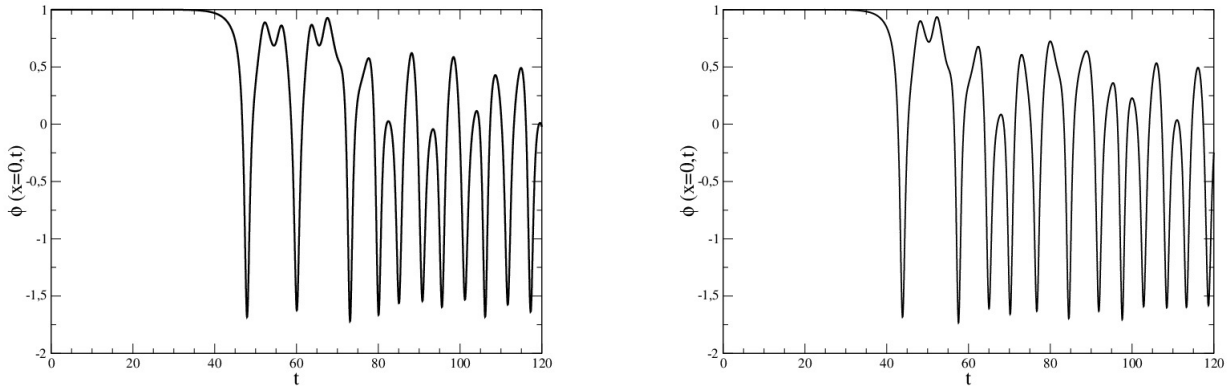

Figure 2.2: Left panel: Formation of a chaotic bound state for $v_{in} = 0.19$. Right panel: Formation of a chaotic bound state for $v_{in} = 0.209$.

collide, reflect, recede to finite separation, return to collide again and reflect to infinity. These effects are the so-called resonance windows, referring to the number of reflections as illustrated in Figure 2.3. In this case, after the first collision the kink and antikink pair are bounded by their attractive potential such that, due to radiation, they do not have enough energy any more to escape to infinity, but after the second collision they regain their lost energy to escape their absorption. An explanation of the phenomenon of transferring and storing energy will be discussed in section 2.6.

From the numerical simulation we estimate the time-dependent trajectory of the antikink by defining its mean position as

$$\langle x \rangle_n(t) = \frac{\int_0^\infty x \mathcal{E}_4^n(x,t)\,\mathrm{d}x}{\int_0^\infty \mathcal{E}_4^n(x,t)\,\mathrm{d}x}, \tag{2.5.5}$$

where $\mathcal{E}_4(x,t)$ is given in equation (2.3.1) with the solution from the PDE substituted and n is a positive integer. We found that, for initial velocities above the critical velocity the kink and antikink pair exhibit pseudo-bounces as shown in Figure 2.4. In this case, the collision process is too short to emit enough energy to bind the kink-antikink system.

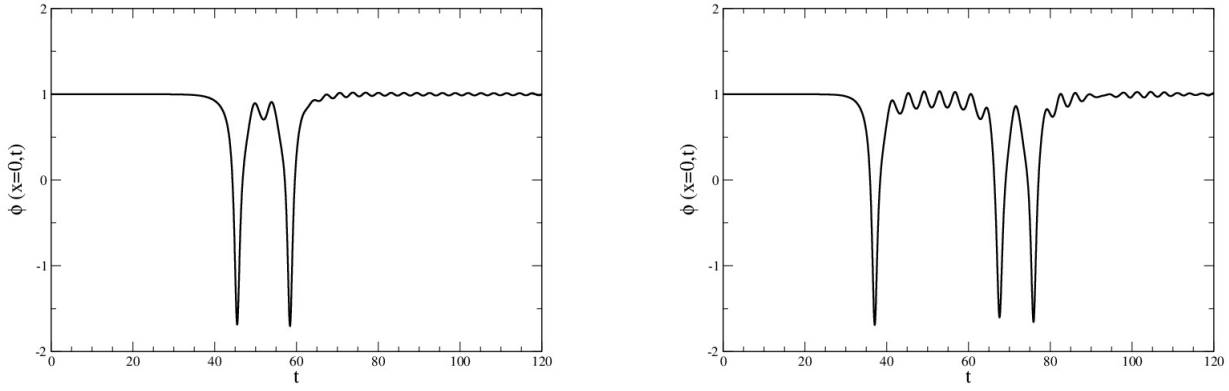

Figure 2.3: Left panel : First two-bounce window shown here with $v_{in} = 0.201$. Right panel: First three-bounce window with $v_{in} = 0.251$.

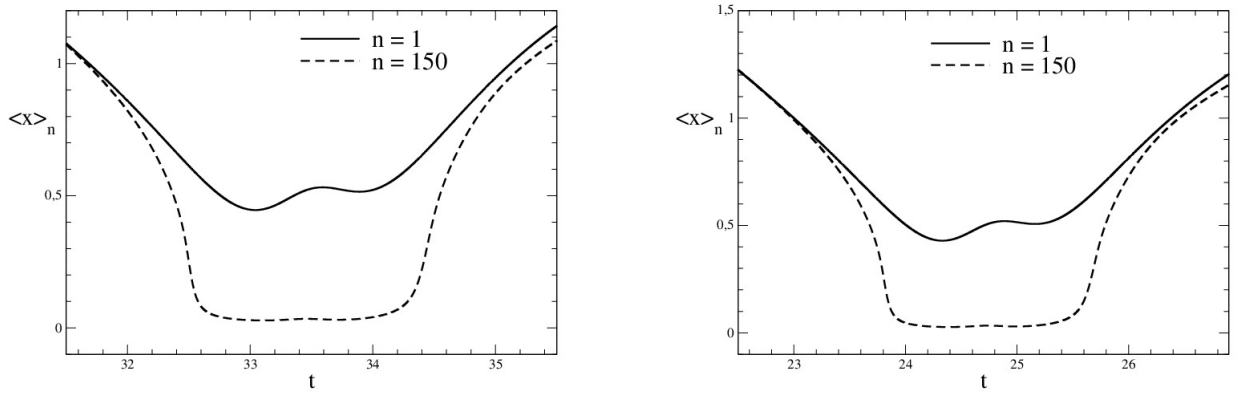

Figure 2.4: Pseudo-bounces in the kink-antikink system; for large n values, the trajectory feigns mini-bounces. Left panel: $v_{in} = 0.28$. Right panel: $v_{in} = 0.389$.

2.6 Excitations of the Kink Solution

In order to explain the phenomenon of transferring and storing energy in the kink and antikink bounces, we consider the fluctuation modes around the kink (or the antikink) solutions, by introducing $\eta(x,t)$ as a small perturbation:

$$\phi(x,t) = \phi_K(x) + \eta(x,t). \tag{2.6.1}$$

By considering linear terms in η equation (2.2.1) becomes :

$$\frac{\partial^2\eta(x,t)}{\partial t^2} - \frac{\partial^2\eta(x,t)}{\partial x^2} - 2\eta(x,t) + 6\phi_K^2(x)\eta(x,t) = 0,$$

which, by substituting equation (2.2.4), leads to

$$\frac{\partial^2\eta(x,t)}{\partial t^2} - \frac{\partial^2\eta(x,t)}{\partial x^2} + \left[6\tanh^2(x) - 2\right]\eta(x,t) = 0. \tag{2.6.2}$$

We find the fluctuation eigenfunctions by the separation ansatz

$$\eta(x,t) = e^{\imath\omega t}\chi(x). \tag{2.6.3}$$

This reduces equation (2.6.2) to a modified Sturm-Liouville equation [37, p.729]

$$-\frac{\mathrm{d}^2\chi}{\mathrm{d}x^2} + U(x)\chi = \omega^2\chi, \tag{2.6.4}$$

where the potential

$$U(x) = 6\tanh^2(x) - 2, \tag{2.6.5}$$

is symmetric under the reflection $x \to -x$ as shown in Figure 2.5. As for fluctuations about the homogeneous vacuum, section (2.1), we find the mass squared $m_\eta^2 = U(\pm\infty) = 4$. In the

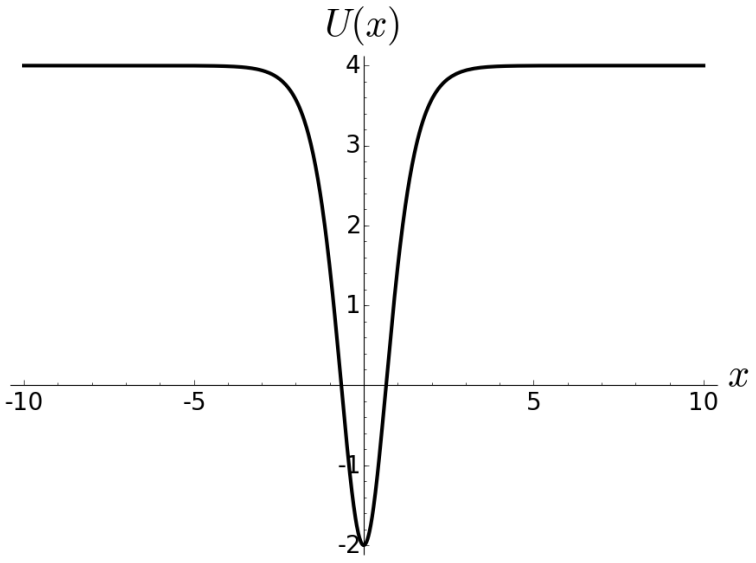

Figure 2.5: A sketch of the potential $U(x)$ for the ϕ^4 soliton, with the boson mass $m_\eta^2 = 4$.

Drazin and Johnson paper [38] equation (2.6.4) is solved by an associated Legendre polynomial. Here we will present a solution that is based on supersymmetric quantum mechanics [39].

The formalism is set up as follows: let χ_0^0 be the ground-state wave function with zero energy of the supersymmetric Hamiltonian H^0,

$$H^0 = Q^+Q^- = -\frac{1}{2}\frac{\mathrm{d}^2}{\mathrm{d}x^2} + V^0(x), \tag{2.6.6}$$

where $Q^\pm$ are operators defined as

$$Q^\pm = \frac{1}{\sqrt{2}}\left[\mp\frac{\mathrm{d}}{\mathrm{d}x} + \Phi(x)\right], \tag{2.6.7}$$

with $Q^+ = (Q^-)^\dagger$ and

$$\Phi(x) = \frac{-1}{\chi_0^0}\frac{\mathrm{d}\chi_0^0}{\mathrm{d}x}, \tag{2.6.8}$$

ensures that $Q^-\chi_0^0 = 0$ and that $H^0\chi_0^0 = 0$, as postulated. The supersymmetric partner of H^0 is H^1 and is defined as

$$H^1 = Q^-Q^+ = -\frac{1}{2}\frac{\mathrm{d}^2}{\mathrm{d}x^2} + V^1(x), \tag{2.6.9}$$

with the potentials given by

$$V^0 = \frac{1}{2}(\Phi^2 - \Phi') = \frac{1}{2}U(x) \quad \text{and} \quad V^1 = \frac{1}{2}(\Phi^2 + \Phi'). \tag{2.6.10}$$

The prime denotes differentiation with respect to x. Integrating (2.6.8) gives

$$\chi_0^0(x) = \mathcal{N}\exp\left\{-\int_x \Phi(x')\,\mathrm{d}x'\right\}, \tag{2.6.11}$$

where $\mathcal{N}$ is the normalization constant obtained from the normalization condition

$$\int |\chi_0^0|^2\,\mathrm{d}x = 1. \tag{2.6.12}$$

Also, let χ_k^0 and χ_k^1 be the wave functions of H^0 and H^1 with energy eigenvalues ω_k^0 and ω_k^1 respectively. From $\langle\chi_k^0|H^0|\chi_k^0\rangle = \omega_k^0\langle\chi_k^0|\chi_k^0\rangle$, if $|\chi_k^0\rangle$ is normalised to unity, then

$$|\chi_k^1\rangle = \frac{1}{\sqrt{\omega_k^0}}Q^-|\chi_k^0\rangle, \tag{2.6.13}$$

is also normalised to unity.

Proof. From $Q^+ = (Q^-)^\dagger$, we have $\langle\chi_k^1| = \dfrac{1}{\sqrt{\omega_k^0}}\langle\chi_k^0|Q^+$. Hence

$$\begin{aligned}\langle\chi_k^1|\chi_k^1\rangle &= \frac{1}{\omega_k^0}\langle\chi_k^0|Q^+Q^-|\chi_k^0\rangle \\ &= \frac{1}{\omega_k^0}\omega_k^0\langle\chi_k^0|\chi_k^0\rangle = 1.\end{aligned}$$

□

An analogous relation holds for $|\chi_k^1\rangle$:

$$|\chi_k^0\rangle = \frac{1}{\sqrt{\omega_k^1}}Q^+|\chi_k^1\rangle. \tag{2.6.14}$$

Now, choosing

$$\Phi(x) = 2\tanh x,$$

the two potentials become

$$\frac{1}{2}U(x) = V^0(x) = 2 - \frac{3}{\cosh^2 x} \quad \text{and} \quad V^1(x) = \frac{3}{2} + \frac{1}{2}\left(1 - \frac{2}{\cosh^2 x}\right), \tag{2.6.15}$$

with the operators given as

$$Q_2^\pm = \frac{1}{\sqrt{2}}\left[\mp\frac{\mathrm{d}}{\mathrm{d}x} + 2\tanh x\right].$$

Let the supersymmetric Hamiltonians be H^0 and H^2 respectively. Observe that H^0 has the eigenvalues as in equation (2.6.4) that we are seeking. Using (2.6.11) and (2.6.12) we have

$$\chi_0^0(x) = \frac{\sqrt{3}}{2}\operatorname{sech}^2 x, \tag{2.6.16}$$

as the ground-state wave function with eigenvalue $(\omega_0^0)^2 = 0$. To find the other eigenvalues of H^0, we are required to solve the eigenvalue problem related to the potential $V^1(x)$. This potential corresponds to the case of choosing $\Phi(x) = \tanh x$, with a shift of the energy by $\frac{3}{2}$ and the supersymmetric Hamiltonians given as H^3 and H^1 respectively. Using equations (2.6.11) and (2.6.12) we have the normalised ground state wave function of the Hamiltonian H^3 as

$$\chi_0^3(x) = \frac{1}{\sqrt{2}}\frac{1}{\cosh x},$$

with energy $\omega_0^3 = 0$. The eigenstates χ_k^1 of H^1 and the energy eigenvalues ω_k^1 are

$$\chi_k^1 = e^{\imath kx} \quad \text{and} \quad \omega_k^1 = \frac{1}{2}(1+k^2),$$

where k is a momentum coordinate. Using the operators $Q_1^{\pm} = \frac{1}{\sqrt{2}}\left[\mp\frac{\mathrm{d}}{\mathrm{d}x} + \tanh x\right]$ and equation (2.6.14), the scattering eigenfunctions are given by

$$\chi_k^3(x) = \frac{1}{\sqrt{\omega_k^1}}Q_1^+\chi_k^1 = \frac{-\imath k + \tanh x}{\sqrt{1+k^2}}e^{\imath kx}.$$

From this, we have the eigenstates χ_1^2 and χ_k^2 of the supersymmetric Hamiltonian H^2 as

$$\chi_1^2 = \frac{1}{\sqrt{2}}\frac{1}{\cosh x} \quad \text{and} \quad \chi_k^2 = \frac{-\imath k + \tanh x}{\sqrt{1+k^2}}e^{\imath kx}. \tag{2.6.17}$$

The other eigenfunctions of H^0 arise by employing equation (2.6.14), this gives the second bound state as

$$\begin{aligned}\chi_1^0 &= Q_2^+\chi_1^2(x),\\ &= \sqrt{\frac{2}{3}}\frac{1}{\sqrt{2}}\left(-\frac{\mathrm{d}}{\mathrm{d}x} + 2\tanh x\right)\frac{1}{\sqrt{2}\cosh x},\\ &= \sqrt{\frac{3}{2}}\frac{\tanh x}{\cosh x} = \sqrt{\frac{3}{2}}\frac{\sinh x}{\cosh^2 x},\end{aligned} \tag{2.6.18}$$

and its eigenvalue is $\frac{1}{2}(\omega_1^0)^2 = \frac{3}{2} \implies (\omega_1^0)^2 = 3 < m_\eta^2$. These two solutions are referred to as the bound states solutions [19]. The $\omega_0^0 = 0$ mode is called the "translational zero mode" [40]. Its existence arises from translational invariance of the theory. That is, $\chi_0^0(x)$ is the infinitesimal translation correction to the kink solution that can be excited without costing energy, from equation (2.4.1) we have

$$\begin{aligned}\Delta\phi_K &\approx \phi_K(x-\delta x_0) - \phi_K(x)\\ &= (-\delta x_0)\frac{\partial\phi_K(x)}{\partial x} = -\delta x_0 \operatorname{sech}^2 x.\end{aligned}$$

The other solution, χ_1^0 is also referred to as the "internal shape mode" (bounce solution) and represents a localised deformation of the kink-antikink solution [33]. Campbell *et al.* [33] proposed that the transfer and storage of energy in the kink and antikink pair bounces is a result of the internal shape and translational zero modes, respectively. They argued that during the first collision of the kink-antikink there is transfer of energy to the internal shape mode such that kink and antikink are unable to overcome their attractive potential, resulting in binding them together. In the second collision, the internal shape is destroyed and its energy is transferred into the translational mode, unbinding the kink-antikink pair.

For a continuous spectrum we have the eigenvalues

$$\frac{1}{2}(\omega_k^0)^2 = \frac{3}{2} + \frac{1}{2}(k^2+1) = \frac{1}{2}(k^2+4),$$

thus $(\omega_k^0)^2 = k^2 + m_\eta^2$, where m_η is as given in (2.1.8). Physically this corresponds to non-dissipative waves propagating to spatial infinity [33]. Their eigenfunctions are

$$\begin{aligned}\chi_k^0(x) &= Q_2^+\chi_k^2,\\ &= \frac{1}{\sqrt{2}}\left(-\frac{\mathrm{d}}{\mathrm{d}x} + 2\tanh x\right)\left(\frac{-\imath k + \tanh x}{\sqrt{1+k^2}}\right)e^{\imath kx}\\ &= \frac{1}{\sqrt{2(1+k^2)}}\left(3\tanh^2 x - 3\imath k\tanh x - 1 - k^2\right)e^{\imath kx}.\end{aligned}$$

Since the eigenvalues are $\omega_k^2 = k^2 + m_\eta^2$, we have the normalised continuum (scattering) states as

$$\chi_k^0 = \frac{1}{\sqrt{(m_\eta^2+k^2)(1+k^2)}}\left(3\tanh^2 x - 3\imath k\tanh x - 1 - k^2\right)e^{\imath kx}. \tag{2.6.19}$$

It must be emphasized that the potentials in equation (2.6.15) are reflectionless: the scattering states are fully transmitted with an identical phase shift in the two (parity) channels and the reflection coefficient vanishes. The transmission is attributed to the fact that as $x \to \pm\infty$,

$$\chi_k^0(x) \to \frac{[-1 \pm 3 - k(k \pm 3\imath)]}{\sqrt{(m_\eta^2+k^2)(1+k^2)}}e^{\imath\left[kx \pm \frac{1}{2}\delta(k)\right]}. \tag{2.6.20}$$

The momentum dependent total phase shift $\delta(k)$ (i.e. sum over the parity channels) of the scattering states is given by:

$$\delta(k) = -2\arctan\left(\frac{3k}{2-k^2}\right). \tag{2.6.21}$$

In summary, the eigenfunctions and eigenvalues of equation (2.6.4) have two discrete levels:

$$\omega_0^0 = 0 \quad \text{with} \quad \chi_0^0(x) = \frac{\sqrt{3}}{2}\operatorname{sech}^2 x$$
$$\omega_1^0 = \sqrt{3} \quad \text{with} \quad \chi_1^0(x) = \sqrt{\frac{3}{2}}\frac{\sinh x}{\cosh^2 x},$$

and continuum levels

$$\omega_k^0 = \frac{1}{2}(k^2 + 4)$$

with

$$\chi_k^0(x) \to \frac{[-1 \pm 3 - k(k \pm 3\imath)]}{\sqrt{(m_\eta^2 + k^2)(1 + k^2)}} e^{\imath\left[kx \pm \frac{1}{2}\delta(k)\right]}.$$

Chapter 3

Kink-Antikink Configuration for the ODE Equation

We treat the "zero mode" that arises due to the translational invariance of the kink solution by introducing a collective coordinate parameter $X(t)$ [18] that now is time dependent. As mentioned earlier it is half the distance between the kink and antikink. Using the analogy of equation (2.5.1) Refs [9], [23] and [22] introduce an ansatz field configuration for the colliding kink-antikink system as

$$\phi_{cc}(x,t) = \phi_K(\xi_+) - \phi_K(\xi_-) - 1 + \sqrt{\frac{3}{2}}A(t)\left[\chi_1^0(\xi_-) - \chi_1^0(\xi_+)\right], \tag{3.0.1}$$

where $A(t)$ is the amplitude of the peak around the kink and antikink centers. This peak is parametrized by the internal shape mode. But in their discussion the interaction between the shape modes at $\pm X(t)$ was omitted. This, unfortunately, suggests a null-vector problem, that arises when $X \to 0$: the A coordinate blew up during the colission. This problem corresponds to the projection of the function $\phi_{cc}(x,t) = \sqrt{\frac{3}{2}}A(t)\left[\chi_1^0(\xi_-) - \chi_1^0(\xi_+)\right]$ on a null vector [24]: the amplitude $A(t)$ is ill-defined as $X \to 0$. In section 3.1, we give an alternative field configuration with two independent amplitudes so as to avoid this null vector problem. Also in that section we quantitatively compare the solutions of the ODE configuration to those of the PDE for the full field equation from the previous chapter.

3.1 Collective Coordinates Description

In order to treat the shape modes at $\pm X(t)$ independently, we introduce the following parametrization for the amplitudes of the two peaks around the kink and antikink, giving rise to three collective coordinates (X, A, B) with

$$\phi_{cc}(x,t) = \phi_K(\xi_+) - \phi_K(\xi_-) - 1 + \sqrt{\frac{3}{2}}\left[A(t)\chi_1^0(\xi_-) + B(t)\chi_1^0(\xi_+)\right]. \tag{3.1.1}$$

Defining

$$\phi_0(x, X(t)) = \phi_K(\xi_+) - \phi_K(\xi_-) - 1 \tag{3.1.2}$$

and substituting the ansatz, equation (3.1.1) into the Lagrange density equation (2.1.1) and integrating over all space, from $-\infty$ to ∞, we obtain the Lagrangian for the collective coordinates as

$$\begin{aligned} L_4(A,\dot{A},B,\dot{B},X,\dot{X}) &= \int \mathcal{L}_4(\phi_{cc})\mathrm{d}x, \\ &= a_1\dot{X}^2 - a_2 + a_3\dot{A}^2 - a_4A^2 + a_5A + a_6\dot{X}^2A + a_7\dot{X}\dot{A} \\ &\quad + a_8\dot{X}^2A^2 + a_9A\dot{X}\dot{A} - a_{10}A^3 - a_{11}A^4 + b_3\dot{B}^2 - b_4B^2 \\ &\quad + b_5B + b_6\dot{X}^2B + b_7\dot{X}\dot{B} + b_8\dot{X}^2B^2 + b_9B\dot{X}\dot{B} - b_{10}B^3 \\ &\quad - b_{11}B^4 + d_1\dot{A}\dot{B} + d_2\dot{X}^2AB + d_3B\dot{X}\dot{A} + d_4A\dot{X}\dot{B} - d_5AB \\ &\quad - d_6A^2B^2 - d_7A^2B - d_8AB^2 - d_9A^3B - d_{10}AB^3. \end{aligned} \tag{3.1.3}$$

The coefficients functions $a_1, \cdots, d_{10}$ are spatial integrals that depend non-linearly on X. Explicit expressions are given in Appendix A.1. They can be computed analytically (via analytic function theory) in the ϕ^4 model. However, we treat them numerically in view of later application to the ϕ^6 model.

3.1.1 Equations of Motion and the Energy Density for the Collective Coordinates

Since the Lagrangian is made up of three independent variables A, B and X we have three independent equations of motion

$$\frac{\mathrm{d}}{\mathrm{d}t}\frac{\partial L_4}{\partial \dot{X}} = \frac{\partial L_4}{\partial X}, \quad \frac{\mathrm{d}}{\mathrm{d}t}\frac{\partial L_4}{\partial \dot{A}} = \frac{\partial L_4}{\partial A} \quad \text{and} \quad \frac{\mathrm{d}}{\mathrm{d}t}\frac{\partial L_4}{\partial \dot{B}} = \frac{\partial L_4}{\partial B}. \tag{3.1.4}$$

The dot indicates a total time derivative $\dot{X}(t) = \dfrac{\mathrm{d}}{\mathrm{d}t}X(t)$, etc. These give derivative couplings between X, A and B that are most conveniently written as a matrix equation

$$\begin{pmatrix} a_{11} & a_{12} & a_{13} \\ a_{21} & a_{22} & a_{23} \\ a_{31} & a_{32} & a_{33} \end{pmatrix} \begin{pmatrix} \ddot{X} \\ \ddot{A} \\ \ddot{B} \end{pmatrix} = \begin{pmatrix} f_1 \\ f_2 \\ f_3 \end{pmatrix}, \tag{3.1.5}$$

with

$$\begin{aligned} a_{11} &= 2a_1 + 2a_6A + 2a_8A^2 + 2b_6B + 2b_8B^2 + 2d_2AB, \\ a_{12} &= a_{21} = a_7 + a_9A + d_3B, \\ a_{13} &= a_{31} = b_7 + b_9B + d_4A, \\ a_{22} &= 2a_3, \\ a_{23} &= a_{32} = d_1, \\ a_{33} &= 2b_3. \end{aligned}$$

The 3×3 matrix structure of (3.1.5) arises from the kinetic energy term in the Lagrangian (2.1.1). We notice that the matrix elements a_{ij} depend on $X(t)$, since the integral coefficients $a_1, \cdots, d_{10}$ depend on X. Solving equation (3.1.5) by inversion gives

$$\begin{pmatrix} \ddot{X} \\ \ddot{A} \\ \ddot{B} \end{pmatrix} = \frac{1}{a_{11}a_{22}a_{33} - a_{11}a_{23}^2 - a_{22}a_{13}^2 - a_{33}a_{12}^2 + 2a_{12}a_{13}a_{23}} \times \begin{pmatrix} a_{22}a_{33} - a_{23}^2 & a_{13}a_{32} - a_{12}a_{33} & a_{12}a_{23} - a_{13}a_{22} \\ a_{23}a_{31} - a_{21}a_{33} & a_{11}a_{33} - a_{13}^2 & a_{21}a_{13} - a_{11}a_{23} \\ a_{21}a_{32} - a_{31}a_{22} & a_{12}a_{31} - a_{11}a_{32} & a_{11}a_{22} - a_{12}^2 \end{pmatrix} \begin{pmatrix} f_1 \\ f_2 \\ f_3 \end{pmatrix}. \tag{3.1.6}$$

We note that technically the null-vector problem of the two component approach, equation (3.1.1) would be reflected by a singularity in this inversion. Using the Euler-Lagrange equation (3.1.4) and the Lagrangian (3.1.3) we have

$$\begin{aligned} f_1 = &-a_1'\dot{X}^2 - a_2' + a_3'\dot{A}^2 - a_4'A^2 + a_5'A - a_6'\dot{X}^2A - 2a_6\dot{X}\dot{A} - a_8'\dot{X}^2A^2 \\ &- 4a_8A\dot{X}\dot{A} - a_9\dot{A}^2 - a_{10}'A^3 - a_{11}'A^4 + b_3'\dot{B}^2 - b_4'B^2 + b_5'B - b_6'\dot{X}^2B \\ &- 2b_6\dot{X}\dot{B} - b_8'\dot{X}^2B^2 - 4b_8B\dot{X}\dot{B} - b_9\dot{B}^2 - b_{10}'B^3 - b_{11}'B^4 + d_1'\dot{A}\dot{B} \\ &- d_2'\dot{X}^2AB - 2d_2B\dot{X}\dot{A} - 2d_2A\dot{X}\dot{B} - d_3\dot{B}\dot{A} - d_4\dot{A}\dot{B} - d_5'AB - d_6'A^2B^2 \\ &- d_7'A^2B - d_8'AB^2 - d_9'A^3B - d_{10}'AB^3, \end{aligned}$$

$$\begin{aligned} f_2 = &-2a_3'\dot{X}\dot{A} - 2a_4A + a_5 + a_6\dot{X}^2 - a_7'\dot{X}^2 + 2a_8\dot{X}^2A - a_9'\dot{X}^2A - 3a_{10}A^2 \\ &- 4a_{11}A^3 - d_1'\dot{X}\dot{B} + d_2\dot{X}^2B - d_3'\dot{X}^2B - d_3\dot{X}\dot{B} + d_4\dot{X}\dot{B} - d_5B \\ &- 2d_6AB^2 - 2d_7AB - d_8B^2 - 3d_9A^2B - d_{10}B^3, \end{aligned}$$

and

$$\begin{aligned} f_3 = &-2b_3'\dot{X}\dot{B} - 2b_4B + b_5 + b_6\dot{X}^2 - b_7'\dot{X}^2 + 2b_8\dot{X}^2B - b_9'\dot{X}^2B - 3b_{10}B^2 \\ &- 4b_{11}B^3 - d_1'\dot{X}\dot{A} + d_2\dot{X}^2A + d_3\dot{X}\dot{A} - d_4'\dot{X}^2A - d_4\dot{X}\dot{A} - d_5A \\ &- 2d_6A^2B - d_7A^2 - 2d_8AB - d_9A^3 - 3d_{10}AB^2. \end{aligned}$$

In the above equations for f_i the primes denote differentiation respect with to X. These derivatives are taken under the integrals in appendix A.1. We end up with coupled second order differential equations:

$$\begin{aligned} \ddot{X} &= \frac{f_1\left(a_{22}a_{33} - a_{23}^2\right) + f_2\left(a_{13}a_{32} - a_{12}a_{33}\right) + f_3\left(a_{12}a_{23} - a_{13}a_{22}\right)}{a_{11}a_{22}a_{33} - a_{11}a_{23}^2 - a_{22}a_{13}^2 - a_{33}a_{12}^2 + 2a_{12}a_{13}a_{23}}, \\ \ddot{A} &= \frac{f_1\left(a_{23}a_{31} - a_{21}a_{33}\right) + f_2\left(a_{11}a_{33} - a_{13}^2\right) + f_3\left(a_{21}a_{13} - a_{11}a_{23}\right)}{a_{11}a_{22}a_{33} - a_{11}a_{23}^2 - a_{22}a_{13}^2 - a_{33}a_{12}^2 + 2a_{12}a_{13}a_{23}}, \\ \ddot{B} &= \frac{f_1\left(a_{21}a_{32} - a_{31}a_{22}\right) + f_2\left(a_{12}a_{31} - a_{11}a_{32}\right) + f_3\left(a_{11}a_{22} - a_{12}^2\right)}{a_{11}a_{22}a_{33} - a_{11}a_{23}^2 - a_{22}a_{13}^2 - a_{33}a_{12}^2 + 2a_{12}a_{13}a_{23}}. \end{aligned} \tag{3.1.7}$$

We have solved these equations of motion numerically for the initial conditions

$$X(0) = 10, \quad \dot{X}(0) = \frac{-v_{in}}{\sqrt{1-v_{in}^2}}, \quad A(0) = B(0) = 0, \quad \text{and} \quad \dot{A}(0) = \dot{B}(0) = 0, \tag{3.1.8}$$

that correspond to the kink-antikink interaction discussed in the previous chapter. The total energy

$$\begin{aligned} E_4 &= \frac{\partial \mathcal{L}_4}{\partial \dot{X}}\dot{X} + \frac{\partial \mathcal{L}_4}{\partial \dot{A}}\dot{A} + \frac{\partial \mathcal{L}_4}{\partial \dot{B}}\dot{B} - \mathcal{L}_4, \\ &= a_1\dot{X}^2 + a_2 + a_3\dot{A}^2 + a_4A^2 - a_5A + a_6\dot{X}^2A + a_7\dot{X}\dot{A} + a_8\dot{X}^2A^2 + a_9A\dot{X}\dot{A} \\ &\quad + a_{10}A^3 + a_{11}A^4 + b_3\dot{B}^2 + b_4B^2 - b_5B + b_6\dot{X}^2B + b_7\dot{X}\dot{B} + b_8\dot{X}^2B^2 + b_9B\dot{X}\dot{B} \\ &\quad + b_{10}B^3 + b_{11}B^4 + d_1\dot{A}\dot{B} + d_2\dot{X}^2AB + d_3B\dot{X}\dot{A} + d_4A\dot{X}\dot{B} + d_5AB + d_6A^2B^2 \\ &\quad + d_7A^2B + d_8AB^2 + d_9A^3B + d_{10}AB^3 \end{aligned} \tag{3.1.9}$$

is conserved in time. It will be used as an accuracy test on our numerical solution.

3.2 Comparison of the Solution of the ODE to those of the PDE

We have solved equation (3.1.7) numerically using a fourth-order Runge-Kutta algorithm (Appendix B.2) with equation (3.1.8) as the initial condition. We want to investigate whether the solutions of the ODE's for the collective coordinate ansätze approximates the solutions to the full PDE's equation reasonably well. To this end we picture the time-dependent trajectory of the antikink (PDE solution) in equation (2.5.5) with $n = 1$ and compare it to $X(t)$ from the ODE. As before we verify the accuracy of our numerical results by ensuring that the total energy (3.1.9) is conserved in all our computations. To better understand our simulations we first describe a number of approximations, that were considered in the literature.

3.2.1 Harmonic Approximation

In this approximation, we consider the approximation used by a number of authors [9, 18, 19, 33, 21]. In their work the non-diagonal terms involving time derivative and non-harmonic contributions were omitted. The first approximation corresponds to setting $a_6, \cdots, a_9, b_6, \cdots, b_9 = 0$ as well as $d_1, \cdots, d_4 = 0$ and the second implies setting $a_{10}, a_{11}, b_{10}, b_{11}, d_6, \cdots, d_{10} = 0$ in equation (3.1.7).

It was assumed that the non-harmonic contributions (the higher order terms) were very small. The determinant

$$D(X) = \begin{Vmatrix} a_{11}(X) & a_{12}(X) & a_{13}(X) \\ a_{12}(X) & a_{22}(X) & a_{23}(X) \\ a_{13}(X) & a_{23}(X) & a_{33}(X) \end{Vmatrix}. \tag{3.2.1}$$

of the system of equations of motion develops a singularity when the non-diagonal terms contribute to the dynamics. As a mechanism to control the numerical solution with the determinant, $D(X) \neq 0$, everywhere the non-diagonal terms were thus omitted.

In earlier numerical studies with only two collective coordinates [22] a formula for $a_5(X) = F(X)$ was usually symmetric under $X \to -X$. However, it was observed in reference [23] that the formula for the coefficient function $F(X)$ from reference [18] was erroneous. If it were symmetric a solution with $X(t) \to -X(t)$ would exist, at least in the harmonic approximation. However,

$$\phi_0(0, X(t)) = 2\tanh X - 1 \to \begin{cases} 1 & \text{for} \quad X \to \infty \\ -3 & \text{for} \quad X \to -\infty \end{cases} \tag{3.2.2}$$

suggests that $\phi_0(0, -\infty)$ is not a solution of the field equation; and as such $a_5(X) = -b_5(X)$ cannot be symmetric under $X \to -X$. The corrected form of $a_5(X) = -b_5(X)$ is [1]

$$a_5(X) = 3\sqrt{6}\pi \left[2 - 2\tanh^3(X) - \frac{3}{\cosh^2(X)} + \frac{1}{\cosh^4(X)} \right]. \tag{3.2.3}$$

The numerical evaluation of $a_5(X) = -b_5(X)$ in appendix A.1 and from equation (3.2.3) indeed yields an unsymmetric function as shown in Figure 3.1.

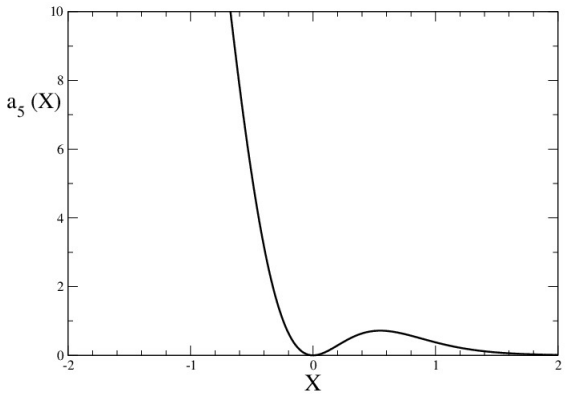

Figure 3.1: The coefficient function $a_5(X) = -b_5(X)$ in equation (3.2.3).

We find that the solutions of the ODE model do not agree with the solutions of the PDE system once this error is been corrected as indicated in Figure 3.2. Our results suggest the associated energy $E_5 = -a_5(X)A - b_5(X)B$ may become big thus producing trapping solutions with large amplitudes of the internal shape mode $A(t)$ and $B(t)$. This is shown in Figure 3.3. This disqualifies the harmonic approximation.[2]

[1] The origin of the error seems a misprint in reference [18] which has $\tanh^2(X)$ instead of $\tanh^3(X)$.

[2] Substituting the incorrect form of $a_5(X)$, we indeed reproduce the earlier numerical results.

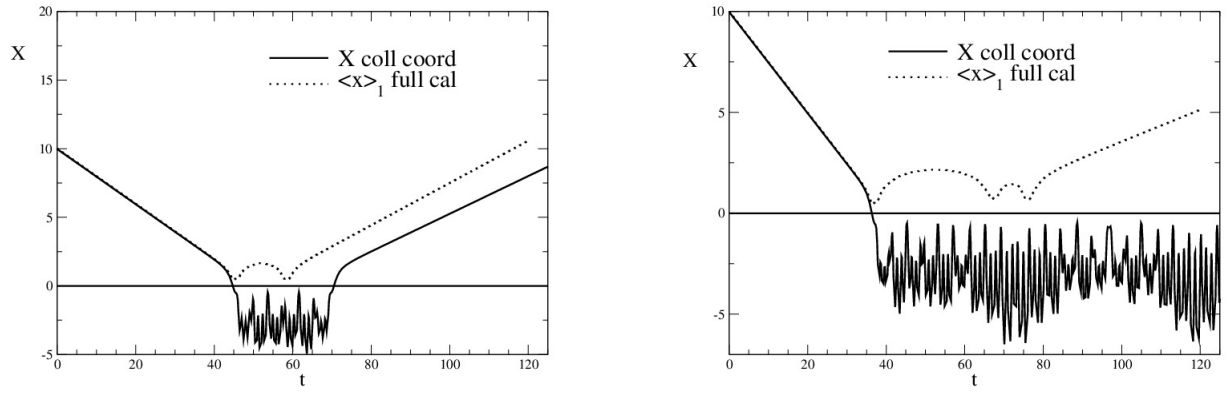

Figure 3.2: Comparison of the time dependence of the collective coordinate $X(t)$ with that of the PDE $\langle x \rangle_1$ in equation (2.5.5). Left panel: $v_{in} = 0.201$. Right panel: $v_{in} = 0.251$.

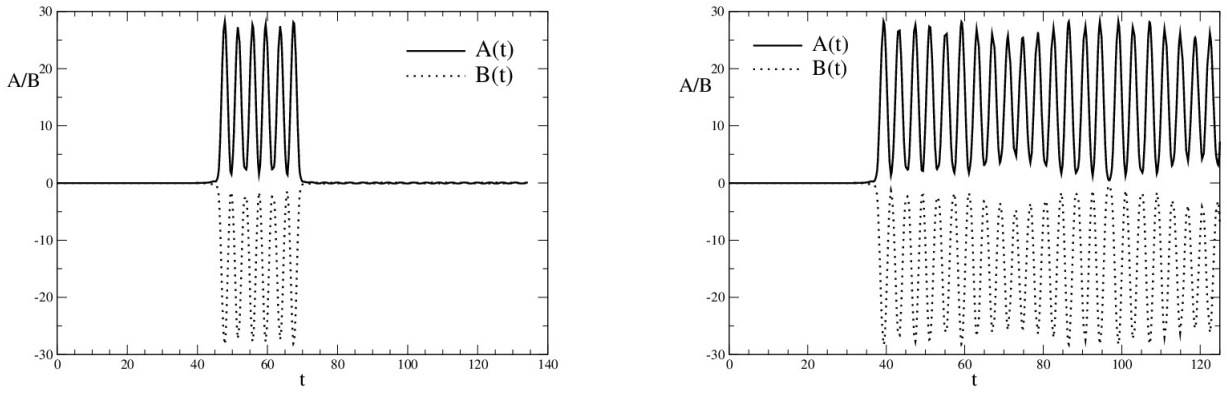

(a) (b)

Figure 3.3: Amplitude of the internal mode vibrations $A(t)$ and $B(t)$ showing a trapping solution with (a) $v_{in} = 0.201$ and (b) $v_{in} = 0.251$.

3.2.2 Beyond the Harmonic Approximation

In view of the above observations it will be interesting to investigate the contribution of all non-diagonal terms involving time derivatives and the non-harmonic terms to the dynamics of the kink-antikink system. As a mechanism to control the numerical solutions such that the determinant $D(X) \neq 0$ everywhere,[3] we modify the mismatch of the configuration by introducing

$$\phi_0(x, X(t)) \to \phi_0(x, X(t)) + 1 - \tanh(qX). \tag{3.2.4}$$

Here q is a large but adjustable parameter and $\phi_0(x, X(t))$ is given in equation (3.1.2). This modification affects the coefficient functions $a_1(X), a_6(X), a_7(X), b_6(X), b_7(X)$. For scenarios with $A(t) = -B(t)$ the contributions of $a_6(X), a_7(X)$ and their counterparts $b_6(X), b_7(X)$ cancel

[3] We discuss later that $D(X)$ may vanish for particular initial conditions with $A(0) + B(0) = 0$.

out and the only affected coefficient is $a_1(X)$. Numerically it turns out the above adjustment mainly concerns the regime with $X < 0$ and adds a strong repulsion when $X \sim 0$. In turn it yields reflections with one or two bounces.

We want to investigate whether a suitable choice of q can improve the agreement of the collective coordinate approach with the full PDE solutions. Using a large value of q (for example $q = 10$) we find that the ODE solutions yield better agreement to the solutions of the PDE system than for smaller values of q (for example $q = 5$). This is shown in Figure 3.4. For $q = 5$ we find that for all initial velocities a trap oscillatory state solution is produced as indicated in Figure 3.5. From the above analysis we conclude that larger q values provide a better account of the actual dynamics of the full PDE results in the ODE approximation. The reason is that, the larger q is, the smaller the regime in which the repulsion from the change performed in equation (3.2.4) is effective for $X > 0$.

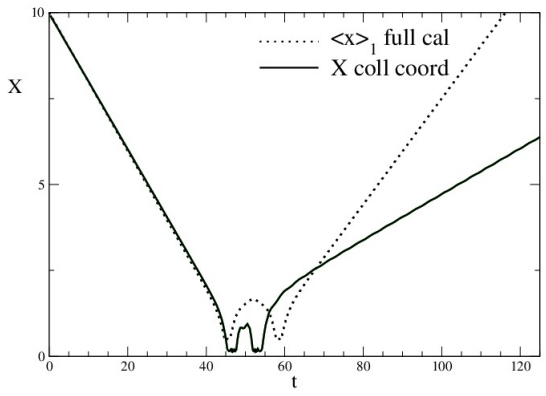

(a)

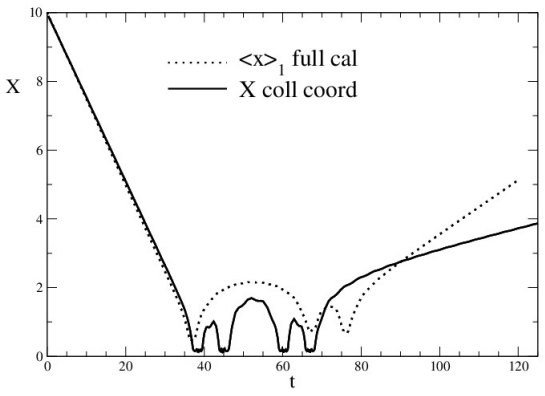

(b)

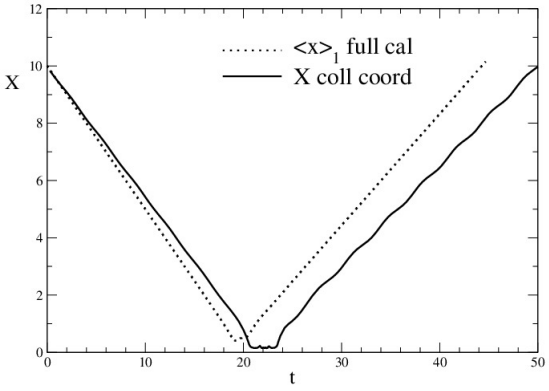

(c)

Figure 3.4: Comparison of the time dependence of the collective coordinate $X(t)$ with that of the PDE $\langle x \rangle_1$ for $q = 10$ in equation (3.2.4): (a) $v_{in} = 0.201$, (b) $v_{in} = 0.251$ and (c) $v_{in} = 0.50$.

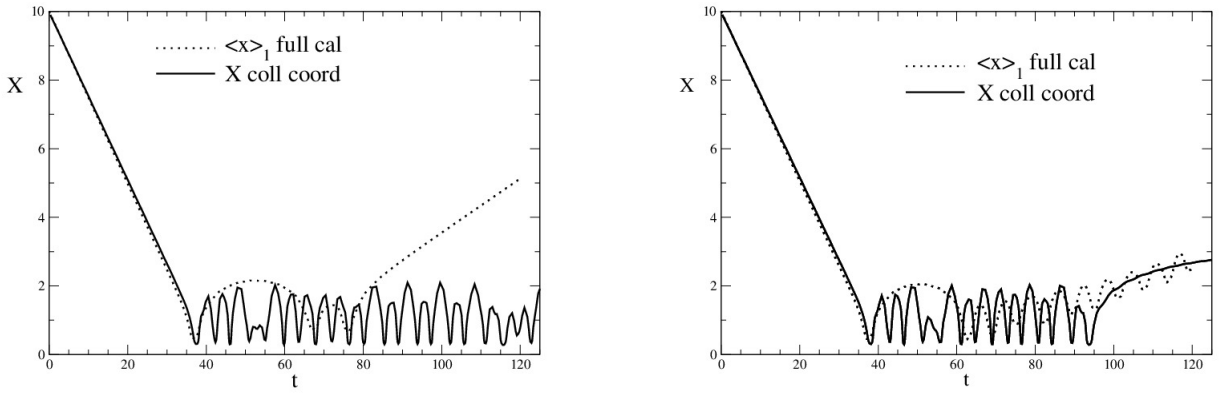

Figure 3.5: Comparison of the time dependence of the collective coordinate $X(t)$ with that of the PDE $\langle x \rangle_1$ for $q = 5$ in equation (3.2.4), Left panel: $v_{in} = 0.251$, Right panel: $v_{in} = 0.247$.

For the solutions of the ODE approach with $q = 10$ we observe that initial velocities in $0.14 \leq v_{in} \leq 0.243$ yield a double bounce, the same result is observed for initial velocities in $0.260 \leq v_{in} \leq 0.289$. Furthermore, for the ODE model, we find three bounce solutions for $v_{in} = 0.421$ and four bounces for $v_{in} = 0.251$. For large velocities $v_{in} \geq 0.425$ a single bounce is observed in the ODE model. For initial velocities in $0.245 \leq v_{in} \leq 0.249$ and $0.301 \leq v_{in} \leq 0.420$ we find a trapped oscillatory state. Figure 3.6 (b) shows the two-dimensional phase space of the collective coordinate system with a bounded and an unbounded phase orbit. In this framework the bounded orbits represent trapped oscillatory states whereas the unbounded orbits represent reflected kink-antikink systems. From this we found that the ODE solutions predict a critical velocity of $v_{cr,ODE} \approx 0.4245$ above which bound state solution cease to exist. Further, Figures 3.6 (a), (c) and (d) show the behaviour of the solutions of $X(t)$, $A(t)$ and $B(t)$ for different initial velocities v_{in}.

The results of the ODE model for $q = 10$ agree with that of the PDE system for certain values of v_{in}. For example in the PDE system, for initial velocities $v_{in} = 0.201$, $v_{in} = 0.198$, $v_{in} = 0.2265$ and $v_{in} = 0.2384$ we observe a double bounce which agrees well to the two bounce window $0.14 \leq v_{in} \leq 0.243$ of the ODE model system. Further, single bounce solutions for the ODE model for initial velocities $v_{in} \geq 0.425$ are also observed in the PDE system. However, there were other instances in which the solutions of the ODE model do not agree with those of the PDE system. For example, in the PDE system for initial velocities in $0.14 \leq v_{in} \leq 0.19$ we observe a bound oscillatory state whereas in the ODE model we observe a double bounce solution. Furthermore in the PDE system we observe a three bounce solution for $v_{in} = 0.251$ while in the ODE model this value yields a four bounce solution.

From relations like $a_5(X) = -b_5(X)$ among the coefficient functions it can be analytically shown that $A(t) = -B(t)$ is a possible solution to the ODE system. Hence initial conditions $A(0) = -B(0)$ will lead to this particular solution. We have numerically verified this results

for $A(0) = -B(0) = 0$ and $v_{in} = 0.201$. These numerical results are shown in Figures 3.6 (c) and (d) as well as in Table 3.1. Thus our initial configuration with two separated (anti)kinks and zero amplitudes for the shape mode leads to the singularity $D(X) \to 0$ as $X \to 0$ unless $q \neq 0$.

We performed a rigorous numerical study in choosing initial conditions for $A(0) = B(0) \neq 0$ with $q = 0$ and $q \neq 0$, that is not subject to this singularity. The two cases essentially yield identical results for $X(t)$ and deviate faintly for the amplitudes $A(t)$ and $B(t)$. Here we discuss the $q = 10$ case in detail. The interesting question is whether the ODE solutions show good resemblance to those from the PDE system. We use the initial velocity $v_{in} = 0.251$ as a case study. For initial conditions of $A(0) = B(0) \neq 0$ we find an oscillatory bound state in the interval $0.01 \leq A(0), B(0) \leq 0.05$; the interval $0.07 \leq A(0), B(0) \leq 0.09$ has two bounces and

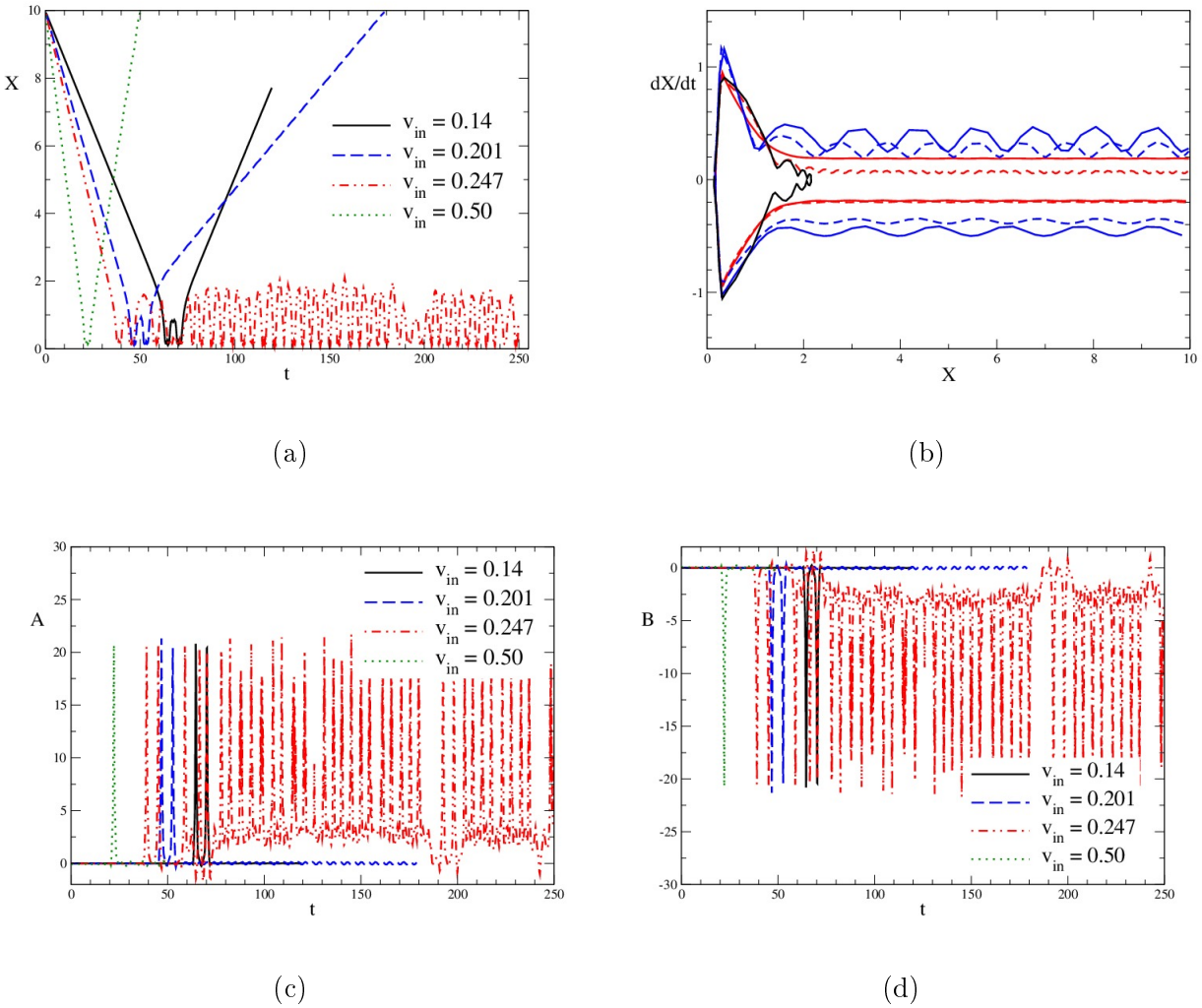

Figure 3.6: (a) The solutions to the ODE configuration. (b) Trajectory in the $X - \dot{X}$ phase plane in the reduced system, the blue lines were calculated with initial velocity above the critical velocity and the red lines with initial velocity less than the critical velocity. Both solutions show reflected systems of the kink-antikink pairs. The amplitudes of the internal shape modes $A(t)$ and $B(t)$ are show in the subgraphs (c) and (d), respectively.

time (t)	A(t)	B(t)
0.2979	-0.0017	0.0017
0.7647	-0.0098	0.0098
46.3345	5.7734	-5.7734
46.4153	8.4117	-8.4117
51.8251	2.4965	-2.4965
51.9675	4.2068	-4.2068
63.5582	11.4982	-11.4982
86.6211	-0.1142	0.1142
178.4420	-0.0029	0.0029
178.8520	0.0803	-0.0803

Table 3.1: The amplitudes of the internal shape modes for $v_{in} = 0.201$ with the initial condition $A(0) = B(0) = 0$.

time(t)	A(t)	B(t)
0.3820	-0.0018	0.0037
0.8442	-0.0114	0.0117
45.9967	3.0948	-3.0959
46.2027	4.4513	-4.4506
51.3065	0.7435	-0.7444
51.5782	1.1157	-1.1156
53.1037	5.6098	-5.6111
91.0534	-0.0607	0.0619
105.6830	-0.0391	0.0403
178.4180	-0.0069	0.0094

Table 3.2: The amplitudes of the internal shape modes for $v_{in} = 0.201$ with the initial condition $A(0) = B(0) = 0.001234$.

we see five bounces in the interval $0.007 \leq A(0), B(0) \leq 0.009$. For $A(0) = B(0) \geq 1$ we observe another oscillatory bound state. For initial conditions in the interval $0 < A(0), B(0) < 0.007$, we observe four bounce solutions with the magnitude of the amplitudes being different from each other.

We now compare this solution to the one from the PDE with identical initial condition. We therefore solve equation (2.2.1) with the initial configuration

$$\begin{aligned}\phi_{K\bar{K}} = &\tanh(\gamma x + X_0) - \tanh(\gamma x - X_0) - 1 \\ &+ \sqrt{\frac{3}{2}} A_0 \frac{\sinh(\gamma x - X_0)}{\cosh^2(\gamma x - X_0)} + \sqrt{\frac{3}{2}} B_0 \frac{\sinh(\gamma x + X_0)}{\cosh^2(\gamma x + X_0)},\end{aligned} \tag{3.2.5}$$

and the initial velocity

$$\begin{aligned}\frac{\partial \phi_{K\bar{K}}}{\partial t} = &\dot{X}_0 \operatorname{sech}^2(\gamma x + X_0) + \dot{X}_0 \operatorname{sech}^2(\gamma x - X_0) \\ &- \sqrt{\frac{3}{2}} A_0 \dot{X}_0 \left\{ \frac{1 - \sinh^2(\gamma x - X_0)}{\cosh^3(\gamma x - X_0)} \right\} \\ &+ \sqrt{\frac{3}{2}} B_0 \dot{X}_0 \left\{ \frac{1 - \sinh^2(\gamma x + X_0)}{\cosh^3(\gamma x + X_0)} \right\},\end{aligned} \tag{3.2.6}$$

where

$$X_0 = X(0) = 10, \quad \dot{X}_0 = \dot{X}(0) = \frac{-v_{in}}{\sqrt{1 - v_{in}^2}}, \quad A_0 = A(0) = B_0 = B(0) = 0.001234. \tag{3.2.7}$$

Results from sample calculation are shown in Figure 3.7. In these cases the ODE approximation reproduces the key features of the full solutions. For these calculations $A(0) = B(0) \ll 1$ and the modification of the initial conditions is minor. Hence it is not surprising that $X(t)$ is essentially identical to the $A(0) = B(0) = 0$ case. This can seen by comparing Figures 3.6 (a) and 3.7 (c). Besides this, we find that before and after collision the magnitude of the amplitudes

are different while during collision they are approximately equal as seen in Table 3.2 for the initial velocity $v_{in} = 0.201$.

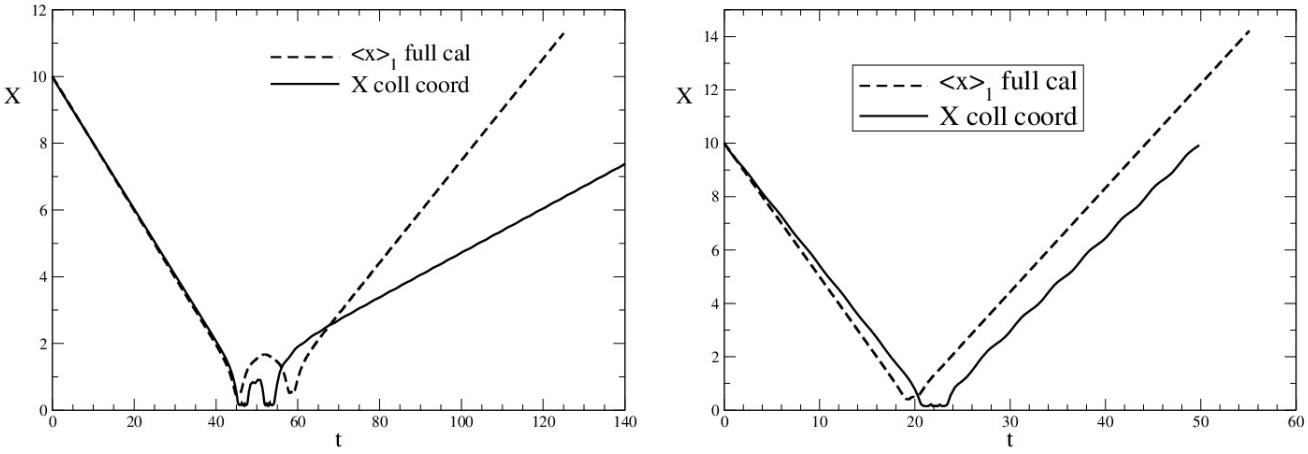

(a) (b)

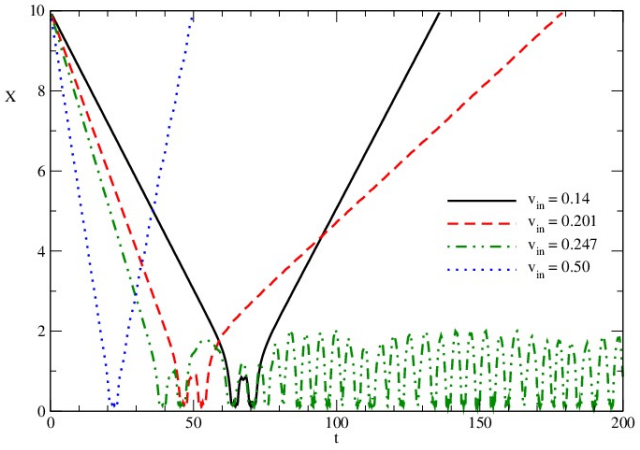

(c)

Figure 3.7: Comparison of the ODE solutions to the PDE solutions subject to the initial conditions of equations (3.2.5) and (3.2.6) for (a) $v_{in} = 0.201$ and (b) $v_{in} = 0.50$. (c) The ODE solutions for various initial velocities, under the initial condition $A(0) = B(0) = 0.001234$.

Chapter 4

The ϕ^6 Theory

In this chapter we introduce the ϕ^6 model. As for the ϕ^4 model, it is characterised by the interaction potential in the Lagrangian density. The static solutions of this model are again boson particles and are referred as kink solitons (and the antiparticle referred as antikink). We have three distinct vacuum solutions in the ϕ^6 model, based on this we investigate two distinct configurations (kink-antikink and antikink-kink configurations) numerically by solving the time-dependent equation of motion (4.2.1). To interpret the solutions of these configurations, we investigate the fluctuation modes around the kink-antikink system in section 4.6.

4.1 Introduction

We discuss another model of a kink solution, which involves three vacua. To obtain these vacua, we consider a single scalar field $\phi(x,t)$, in one space (x) and one time (t) dimension whose potential $U(\phi)$ is cubic in ϕ^2 and is given by [34, p.111–113]

$$U(\phi) = \nu\phi^2 + \varrho\phi^4 + \lambda\phi^6. \tag{4.1.1}$$

Here ν, ϱ and λ are real constants with $\lambda > 0$ such that the energy that arises from the Lagrangian density is bounded from below. For static solutions to exist, we again assume $\varrho < 0$ and choose ϱ and ν as in (2.1.3). In this case the potential becomes

$$U(\phi) = \lambda\phi^2(\phi^2 - m^2)^2.$$

Again we may scale the coordinates and fields such that $\lambda = \frac{1}{2}$ and $m = 1$ yielding

$$U(\phi) = \frac{1}{2}\phi^2(\phi^2 - 1)^2. \tag{4.1.2}$$

This potential has three degenerate minima: a central minimum given by $\phi(x,t) = 0$, and two minima $\phi = \pm 1$ the latter are connected by the symmetry operation $\phi \to -\phi$. The full

Lagrangian density of this model is given as

$$\begin{aligned}\mathcal{L} &= \frac{1}{2}\partial_\mu\phi\partial^\mu\phi - U(\phi),\\ &= \frac{1}{2}(\phi_t)^2 - \frac{1}{2}(\phi_x)^2 - \frac{1}{2}\phi^2(\phi^2-1)^2.\end{aligned} \tag{4.1.3}$$

Since we have three degenerate minima, we can have four static solutions to the Lagrangian density [4, p.19] that connect these vacua at spatial infinity.

As before the Lagrangian density is invariant under the symmetry $\phi \leftrightarrow -\phi$. Now, considering the central minimum, $\phi(x,t) = 0 = \phi_0(\text{say})$ and expanding in the shifted field $\phi(x,t) = \eta(x,t) + \phi_0$, we have the Lagrangian density as

$$\mathcal{L} = \frac{1}{2}\partial_\nu\eta\partial^\nu\eta - \frac{1}{2}(\eta^2 - 2\eta^4 + \eta^6).$$

Comparing to the Lagrangian density of the Klein-Gordon equation (1.3.3) we have

$$m_\eta^2 = 1,$$

thus the boson states built on this vacuum have mass $m_\eta = 1$. Further, we consider the minima $\phi(x,t) = \pm 1$, choosing $\phi(x,t) = 1$ and expanding in the shifted field $\phi(x,t) = \zeta(x,t) + 1$, we have the Lagrangian density as

$$\mathcal{L} = \frac{1}{2}\partial_\nu\zeta\partial^\nu\zeta - \frac{1}{2}(4\zeta^2 + 12\zeta^3 + 13\zeta^4 + 6\zeta^5 + \zeta^6).$$

Comparing it to the Lagrangian density of the Klein-Gordon equation (1.3.3) as before, we have

$$m_\zeta^2 = 4,$$

thus the boson states built on this vacuum have mass $m_\zeta = 2$. As before, choosing either of the vacuum configuration $\phi(x,t) = \pm 1$ breaks the symmetry of $\phi \leftrightarrow -\phi$ [35, p.369].

4.2 The Kink and Antikink Solitons of the ϕ^6 Theory

Using (1.3.2) the equation of motion becomes

$$(\phi_t)^2 - (\phi_x)^2 = -\phi(3\phi^4 - 4\phi^2 + 1). \tag{4.2.1}$$

For static solutions we set the time derivative to zero

$$\frac{\mathrm{d}^2\phi}{\mathrm{d}x^2} = 3\phi^5 - 4\phi^3 + \phi. \tag{4.2.2}$$

Again the stable static (vacuum) solutions of equation (4.2.2) are just the minima of the scalar potential energy since the kinetic energy part of the Lagrange is quadratic in time derivatives [36, p.7], thus

$$\phi_{\text{vac}} = 0, \pm 1. \tag{4.2.3}$$

Multiplying both sides of (4.2.2) by $\phi'(x)$ and integrating over space using the boundary conditions

$$\phi'(-\infty) = 0 \quad \text{and} \quad U(\phi(-\infty)) = 0,$$

we obtain by the first order differential equation

$$\frac{\mathrm{d}\phi}{\mathrm{d}x} = \pm\phi(\phi^2 - 1). \tag{4.2.4}$$

Integrating this equation and taking the integration constant to be zero we have

$$x = \pm\frac{1}{2}\ln\left(\frac{1-\phi^2}{\phi^2}\right).$$

This gives

$$\phi^2(x) = [1 + \exp(\pm 2x)]\,. \tag{4.2.5}$$

Thus there are four possible solutions. Pairs of which are related by $x \leftrightarrow -x$. Taking the negative square root

$$\phi(x) = -\left[1 + \exp(2x)\right]^{-\frac{1}{2}}, \tag{4.2.6}$$

we find a kink interpolating between $\phi(-\infty) = -1$ and $\phi(\infty) = 0$, and an antikink interpolating between $\phi(-\infty) = 0$ and $\phi(\infty) = -1$, given by $-\left[1 + \exp(-2x)\right]^{-\frac{1}{2}}$. Similarly taking the positive square root

$$\phi(x) = \left[1 + \exp(-2x)\right]^{-\frac{1}{2}}, \tag{4.2.7}$$

we have a kink interpolating between $\phi(-\infty) = 1$ and $\phi(\infty) = 0$ and an antikink interpolating between $\phi(-\infty) = 0$ and $\phi(\infty) = 1$, given by $\left[1 + \exp(2x)\right]^{-\frac{1}{2}}$. These features were discussed in [41] and [42]. Taking a Lorentz boost of the kink solutions of equation (4.2.6) and (4.2.7)

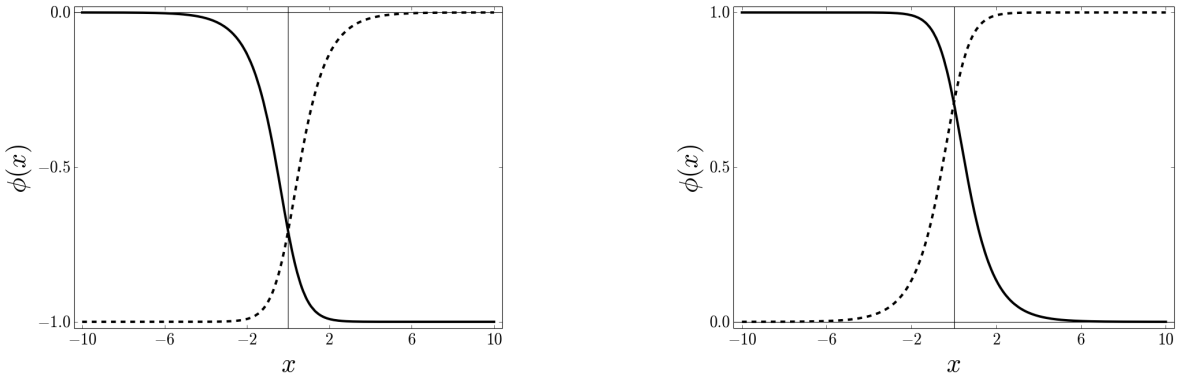

Figure 4.1: Left panel: The kink (dashed line) and antikink (solid line) solutions of equation (4.2.6). Right panel: The kink (dashed line) and antikink (solid line) solutions of equation (4.2.7).

and their respective antikink solutions, we obtain the moving kink solutions as

$$\phi(x,t) = \begin{cases} -\left[1 + \exp(2\gamma(x - vt))\right]^{-\frac{1}{2}} \\ \left[1 + \exp(-2\gamma(x - vt))\right]^{-\frac{1}{2}} \end{cases}, \tag{4.2.8}$$

and the moving antikink solutions as

$$\phi(x,t) = \begin{cases} -\left[1+\exp(-2\gamma(x-vt))\right]^{-\frac{1}{2}} \\ \left[1+\exp(2\gamma(x-vt))\right]^{-\frac{1}{2}} \end{cases}, \tag{4.2.9}$$

where $|v|<1$ is the velocity of the (anti)kink and $\gamma = \dfrac{1}{\sqrt{1-v^2}}$ is the Lorentz factor.

4.3 Energy Density and Energy Functional of the ϕ^6 Kink Solution

As before the energy density is given as

$$\begin{aligned} \mathcal{E}_6(x) &= \frac{1}{2}(\phi_t)^2 + \frac{1}{2}(\phi_x)^2 + U(\phi), \\ &= \frac{1}{2}(\phi_t)^2 + \frac{1}{2}(\phi_x)^2 + \frac{1}{2}\phi^2(\phi^2-1)^2, \end{aligned} \tag{4.3.1}$$

and the total energy is obtained by integration

$$E[\phi] = \int_{-\infty}^{\infty} \mathcal{E}_6(x,t)\,\mathrm{d}x. \tag{4.3.2}$$

It is conserved for any solution of equation (4.2.1). For the kink solution of (4.2.6), we have the energy density using equation (4.2.4) as

$$\mathcal{E}_6(x) = \frac{1}{2}(\phi_x)^2 + U(\phi) = 2U(\phi) = \frac{\exp(4x)}{\left[1+\exp(2x)\right]^3}. \tag{4.3.3}$$

With this the total kink energy becomes

$$E[\phi] = \int_{-\infty}^{\infty} \mathcal{E}_6(x)\,\mathrm{d}x = \int_{-\infty}^{\infty} \frac{\exp(4x)}{\left[1+\exp(2x)\right]^3}\,\mathrm{d}x = \frac{1}{4}. \tag{4.3.4}$$

Thus the classical kink mass (by restoring the units (λ, m)) in this case is

$$M = \frac{\sqrt{2}}{4} m^4 \sqrt{\lambda}.$$

The energy density of the moving kink, equation (4.2.8) attains the form

$$\begin{aligned} \mathcal{E}_6(x) &= \frac{1}{2}\left\{\frac{v^2}{1-v^2} + \frac{1}{1-v^2} + 1\right\} \frac{\exp(4\gamma(x-vt))}{\left[1+\exp(2\gamma(x-vt))\right]^3}, \\ &= \frac{1}{1-v^2} \frac{\exp(4\gamma(x-vt))}{\left[1+\exp(2\gamma(x-vt))\right]^3}, \end{aligned} \tag{4.3.5}$$

and its total energy becomes

$$\begin{aligned} E[\phi] &= \frac{1}{1-v^2} \int_{-\infty}^{\infty} \frac{\exp(4\gamma(x-vt))}{\left[1+\exp(2\gamma(x-vt))\right]^3}\,\mathrm{d}x, \\ &= \frac{1}{\sqrt{1-v^2}} \frac{1}{4} = \frac{M}{\sqrt{1-v^2}}. \end{aligned} \tag{4.3.6}$$

This equation shows that the kink is a particle with mass M moving with velocity v, because it is the Einstein mass-energy relation for a particle. We note that these results remain the same for the kink solution (4.2.7).

4.4 Translational Invariance of the Kink Solution

Translating the kink solution (4.2.6) by

$$x \to x + x_0$$

we obtain

$$\phi(x, x_0) = -\left[1 + \exp(2(x + x_0))\right], \tag{4.4.1}$$

which corresponds to the kink centered at $-x_0$. Shifting the integration variable in equation (4.2.4) accordingly shows that translating the kink solution does not change the energy of the kink. This causes the existence of the "zero mode" of the kink [7, p.4], whose properties will be discussed in a latter section.

4.5 Kink-Antikink Interaction

We now investigate the interaction of the kink-antikink solutions. Since there are two distinct classes of vacua; $\phi_{\text{vac}} = 0$ and $\phi_{\text{vac}} = \pm 1$, we investigate the interaction of the kink-antikink separately on each class of vacua basing our arguments on those used by Dorey *et al.* [17].

Case I In the case of $\phi_{\text{vac}} = 0$, we have a **kink-antikink** configuration $(K\bar{K})$ given by the superposition ansatz:

$$\phi_{K\bar{K}} = \phi_K(\xi_-) + \phi_{\bar{K}}(\xi_+) - 1 = \frac{1}{\sqrt{1 + e^{2\xi_-}}} + \frac{1}{\sqrt{1 + e^{-2\xi_+}}} - 1, \tag{4.5.1}$$

where $\xi_\pm = \dfrac{x}{\sqrt{1 - v_{in}^2}} \pm X_0$, so that X_0 measures the position of the antikink. As in section 2.5, for the PDE X_0 is a not a function of time, but merely an initial parameter. To simplify the equation we have defined $\gamma = \dfrac{1}{\sqrt{1 - v_{in}^2}}$. At initial time $(t = 0)$, the propagation of the kink and antikink towards each other at speed $2v_{in}$ is

$$\begin{aligned}\phi_{K\bar{K}} &= \phi_K(\xi_-) + \phi_{\bar{K}}(\xi_+) - 1 \\ &= \left[1 + \exp(2(\gamma x - X_0))\right]^{-\frac{1}{2}} + \left[1 + \exp(-2(\gamma x + X_0))\right]^{-\frac{1}{2}} - 1,\end{aligned} \tag{4.5.2}$$

and its time derivative with the same initial condition is

$$\frac{\partial \phi_{K\bar{K}}}{\partial t} = \dot{X}_0 \frac{\exp(2(\gamma x - X_0))}{\left[1 + \exp(2(\gamma x - X_0))\right]^{\frac{3}{2}}} + \dot{X}_0 \frac{\exp(-2(\gamma x + X_0))}{\left[1 + \exp(-2(\gamma x + X_0))\right]^{\frac{3}{2}}}, \tag{4.5.3}$$

with $\dot{X}_0 = \dfrac{-v_{in}}{\sqrt{1 - v_{in}^2}}$.

Case II Similarly in the case of $\phi_{\text{vac}} = \pm 1$, we have an **antikink-kink** configuration $\phi(\bar{K}K)$ given by the superposition ansatz:

$$\phi_{\bar{K}K} = \phi_K(\xi_+) + \phi_{\bar{K}}(\xi_-) = \frac{1}{\sqrt{1 + e^{2\xi_+}}} + \frac{1}{\sqrt{1 + e^{-2\xi_-}}}. \tag{4.5.4}$$

Also at initial time ($t = 0$), the propagation of the antikink and kink towards each other at speed $2v_{in}$ is

$$\begin{aligned}\phi_{\bar{K}K} &= \phi_{\bar{K}}(\xi_+) + \phi_{\bar{K}}(\xi_-), \\ &= [1 + \exp(2(\gamma x + X_0))]^{-\frac{1}{2}} + [1 + \exp(-2(\gamma x - X_0))]^{-\frac{1}{2}}\,. \end{aligned} \tag{4.5.5}$$

and its time derivative with the same initial condition is

$$\frac{\partial \phi_{K\bar{K}}}{\partial t} = -\dot{X}_0 \frac{\exp(2(\gamma x + X_0))}{[1 + \exp(2(\gamma x + X_0))]^{\frac{3}{2}}} - \dot{X}_0 \frac{\exp(-2(\gamma x - X_0))}{[1 + \exp(-2(\gamma x - X_0))]^{\frac{3}{2}}}. \tag{4.5.6}$$

As before, we choose the configuration of equations (4.5.2) (respectively equation (4.5.5)) and (4.5.3) (respectively equation (4.5.6)) to solve the partial differential equation (4.2.1) numerically (algorithm discussed in Appendix B.1) by choosing $X_0 \gg 1$ to avoid initial interference and v_{in} such that kink and antikink propagate towards each other. Again the accuracy of our numerically results is tested by verifying that total energy (4.3.2) is conserved at all times.

For the case of the **kink-antikink** configuration, the critical velocity has been computed numerically to be $v_{cr} \approx 0.289$ [17]. This critical velocity is defined as separating two distinct classes of solutions: Figure 4.2 shows that for $v_{in} < v_{cr}$ the kink-antikink pair collide, reflect, recede to finite separation and return to collide again radiating their energy at every time they collide to form a chaotic bound state as in the case of the ϕ^4 model. For $v_{in} > v_{cr}$ the

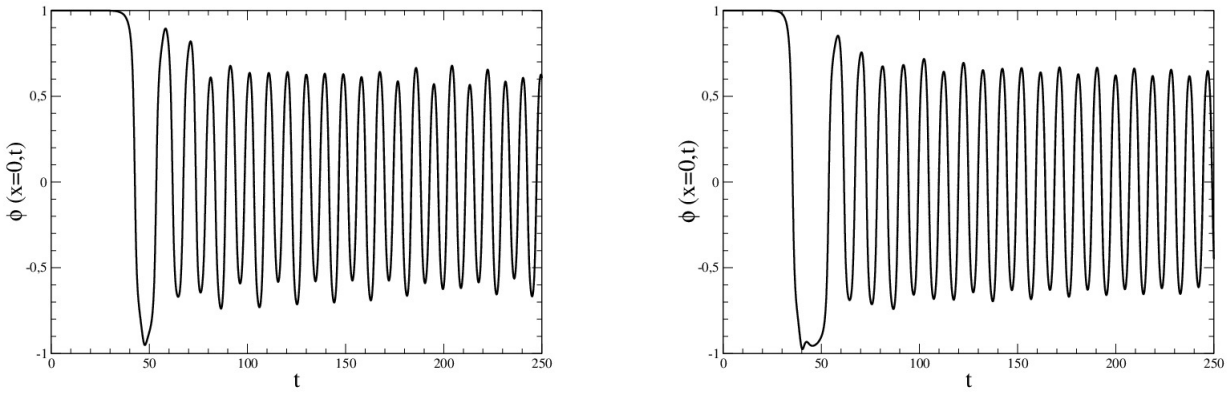

Figure 4.2: Formation of chaotic bound state of the kink-antikink pairs, Left panel: $v_{in} = 0.221$. Right panel: $v_{in} = 0.270$.

kink-antikink pair reflects upon collision without further interaction, since there is not enough energy emitted during the short-time collision process as shown in Figure 4.3.

For the case of **antikink-kink** configuration, the critical velocity was computed numerically to be $v_{cr} \approx 0.0457$ [17], above which the kinks have enough energy to separate. We observe two results, for initial velocities $v_{in} < v_{cr}$, kink and antikink are captured and they slowly annihilate each other to form a chaotic bound state as shown in Figure 4.4.

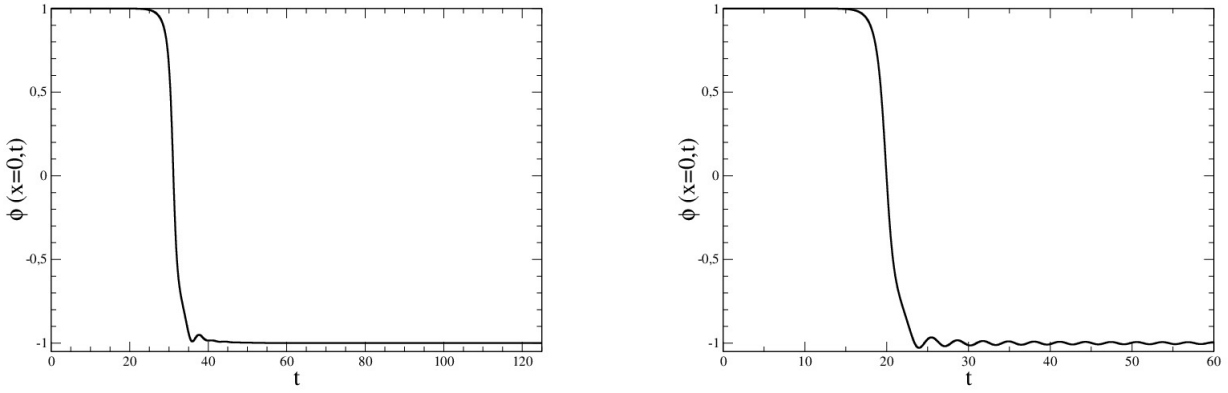

Figure 4.3: Reflection of kink-antikink pair, Left panel: $v_{in} = 0.31$. Right panel: $v_{in} = 0.50$.

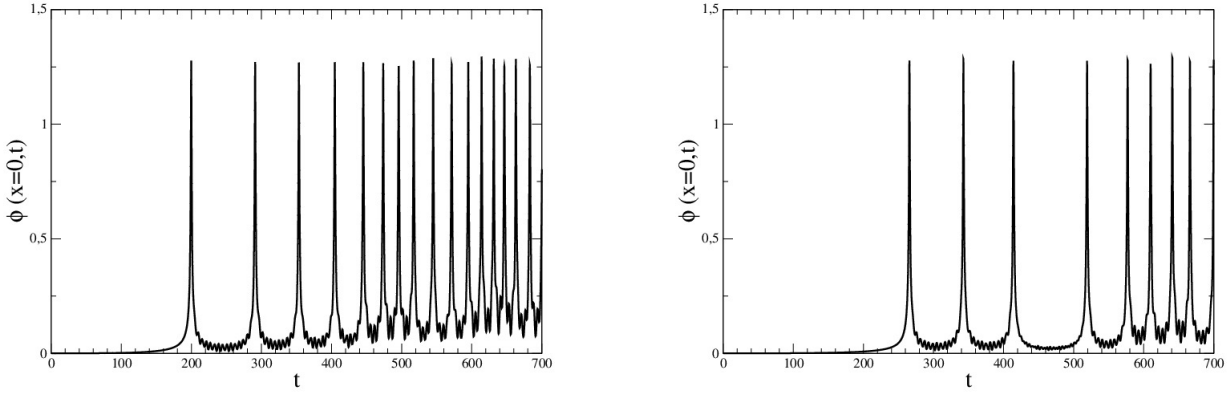

Figure 4.4: Formation of chaotic bound state of antikink-kink pair, Left panel: $v_{in} = 0.031$. Right panel: $v_{in} = 0.022$.

Further, for some specific initial velocities $v_{in} < v_{cr}$, two-resonance windows are observed, Figure 4.5, as in the case of ϕ^4 model . Thus, in this case after the first collision the kink-antikink pair is bounded by an attractive potential such that kink and antikink do not have enough energy to escape to infinity, but after the second collision they regain that lost energy and are able to escape.

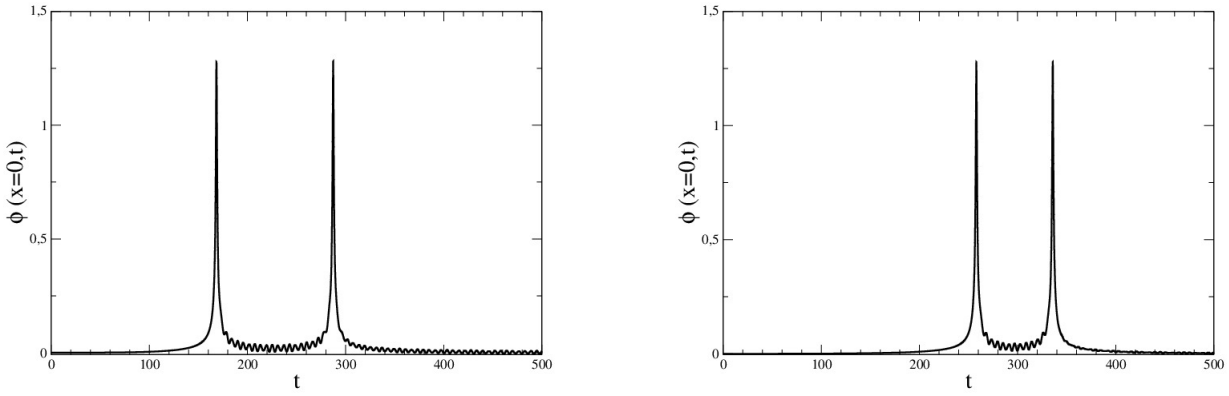

Figure 4.5: Formation of two-bounce windows, Left panel: $v_{in} = 0.038$. Right panel: $v_{in} = 0.0228$.

Adapting the expectation value, equation (2.5.5) to the ϕ^6 model, we found that, for $v_{in} > v_{cr}$ the antikink and kink pair exhibit pseudo-bounces as shown in Figure 4.6. This is because there is no time to emit enough energy during the collision process in binding the antikink-kink system.

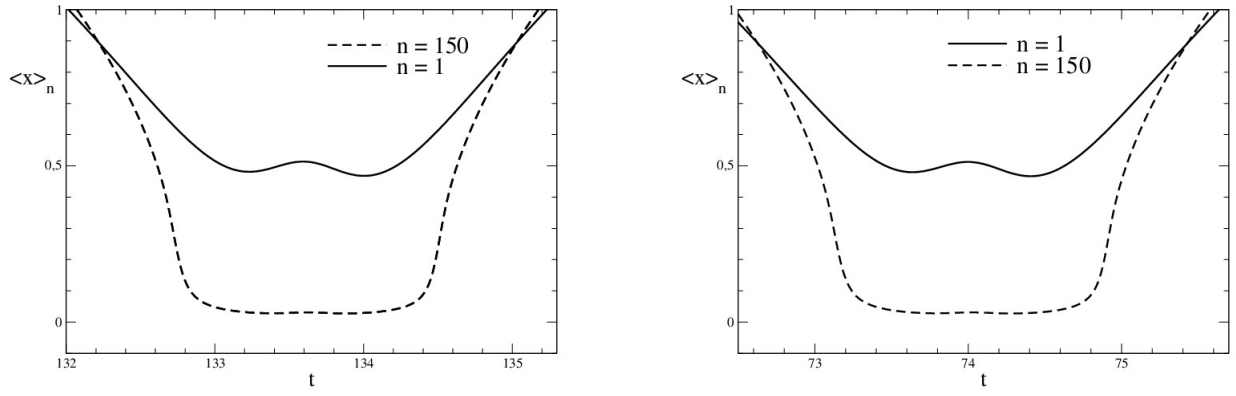

Figure 4.6: Pseudo-bounces in the antikink-kink system; for large n values in equation (2.5.5) with $\mathcal{E}_4 \to \mathcal{E}_6$. Left panel: $v_{in} = 0.050$. Right panel: $v_{in} = 0.10$.

Based on these results, we ask the following questions:

- Does the transfer and storage of energy in the resonance window depend on the excitation modes as conjectured in the case of the ϕ^4 model?
- If such excitation modes exist does the Campbell *et al.* [33] explanation hold in this model?

4.6 Excitation of the Kink Solutions

To answer the questions from the end of section 4.5, we consider the fluctuation modes around the kink solutions by introducing $\eta(x,t)$ as a small perturbation:

$$\phi(x,t) = \phi_K(x) + \eta(x,t), \tag{4.6.1}$$

substituting this into the equation (4.2.1) by considering linear terms of η we have

$$\frac{\partial^2\eta}{\partial t^2} - \frac{\partial^2\eta}{\partial x^2} = -\left[15\phi_K^4\eta - 12\phi_K^2\eta + \eta\right]. \tag{4.6.2}$$

We find the fluctuation eigenfunctions by the separation ansatz

$$\eta(x,t) = e^{\imath\omega t}\chi(x), \tag{4.6.3}$$

and equation (4.6.2) reduces to a modified Sturm-Liouville equation

$$-\frac{\mathrm{d}^2\chi(x)}{\mathrm{d}x^2} + U(x)\chi(x) = \omega^2\chi(x), \tag{4.6.4}$$

where the potential $U(x)$ is given as

$$U(x) = 15\phi_K^4 - 12\phi_K^2 + 1. \tag{4.6.5}$$

Writing the kink solution (4.2.7) as

$$\phi_K(x) = [1+\exp(-2x)]^{-\frac{1}{2}} = \sqrt{\frac{1+\tanh x}{2}},$$

the potential function becomes

$$\begin{aligned} U(x) &= 15\left[\frac{1+\tanh x}{2}\right]^2 - 12\left[\frac{1+\tanh x}{2}\right] + 1, \\ &= -\frac{15}{4}\operatorname{sech}^2 x + \frac{3}{2}\tanh x + \frac{5}{2}, \end{aligned}$$

which is not symmetric under the reflection $x \to -x$ as can be seen in Figure 4.7. As before we solve equation (4.6.4) by using techniques from supersymetric quantum mechanics. In a first step we modify this equation slightly as

$$-\frac{1}{2}\frac{\mathrm{d}^2\chi(x)}{\mathrm{d}x^2} + U^1(x)\chi(x) = \frac{1}{2}\omega^2\chi(x), \tag{4.6.6}$$

where

$$U^1(x) = -\frac{15}{8}\operatorname{sech}^2 x + \frac{3}{4}\tanh x + \frac{5}{4}.$$

For bounded solutions, we seek solutions for $\omega^2 < m_\eta^2$. Let χ_0^0 be the ground-state wave function of the Hamiltonian H^0 whose supersymmetric partner H^1, is defined in equations (2.6.6) and

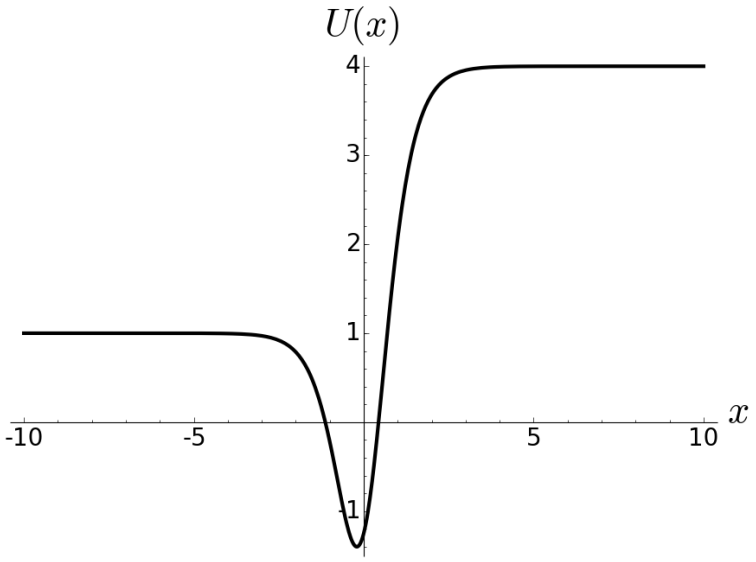

Figure 4.7: A sketch of the potential $U(x)$ of the ϕ^6 model, with the boson masses $m_\eta^2 = 1$ and $m_\zeta^2 = 4$.

(2.6.9). Formally the operators $Q^\pm$ of equation (2.6.7) with the function $\Phi(x)$ and the potentials V^0, V^1 of equation (2.6.10) with their conditions remain the same. Choosing

$$\Phi(x) = \frac{3}{2}\tanh x + \frac{1}{2}, \tag{4.6.7}$$

the two potentials become

$$V^0(x) = -\frac{15}{8}\operatorname{sech}^2 x + \frac{3}{4}\tanh x + \frac{5}{4}, \tag{4.6.8a}$$

$$V^1(x) = -\frac{3}{8}\operatorname{sech}^2 x + \frac{3}{4}\tanh x + \frac{5}{4}, \tag{4.6.8b}$$

with the operators explicitly given as

$$Q^\pm = \frac{1}{\sqrt{2}}\left[\mp\frac{\mathrm{d}}{\mathrm{d}x} + \frac{1}{2}(3\tanh x + 1)\right]. \tag{4.6.9}$$

Using equation (2.6.11) we have

$$\begin{aligned}\chi_0^0(x) &= \mathcal{N}\exp\left\{-\frac{1}{2}\int_x (3\tanh x' + 1)\,\mathrm{d}x'\right\},\\ &= \mathcal{N}e^{-\frac{1}{2}x}\operatorname{sech}^{\frac{3}{2}} x.\end{aligned}$$

Using the normalization condition (2.6.12) we finally obtain the normalized wave function as

$$\chi_0^0(x) = \frac{1}{\sqrt{2}}e^{-\frac{1}{2}x}\operatorname{sech}^{\frac{3}{2}} x. \tag{4.6.10}$$

Clearly $Q^-\chi_0^0 = 0 \implies Q^+Q^-\chi_0^0 = 0$. Hence the ground-state energy is $\omega_0^0 = 0$. It is the translational zero mode arising from the x_0-expansion of equation (4.4.1). The remaining eigenvalues are identical with the problem $V^1(x)$; but this potential has no solution within

$0 < \omega^2 < m_\eta^2$. Thus the only bound state solution is this translational "zero mode " with $\chi_0^0(x)$ given in (4.6.10) with eigenvalue $\omega_0^0 = 0$. This results agrees with the one obtained by Lohe in reference [43]. Thus, we found that there is no internal shape mode which, according to reference [33] would be responsible for the resonance structure exhibited in the kink-antikink interaction.

To better understand the resonance type solutions in this model we pursue a collective coordinate approximation based on the argument of reference [33] (i.e. the shape mode $\chi_1^0(x)$ being responsible for the resonance type solutions) that reduces the partial differential equations to a set of ordinary differential equations in the subsequent chapter.

Chapter 5

The ODE Equation for the ϕ^6 Kink-Antikink Configuration

As before, we tackle the "zero mode" that arises due to the translational invariance of the kink solution by the collective coordinates $X(t)$. Even though an internal shape mode does not exist, we investigate whether a collective coordinate ansatz including the internal shape mode (equation (2.6.18)) will approximate the PDE solution well. Now, since we have two different interaction configurations, we consider two different collective coordinate parametrisations proposed by [23]. In an attempt to avoid the null vector problem, we again introduce independent amplitudes for the two peaks around the kink-antikink centers. In total there are three degrees of freedom (X, A, B), for each parametrisation.

5.1 Collective Coordinates Description of the Kink-Antikink Configuration in the ϕ^6 Theory

For the kink-antikink configuration, we consider the parametrisation, of equation (2.5.2)

$$\begin{aligned}\phi_{cc}(x,t) &= \phi_K(\xi_-) + \phi_{\bar{K}}(\xi_+) - 1 + \sqrt{\frac{3}{2}}\left[A(t)\chi_1^0(\xi_-) + B(t)\chi_1^0(\xi_+)\right], \\ &= \phi_K(\xi_-) + \phi_K(-\xi_+) - 1 + \sqrt{\frac{3}{2}}\left[A(t)\chi_1^0(\xi_-) + B(t)\chi_1^0(\xi_+)\right], \end{aligned} \tag{5.1.1}$$

where

$$\phi_K(\xi) = [1 + \exp(2\xi)]^{-\frac{1}{2}} = \phi_{\bar{K}}(-\xi).$$

Let

$$\phi_0(x, X(t)) = \phi_K(\xi_-) + \phi_K(-\xi_+) - 1, \tag{5.1.2}$$

then we have

$$\phi_{cc}(x,t) = \phi_0(x, X(t)) + \sqrt{\frac{3}{2}}\left[A(t)\chi_1^0(\xi_-) + B(t)\chi_1^0(\xi_+)\right].$$

Substituting this into the Lagrange density (4.1.3) and integrating over all space, from $-\infty$ to ∞, we obtained the Lagrange function for the collective coordinates

$$\begin{aligned} L_6(A,\dot{A},B,\dot{B},X,\dot{X}) &= \int \mathcal{L}_6(\phi_{cc})\,\mathrm{d}x, \\ &= a_1\dot{X}^2 - a_2 + a_3\dot{A}^2 - a_4A^2 + a_5A + a_6\dot{X}^2A + a_7\dot{X}\dot{A} \\ &\quad + a_8\dot{X}^2A^2 + a_9A\dot{X}\dot{A} - a_{10}A^3 - a_{11}A^4 - a_{12}A^5 - a_{13}A^6 \\ &\quad + b_3\dot{B}^2 - b_4B^2 + b_5B + b_6\dot{X}^2B + b_7\dot{X}\dot{B} + b_8\dot{X}^2B^2 \\ &\quad + b_9B\dot{X}\dot{B} - b_{10}B^3 - b_{11}B^4 - b_{12}B^5 - b_{13}B^6 \\ &\quad + d_1\dot{A}\dot{B} + d_2\dot{X}^2AB + d_3B\dot{X}\dot{A} + d_4A\dot{X}\dot{B} - d_5AB \\ &\quad - d_6A^2B^2 - d_7A^2B - d_8AB^2 - d_9A^3B - d_{10}AB^3 \\ &\quad - d_{11}A^4B - d_{12}A^3B^2 - d_{13}A^2B^3 - d_{14}AB^4 - d_{15}A^5B \\ &\quad - d_{16}A^4B^2 - d_{17}A^3B^3 - d_{18}A^2B^4 - d_{19}AB^5, \end{aligned} \tag{5.1.3}$$

where the coefficients $a_1, \cdots, d_{19}$ are again implicit functions of X. Integral representations is given in Appendix A.2.

5.1.1 Equations of Motion and the Energy Density of the Kink-Antikink System

Since the Lagrangian is made up of three independent variables A, B and X we have three independent equations of motion

$$\frac{\mathrm{d}}{\mathrm{d}t}\frac{\partial L_6}{\partial \dot{X}} = \frac{\partial L_6}{\partial X}, \quad \frac{\mathrm{d}}{\mathrm{d}t}\frac{\partial L_6}{\partial \dot{A}} = \frac{\partial L_6}{\partial A} \quad \text{and} \quad \frac{\mathrm{d}}{\mathrm{d}t}\frac{\partial L_6}{\partial \dot{B}} = \frac{\partial L_6}{\partial B}, \tag{5.1.4}$$

where the dot indicates a total time derivative $\dot{X}(t) = \dfrac{\mathrm{d}}{\mathrm{d}t}X(t)$, etc. These give derivative couplings between X, A and B that are most conveniently written as a matrix equation

$$\begin{pmatrix} a_{11} & a_{12} & a_{13} \\ a_{21} & a_{22} & a_{23} \\ a_{31} & a_{32} & a_{33} \end{pmatrix} \begin{pmatrix} \ddot{X} \\ \ddot{A} \\ \ddot{B} \end{pmatrix} = \begin{pmatrix} f_1 \\ f_2 \\ f_3 \end{pmatrix}, \tag{5.1.5}$$

with

$$\begin{aligned} a_{11} &= 2a_1 + 2a_6A + 2a_8A^2 + 2b_6B + 2b_8B^2 + 2d_2AB, \\ a_{12} &= a_{21} = a_7 + a_9A + d_3B, \\ a_{13} &= a_{31} = b_7 + b_9B + d_4A, \\ a_{22} &= 2a_3, \\ a_{23} &= a_{32} = d_1, \\ a_{33} &= 2b_3. \end{aligned}$$

As before, the 3×3 matrix structure of equation (5.1.5) arises from the kinetic energy term in the Lagrangian (4.1.3). Solving equation (5.1.5) by inversion gives

$$\begin{pmatrix} \ddot{X} \\ \ddot{A} \\ \ddot{B} \end{pmatrix} = \frac{1}{a_{11}a_{22}a_{33} - a_{11}a_{23}^2 - a_{22}a_{13}^2 - a_{33}a_{12}^2 + 2a_{12}a_{13}a_{23}} \times \begin{pmatrix} a_{22}a_{33} - a_{23}^2 & a_{13}a_{32} - a_{12}a_{33} & a_{12}a_{23} - a_{13}a_{22} \\ a_{23}a_{31} - a_{21}a_{33} & a_{11}a_{33} - a_{13}^2 & a_{21}a_{13} - a_{11}a_{23} \\ a_{21}a_{32} - a_{31}a_{22} & a_{12}a_{31} - a_{11}a_{32} & a_{11}a_{22} - a_{12}^2 \end{pmatrix} \begin{pmatrix} f_1 \\ f_2 \\ f_3 \end{pmatrix}. \tag{5.1.6}$$

Using the Euler-Lagrange equation (5.1.4) and the Lagrangian (5.1.3) we have

$$\begin{aligned} f_1 = &-a_1'\dot{X}^2 - a_2' + a_3'\dot{A}^2 - a_4'A^2 + a_5'A - a_6'\dot{X}^2A - 2a_6\dot{X}\dot{A} - a_8'\dot{X}^2A^2 \\ &- 4a_8A\dot{X}\dot{A} - a_9\dot{A}^2 - a_{10}'A^3 - a_{11}'A^4 - a_{12}'A^5 - a_{13}'A^6 \\ &+ b_3'\dot{B}^2 - b_4'B^2 + b_5'B - b_6'\dot{X}^2B - 2b_6\dot{X}\dot{B} - b_8'\dot{X}^2B^2 - 4b_8B\dot{X}\dot{B} \\ &- b_9\dot{B}^2 - b_{10}'B^3 - b_{11}'B^4 - b_{12}'B^5 - b_{13}'B^6 + d_1'\dot{A}\dot{B} \\ &- d_2'\dot{X}^2AB - 2d_2B\dot{X}\dot{A} - 2d_2A\dot{X}\dot{B} - d_3\dot{B}\dot{A} - d_4\dot{A}\dot{B} - d_5'AB - d_6'A^2B^2 \\ &- d_7'A^2B - d_8'AB^2 - d_9'A^3B - d_{10}'AB^3 - d_{11}'A^4B - d_{12}'A^3B^2 \\ &- d_{13}'A^2B^3 - d_{14}'AB^4 - d_{15}'A^5B - d_{16}'A^4B^2 - d_{17}'A^3B^3 - d_{18}'A^2B^4 \\ &- d_{19}'AB^5, \end{aligned}$$

$$\begin{aligned} f_2 = &-2a_3'\dot{X}\dot{A} - 2a_4A + a_5 + a_6\dot{X}^2 - a_7'\dot{X}^2 + 2a_8\dot{X}^2A - a_9'\dot{X}^2A - 3a_{10}A^2 \\ &- 4a_{11}A^3 - 5a_{12}A^4 - 6a_{13}A^5 - d_1'\dot{X}\dot{B} + d_2\dot{X}^2B - d_3'\dot{X}^2B - d_3\dot{X}\dot{B} \\ &+ d_4\dot{X}\dot{B} - d_5B - 2d_6AB^2 - 2d_7AB - d_8B^2 - 3d_9A^2B - d_{10}B^3 - 4d_{11}A^3B \\ &- 3d_{12}A^2B^2 - 2d_{13}AB^3 - d_{14}B^4 - 5d_{15}A^4B - 4d_{16}A^3B^2 - 3d_{17}A^2B^3 \\ &- 2d_{18}AB^4 - d_{19}B^5, \end{aligned}$$

and

$$\begin{aligned} f_3 = &-2b_3'\dot{X}\dot{B} - 2b_4B + b_5 + b_6\dot{X}^2 - b_7'\dot{X}^2 + 2b_8\dot{X}^2B - b_9'\dot{X}^2B - 3b_{10}B^2 \\ &- 4b_{11}B^3 - 5b_{12}B^4 - 6b_{13}B^5 - d_1'\dot{X}\dot{A} + d_2\dot{X}^2A + d_3\dot{X}\dot{A} - d_4'\dot{X}^2A \\ &- d_4\dot{X}\dot{A} - d_5A - 2d_6A^2B - d_7A^2 - 2d_8AB - d_9A^3 - 3d_{10}AB^2 \\ &- d_{11}A^4 - 2d_{12}A^3B - 3d_{13}A^2B^2 - 4d_{14}AB^3 - d_{15}A^5 - 2d_{16}A^4B \\ &- 3d_{17}A^3B^2 - 4d_{18}A^2B^3 - 5d_{19}AB^4, \end{aligned}$$

where the prime denotes differentiation with respect to X. These derivatives are taken under the integrals in appendix A.2. We end up with coupled second order differential equations

$$\begin{aligned}
\ddot{X} &= \frac{f_1\left(a_{22}a_{33}-a_{23}^2\right)+f_2\left(a_{13}a_{32}-a_{12}a_{33}\right)+f_3\left(a_{12}a_{23}-a_{13}a_{22}\right)}{a_{11}a_{22}a_{33}-a_{11}a_{23}^2-a_{22}a_{13}^2-a_{33}a_{12}^2+2a_{12}a_{13}a_{23}},\\
\ddot{A} &= \frac{f_1\left(a_{23}a_{31}-a_{21}a_{33}\right)+f_2\left(a_{11}a_{33}-a_{13}^2\right)+f_3\left(a_{21}a_{13}-a_{11}a_{23}\right)}{a_{11}a_{22}a_{33}-a_{11}a_{23}^2-a_{22}a_{13}^2-a_{33}a_{12}^2+2a_{12}a_{13}a_{23}},\\
\ddot{B} &= \frac{f_1\left(a_{21}a_{32}-a_{31}a_{22}\right)+f_2\left(a_{12}a_{31}-a_{11}a_{32}\right)+f_3\left(a_{11}a_{22}-a_{12}^2\right)}{a_{11}a_{22}a_{33}-a_{11}a_{23}^2-a_{22}a_{13}^2-a_{33}a_{12}^2+2a_{12}a_{13}a_{23}}.
\end{aligned} \tag{5.1.7}$$

As before, we have solved these equations of motion numerically for initial conditions

$$X(0)=10,\quad \dot{X}(0)=\frac{-v_{in}}{\sqrt{1-v_{in}^2}},\quad A(0)=B(0)=0,\quad \text{and}\quad \dot{A}(0)=\dot{B}(0)=0. \tag{5.1.8}$$

The total energy

$$\begin{aligned}
E_6 &= \frac{\partial\mathcal{L}_4}{\partial\dot{X}}\dot{X}+\frac{\partial\mathcal{L}_4}{\partial\dot{A}}\dot{A}+\frac{\partial\mathcal{L}_4}{\partial\dot{B}}\dot{B}-\mathcal{L}_4,\\
&= a_1\dot{X}^2+a_2+a_3\dot{A}^2+a_4A^2-a_5A+a_6\dot{X}^2A+a_7\dot{X}\dot{A}+a_8\dot{X}^2A^2+a_9A\dot{X}\dot{A}\\
&\quad+a_{10}A^3+a_{11}A^4+a_{12}A^5+a_{13}A^6+b_3\dot{B}^2+b_4B^2-b_5B+b_6\dot{X}^2B+b_7\dot{X}\dot{B}\\
&\quad+b_8\dot{X}^2B^2+b_9B\dot{X}\dot{B}+b_{10}B^3+b_{11}B^4+b_{12}B^5+b_{13}B^6+d_1\dot{A}\dot{B}+d_2\dot{X}^2AB\\
&\quad+d_3B\dot{X}\dot{A}+d_4A\dot{X}\dot{B}+d_5AB+d_6A^2B^2+d_7A^2B+d_8AB^2+d_9A^3B+d_{10}AB^3\\
&\quad+d_{11}A^4B+d_{12}A^3B^2+d_{13}A^2B^3+d_{14}AB^4+d_{15}A^5B\\
&\quad+d_{16}A^4B^2+d_{17}A^3B^3+d_{18}A^2B^4+d_{19}AB^5
\end{aligned} \tag{5.1.9}$$

is a constant of motion. It has been used as an accuracy test on the numerical solution.

5.2 Collective Coordinates Description of the Antikink-Kink Configuration in the ϕ^6 Theory

For the antikink-kink configuration, we consider the parametrisation

$$\begin{aligned}
\phi_{cc}(x,t) &= -\phi_K(\xi_+)-\phi_{\bar{K}}(\xi_-)+\sqrt{\frac{3}{2}}\left[A(t)\chi_1^0(\xi_-)+B(t)\chi_1^0(\xi_+)\right],\\
&= -\phi_K(\xi_+)-\phi_K(-\xi_-)+\sqrt{\frac{3}{2}}\left[A(t)\chi_1^0(\xi_-)+B(t)\chi_1^0(\xi_+)\right].
\end{aligned} \tag{5.2.1}$$

With

$$\phi_0(x,X(t))=-\phi_K(\xi_+)-\phi_K(-\xi_-) \tag{5.2.2}$$

we have

$$\phi_{cc}(x,t)=\phi_0(x,X(t))+\sqrt{\frac{3}{2}}\left[A(t)\chi_1^0(\xi_-)+B(t)\chi_1^0(\xi_+)\right],$$

substituting this into the Lagrange density (4.1.3) and integrating over all space, from $-\infty$ to ∞, we obtain the Lagrangian of the collective coordinates formally as the one of the kink-antikink

configuration (i.e. equation (5.1.3)) with the only difference being the function $\phi_0(x, X(t))$ in the integrals $a_1, \cdots, d_{19}$. Formally, the equation of motion (5.1.7), and the matrix elements of (5.1.5) remain the same, so is the total energy of the system (5.1.9). Numerically the coefficients functions obtained from the Lagrangian of course differ from that of the kink-antikink system and are given in Appendix A.3.

5.3 Comparison of the Solution of the ODE to those of the PDE

We have solved equation (5.1.7) numerically using a fourth-order Runge-Kutta algorithm with equation (5.1.8) as the initial condition. We quantitatively compare the solutions of the ODE to those of the PDE. We compute the time-dependent trajectory of the antikink as in equation (2.5.5) by replacing the energy density by equation (4.3.1). The accuracy of our numerically results has been tested by computing the conserved energy (5.1.9) at all times. In all computations we have included the non-harmonic terms. We will report those results in this section.

5.3.1 Numerical Results for the Kink-Antikink Configuration

The kink-antikink system in the ϕ^6 model is quite different from that in the ϕ^4 model. The main difference lies in the potential term $a_2(X)$. While it diverges in the ϕ^4 model as $X \to -\infty$ [18] it tends to a finite value in the ϕ^6 model as seen in the left panel of Figure 5.1.

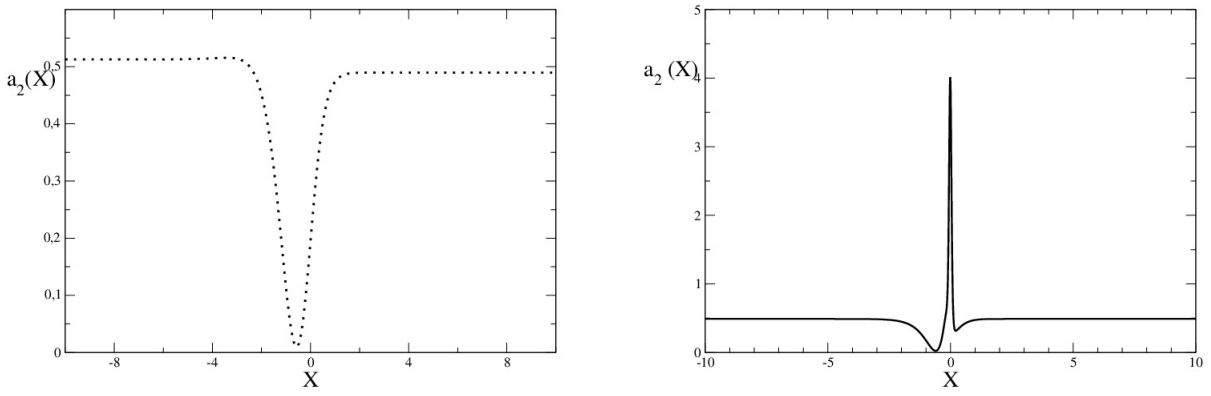

Figure 5.1: Potential $a_2(X)$ for $v_{in} = 0.201$. Left panel: without variation. Right panel: with variation for $q = 10$.

When all coefficient functions contribute to the dynamics (i.e no further approximation applied) we also consider the following variation

$$\phi_0(x, X(t)) \to \phi_0(x, X(t)) + 1 - \frac{1}{2}\left[\tanh(qX) + 1\right] \tag{5.3.1}$$

as a mechanism to control the singularity around $X \to 0$. Here q is an adjustable parameter and $\phi_0(x, X(t))$ is given in equation (5.1.2). This variation is obviously analogy to our treatment of the ϕ^4 model. Without this variation we have a finite potential at negative infinity with $a_2(-\infty) > a_2(+\infty)$. Including this variation we find the symmetry $a_2(-\infty) = a_2(+\infty)$ at the expense of a strong repulsion around $X = 0$. This is also shown in the right panel of Figure 5.1.

We note that the kink-antikink solutions of the ϕ^6 model discussed in section 4.2 form bubbles similar to the detailed study in reference [44]. It was further studied by the authors in references [45, 46] that these soliton-like bubbles, when unstable, can have repercussion on the dynamics of the kink interaction system. We find some 'noise' behaviour of the mean distance of the antikink in the PDE system when they reflect to infinity as seen in Figure 5.2 (a). Such 'noises' was also observe in the solutions of the ODE system for large initial velocities v_{in} when they reflect off each other (Figure 5.2 (b)).

The solutions of the ODE approximation with $q = 10$ match the solutions of the PDE system (only) qualitatively as shown in Figure 5.2. For the solutions for the PDE model we find an oscillatory bound state for initial velocities in $0.10 \leq v_{in} \leq 0.286$, and for initial velocities above this window we observe a single bounce. In the solutions for the ODE model for $q = 10$,

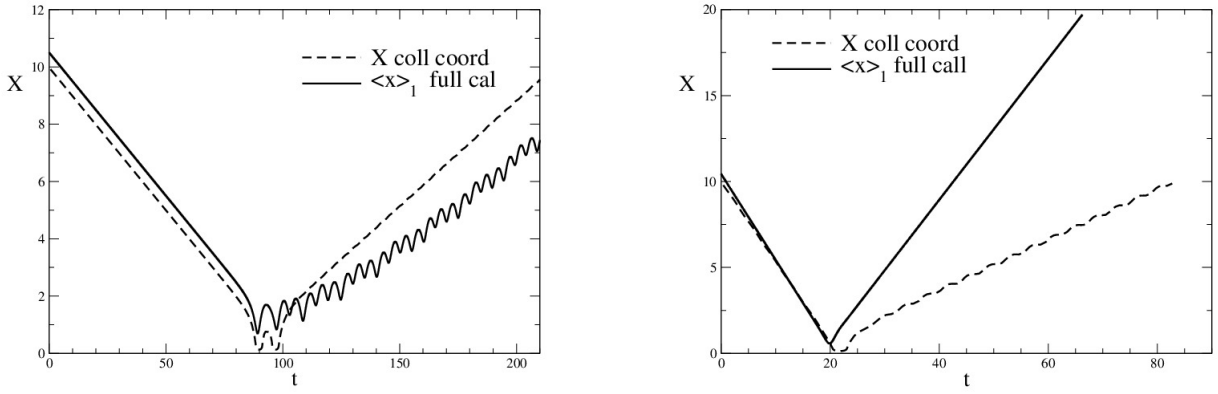

(a) (b)

Figure 5.2: Comparison of the time dependence of the collective coordinate $X(t)$ with that of the PDE $\langle x \rangle_1$: (a) $v_{in} = 0.10$ and (b) $v_{in} = 0.50$ for the case of $q = 10$.

we observe exactly two bounces for $v_{in} = 0.10, v_{in} = 0.20$ and $v_{in} = 0.260$. Furthermore, we observe exactly three bounces for $v_{in} = 0.40$ and $v_{in} = 0.415$, and four bounces for $v_{in} = 0.425$, and five bounces for $v_{in} = 0.340$ and $v_{in} = 0.412$. For large velocities $v_{in} \geq 0.443$ a single bounce was observed and this agrees well with the solutions of the PDE system, but for initial velocities in the regime $0.270 \leq v_{in} \leq 0.330$ we find a single oscillatory bound state in the ODE, even though $v_{cr} = 0.289$ from the PDE. Figure 5.3 (a) shows solutions of the ODE for various

initial velocities and (d) shows the two-dimensional phase space of the reduced system. In this framework, the ODE configuration predicts a critical velocity of $v_{cr,ODE} \approx 0.4424$ above which bound state solution cease to exist. This is large as compared with the critical velocity (0.289) from the PDE calculation [17].

The amplitudes of the internal shape modes $A(t)$ and $B(t)$ (Figure 5.3 (b), (c), respectively) of the ODE solutions increase monotonically and then oscillate a finite number of times before settling down to a steady oscillation as $X \to \infty$.[1] The larger amplitudes occur when the system is bound.

[1] We have used $X(0) \sim 10$ as an adequate representation of infinity in our numerical simulation.

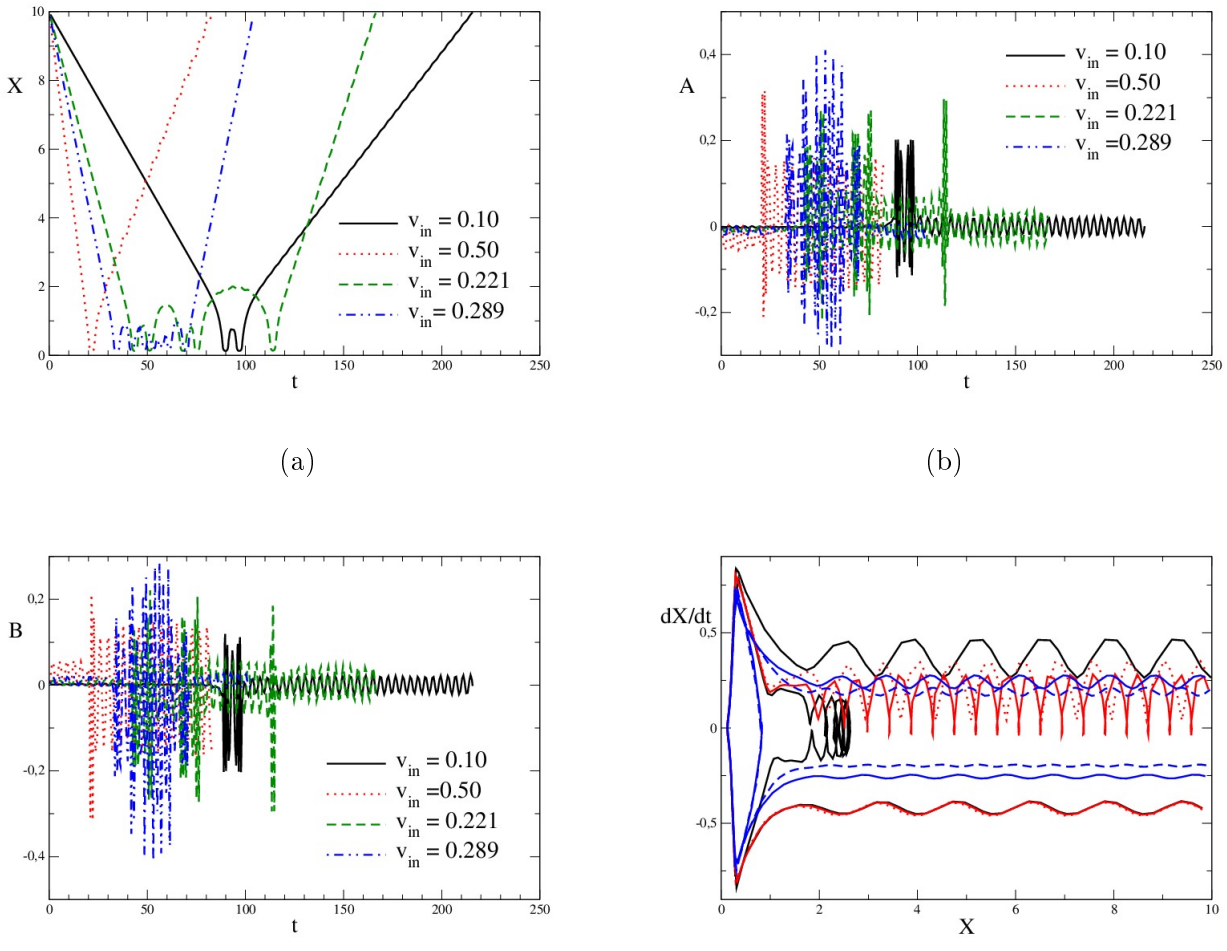

(a) (b)

(c) (d)

Figure 5.3: (a) Solutions of the ODE configuration. The amplitudes of the internal shape modes (b) $A(t)$ and (c) $B(t)$. (d) Trajectory in the $X - \dot{X}$ phase plane in the reduced system, the blue lines were calculated with initial velocity above the critical velocity and the red lines with initial velocity below the critical velocity.

time (t)	A(t)	B(t)
0.8257	-0.0246	0.0246
1.4041	-0.0509	0.0509
4.0092	-0.0061	0.0061
4.5105	-0.0276	0.0276
20.8929	0.2938	-0.2938
21.1413	0.2261	-0.2261
23.0743	-0.0177	0.0177
60.5406	-0.0798	0.0798
61.1232	-0.1450	0.1450
82.0640	0.1456	-0.1456

Table 5.1: The amplitudes of the internal shape modes for $v_{in} = 0.221$ with the initial condition $A(0) = B(0) = 0$.

time (t)	A(t)	B(t)
0.4399	-0.000569	0.0025
43.5197	-0.0713	0.0696
44.2574	-0.0202	0.0189
58.6185	0.0378	-0.0393
68.6915	-0.0436	0.0451
75.5592	-0.2062	0.2057
91.3419	0.0681	-0.0653
113.0720	0.02897	-0.02695
114.1620	-0.1746	0.1748
133.1020	0.02299	-0.02433

Table 5.2: The amplitudes of the internal shape modes for $v_{in} = 0.221$ with the initial condition $A(0) = B(0) = 0.001234$.

The magnitudes of these amplitudes are equal, as can be seen in the detailed data in Table 5.1. As in the ϕ^4 model $A(t) = -B(t)$ is an allowed solution to the ODE. Therefore the solution that starts with $A(0) = B(0)$ will run into the singularity unless $X \to 0$ is prevented, for example by setting $q \neq 0$. To see whether or not the ODE can nevertheless be a suitable approximation, we choose the initial condition $A(0) = B(0) = 0.001234$ and solve equation (5.1.7). For the PDE we impose the following initial field configuration:

$$\begin{aligned}\phi_{K\bar{K}} = &\frac{1}{\sqrt{1+\exp\left[2(\gamma x - X_0)\right]}} + \frac{1}{\sqrt{1+\exp\left[-2(\gamma x + X_0)\right]}} - 1 \\ &+ \sqrt{\frac{3}{2}} A_0 \frac{\sinh(\gamma x - X_0)}{\cosh^2(\gamma x - X_0)} + \sqrt{\frac{3}{2}} B_0 \frac{\sinh(\gamma x + X_0)}{\cosh^2(\gamma x + X_0)},\end{aligned} \tag{5.3.2}$$

and

$$\begin{aligned}\frac{\partial \phi_{K\bar{K}}}{\partial t} = &\dot{X}_0 \frac{\exp\left[2(\gamma x - X_0)\right]}{\left[1+\exp\left[2(\gamma x - X_0)\right]\right]^{\frac{3}{2}}} + \dot{X}_0 \frac{\exp\left[-2(\gamma x + X_0)\right]}{\left[1+\exp\left[-2(\gamma x + X_0)\right]\right]^{\frac{3}{2}}} \\ &- \sqrt{\frac{3}{2}} A_0 \dot{X}_0 \left\{ \frac{1-\sinh^2(\gamma x - X_0)}{\cosh^3(\gamma x - X_0)} \right\} \\ &+ \sqrt{\frac{3}{2}} B_0 \dot{X}_0 \left\{ \frac{1-\sinh^2(\gamma x + X_0)}{\cosh^3(\gamma x + X_0)} \right\},\end{aligned} \tag{5.3.3}$$

with

$$X_0 = X(0) = 10, \quad \dot{X}_0 = \dot{X}(0) = \frac{-v_{in}}{\sqrt{1-v_{in}^2}}, \quad A_0 = B_0 = A(0) = 0.001234. \tag{5.3.4}$$

The solutions that we obtain from this initial condition (shown in Figure 5.4) are almost the same as the case of using the initial condition of equation (5.1.8). The only difference is that,

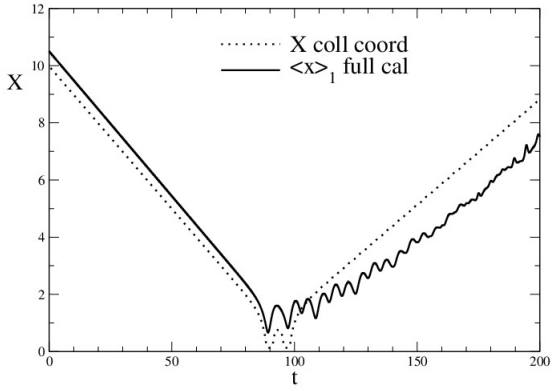

(a)

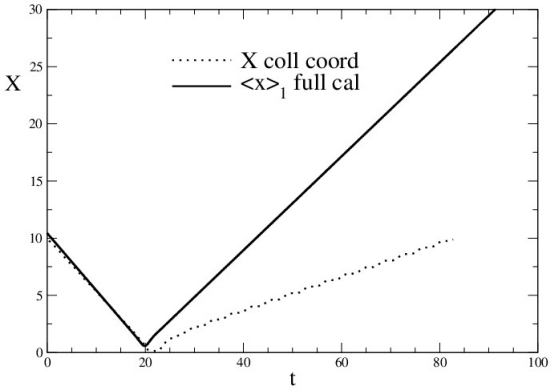

(b)

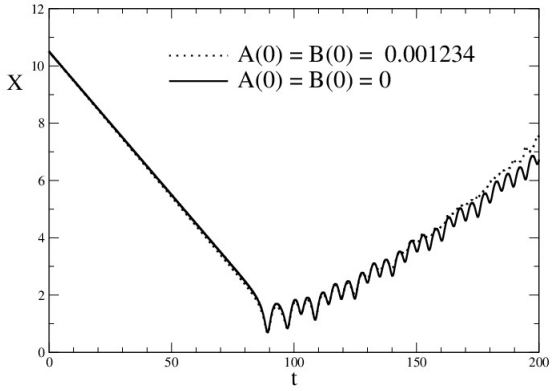

(c)

Figure 5.4: Time dependence of the collective coordinate $X(t)$ with that of the PDE $\langle x\rangle_1$ (a) for $v_{in} = 0.10$, (b) for $v_{in} = 0.50$. (c) Comparison of the PDE solution subject to the initial condition $A(0) = B(0) = 0$ to that of $A(0) = B(0) = 0.001234$ with initial velocity $v_{in} = 0.10$.

before and after collision the magnitude of the amplitudes are different but are approximately equal during collision as seen in Table 5.2. This suggest that the kink-antikink interaction dominantly excites the $A - B$ mode via the linear $a_5(X) = -b_5(X)$ coupling.

5.3.2 Numerical Results for the Antikink-Kink Configuration

We consider the antikink-kink interaction based on the configuration (5.2.1). Since

$$\phi_0(0, X) = \frac{-1}{\sqrt{1+e^{2X}}} - \frac{1}{\sqrt{1+e^{2X}}} \to \begin{cases} 0 & \text{for} \quad X \to \infty \\ -2 & \text{for} \quad X \to -\infty, \end{cases} \tag{5.3.5}$$

we see that $\phi_0(0, -\infty)$ is not a solution as the kink-antikink interpolates between neighbouring vacua of $\phi_{vac} \in \{-1, 0, 1\}$. As a mechanism to control the numerical solutions at $X \to 0$ and

to render $X \to -\infty$ a solution, we consider

$$\phi_0(x, X(t)) \to \phi_0(x, X(t)) + \frac{3}{\sqrt{1 + e^{2qX}}}, \tag{5.3.6}$$

where q is again an adjustable parameter. As before, this changes the function $\phi_0(x, X(t))$ and affects the coefficient function $a_1(X)$. It should be noted that large q values provide a better account of the actual dynamics of the PDE results in the ODE computation. For this reason

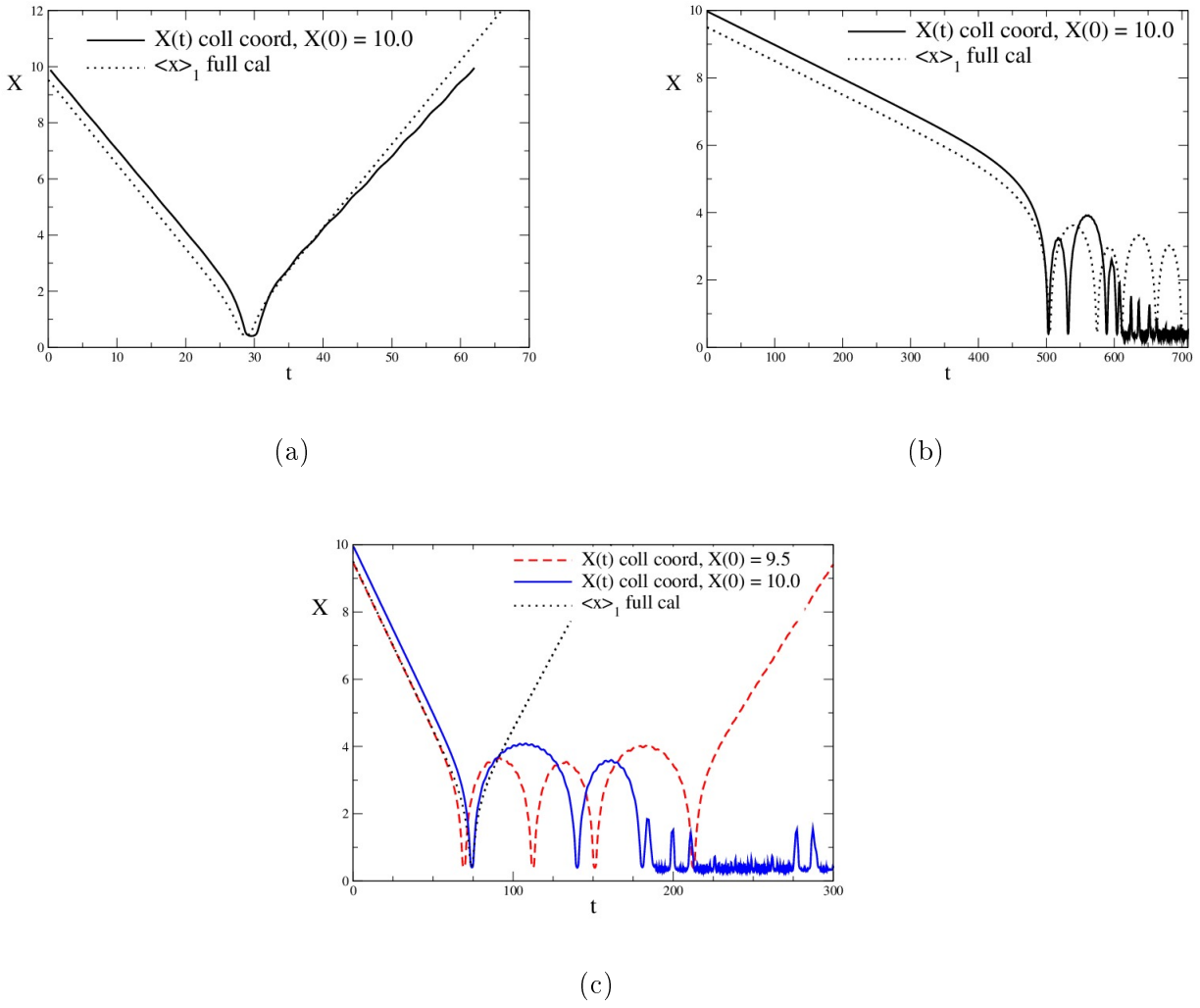

Figure 5.5: Comparison of the time dependence of the collective coordinate $X(t)$ from equation (5.3.6) with that of the PDE $\langle x \rangle_1$: (a) $v_{in} = 0.30$, (b) $v_{in} = 0.010$, (c) $v_{in} = 0.10$.

we use $q = 10$ in all calculations.

We find that the ODE solutions essentially resemble those of the PDE: they possess large bounce frequencies as they interact. We note that the ODE solutions are sensitive to the choice of the initial value $X(0)$, that is supposed to represent infinity. As is typical for non-linear systems, a chaotic behaviour emerges. As can be seen from Figure 5.5 (c), a moderate change in this initial value has a large effect: after several similar bounces, the $X(0) = 10$ configuration

remains confined, while for $X(0) = 9.5$, kink and antikink separate again. Whenever there are bounces, large amplitudes of the internal shape modes ($A(t)$ and $B(t)$) emerge. For $X(0) = 10.0$, we observe exactly two bounces for initial velocities $v_{in} = 0.103$ and $v_{in} = 0.108$. Furthermore, we observe that the solutions of the ODE model predict a critical velocity of $v_{cr,ODE} = 0.1119$, above which bounce type solutions cease to exist. For velocities $v_{cr,ODE} > v_{in} > 0.111$ a single

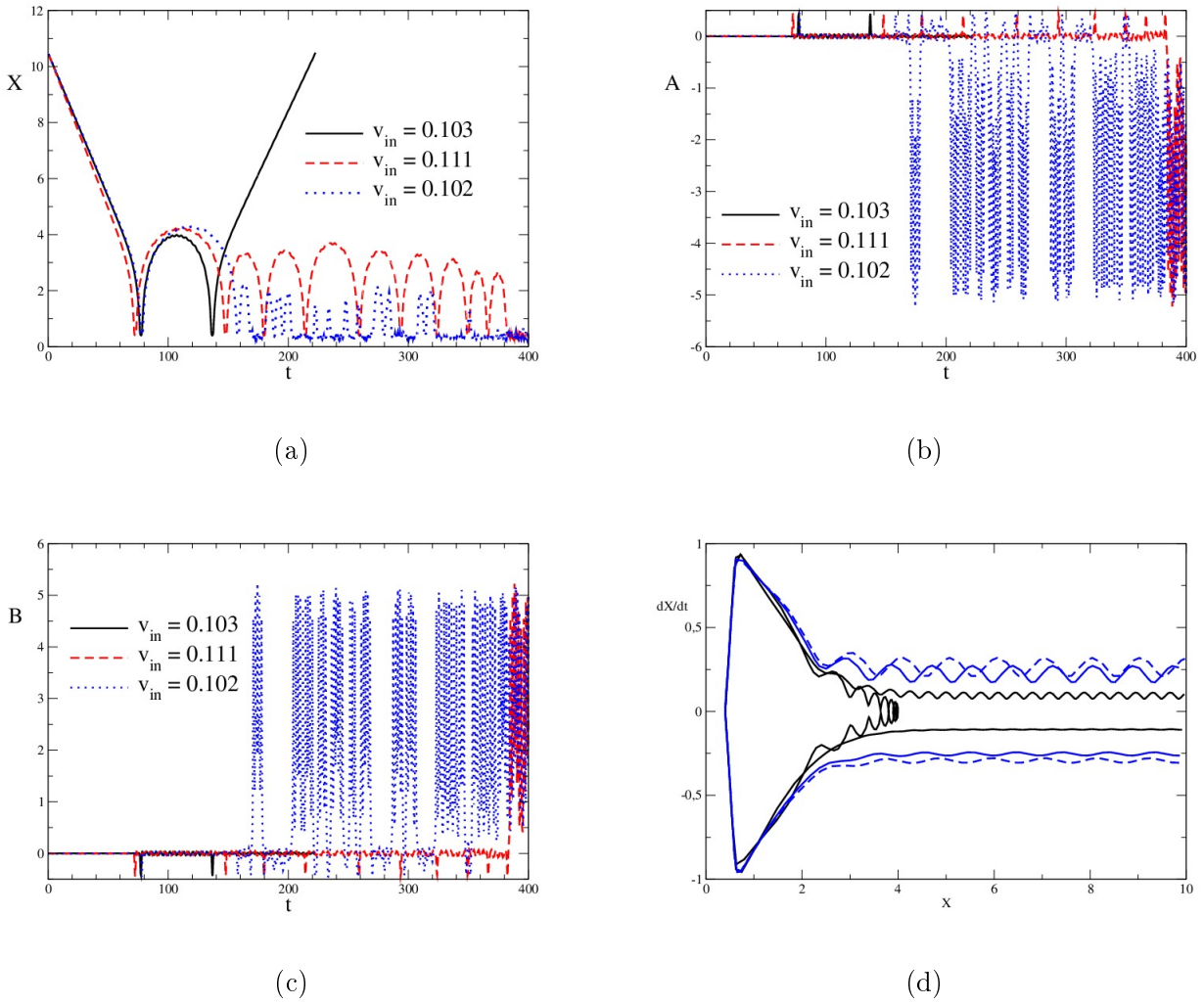

Figure 5.6: (a) Solutions of the ODE configuration. The amplitudes of the internal shape modes (b) $A(t)$ and (c) $B(t)$. (d) Trajectory in the $X - \dot{X}$ phase plane in the reduced system, the blue lines were calculated with initial velocity above the critical velocity and the red lines with initial velocity below the critical velocity.

bounce was observed. Figures 5.3 (a),(b) and (c) shows the ODE solutions and the amplitudes of the internal shape modes $A(t)$ and $B(t)$ for various initial velocities for $X(0) = 10.0$, with the larger amplitudes occurring when the system is bound. The comparison with the PDE solutions indicates a good agreement for large initial velocities.

As in our previous discussion, the amplitudes of the internal shape modes are equal in magnitude but of opposite sign as seen in Table 5.3 for $v_{in} = 0.010$. This may result in a singularity for

the antikink-kink configuration. Again we choose the initial condition $A(0) = B(0) = 0.001234$ and solve the ordinary differential equations for this configuration so that we can test the ODE approximation for $A(t) \neq -B(t)$, for configurations without this singularity. The comparison requires to solve the partial differential equation (4.2.1) subject to the following initial condition

$$\phi_{K\bar{K}} = \frac{1}{\sqrt{1+\exp\left[2(\gamma x + X_0)\right]}} + \frac{1}{\sqrt{1+\exp\left[-2(\gamma x - X_0)\right]}} - 1 + \sqrt{\frac{3}{2}} A_0 \frac{\sinh(\gamma x - X_0)}{\cosh^2(\gamma x - X_0)} + \sqrt{\frac{3}{2}} B_0 \frac{\sinh(\gamma x + X_0)}{\cosh^2(\gamma x + X_0)}, \tag{5.3.7}$$

and

$$\frac{\partial \phi_{K\bar{K}}}{\partial t} = -\dot{X}_0 \frac{\exp\left[2(\gamma x + X_0)\right]}{\left[1+\exp\left[2(\gamma x + X_0)\right]\right]^{\frac{3}{2}}} - \dot{X}_0 \frac{\exp\left[-2(\gamma x - X_0)\right]}{\left[1+\exp\left[-2(\gamma x - X_0)\right]\right]^{\frac{3}{2}}} - \sqrt{\frac{3}{2}} A_0 \dot{X}_0 \left\{ \frac{1-\sinh^2(\gamma x - X_0)}{\cosh^3(\gamma x - X_0)} \right\} + \sqrt{\frac{3}{2}} B_0 \dot{X}_0 \left\{ \frac{1-\sinh^2(\gamma x + X_0)}{\cosh^3(\gamma x + X_0)} \right\}, \tag{5.3.8}$$

and quantitatively compare it to the ODE solutions subject to the initial conditions

$$X_0 = X(0) = 10, \quad \dot{X}_0 = \dot{X}(0) = \frac{-v_{in}}{\sqrt{1-v_{in}^2}}, \quad A_0 = A(0) = B_0 = B(0) = 0.001234. \tag{5.3.9}$$

time (t)	A(t)	B(t)
0.8161	-0.971 $\times 10^{-05}$	0.971 $\times 10^{-05}$
1.4241	-0.214 $\times 10^{-04}$	0.214 $\times 10^{-04}$
78.5897	-0.253 $\times 10^{-04}$	0.253 $\times 10^{-04}$
99.3236	-0.194 $\times 10^{-05}$	0.194 $\times 10^{-05}$
198.9360	-0.260 $\times 10^{-05}$	0.260 $\times 10^{-05}$
505.0310	-0.00202	0.00202
518.5220	0.00470	-0.00470
590.1710	-0.0727	0.0727
618.7800	-5.0705	5.0705
708.7420	-1.0114	1.0114

Table 5.3: The amplitudes of the internal shape modes for $v_{in} = 0.010$ with the initial condition $A(0) = B(0) = 0$.

time (t)	A(t)	B(t)
0.670	0.571 $\times 10^{-03}$	0.584 $\times 10^{-03}$
1.0990	-0.175 $\times 10^{-03}$	-0.148 $\times 10^{-03}$
75.8233	-0.427 $\times 10^{-03}$	-0.460 $\times 10^{-03}$
502.0740	0.00893	-0.00644
504.080	-0.03365	0.03145
533.1720	-0.00595	0.00741
590.7830	0.2512	-0.2506
673.5120	-0.01477	0.01635
752.6520	0.01981	-0.01692
775.8080	-0.08198	0.08539

Table 5.4: The amplitudes of the internal shape modes for $v_{in} = 0.010$ with the initial condition $A(0) = B(0) = 0.001234$.

Surprisingly the solutions we obtain from this initial condition do not show chaotic behaviour as compared to the former (with $A(0) = B(0) = 0$) as seen in Figure 5.7 (a). Besides this,

the ODE solutions show much resemblance of the PDE solutions (Figure 5.7 (b)). It must be emphasized that in this regime the ODE solutions predict a critical velocity of $v_{cr,ODE} = 0.1119$ the same as that of the former. Interestingly, the amplitudes of the internal shape modes differ in magnitude, as can be seen from Table 5.4.

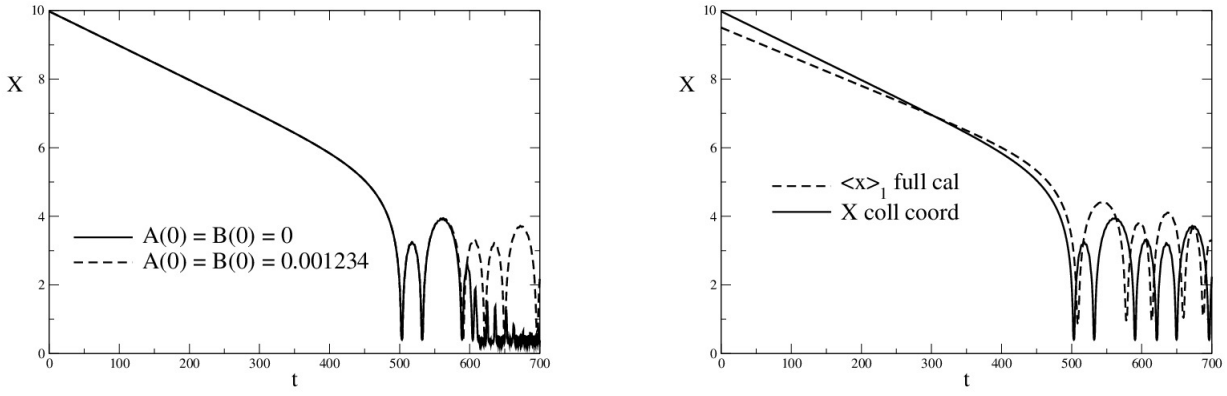

(a) (b)

Figure 5.7: (a) Comparison of the ODE solution for $A(0) = B(0) = 0$ to that for $A(0) = B(0) = 0.001234$ with initial velocity $v_{in} = 0.010$. (b) Comparison of the ODE (coll coord) solutions to that of the PDE (full cal) solutions for $v_{in} = 0.010$.

In summary it occurs that solutions to the ODE system whose initial conditions avoid the null-vector problem lead to better agreement with exact PDE solutions. Note that we have made only small modifications to the initial conditions $A(0) \sim 10^{-3}$ to circumvent the problem.

Chapter 6

Conclusion

We have investigated the kink-antikink interaction in the ϕ^4 and ϕ^6 models in one space dimension. We have considered both, the full field equations, i.e the partial differential equations (PDE), and an approximation based on the introduction of three collective coordinates. This approximation simplifies the field equations to a set of (here three) ordinary differential equations (ODE).

The solutions show a number of interesting features, for example bouncing or being fully trapped etc. Which of the features emerges depends on the initial relative velocity between the kink and the antikink.

The idea of using collective coordinates with three degrees of freedom was first introduced in reference [18] for the ϕ^4 model, but in that work a number of approximations were used: all non-harmonic terms $(a_{10}, \cdots, a_{13}, b_{10}, \cdots, b_{13})$ and $(d_6, \cdots, d_{19})$ in eqs ((3.1.3), (5.1.3)) were omitted. The terms $a_8, a_9, b_8, b_9, d_2, d_3, d_4$ were also ignored under the assumptions that they were small. With these approximations critical velocities that separate regimes of different features were produced in remarkable agreement to those obtained in the PDE system.

Subsequently the authors of references [19], [22] and [40] considered the amplitudes of the shape mode to be dependent on each other thereby reducing the system to two degrees of freedom. Although, they reproduced remarkable agreement to the full PDE system, their calculation from the collective coordinate system suffered from two setbacks. Firstly in reference [24] it was found that the direct interaction between the internal shape modes at $\pm X(t)$ leads to the so-called null-vector problem. Secondly a typographical error in reference [18] has propagated through the literature invalidating the calculations and conclusions.

The latter case has been dealt with in reference [23] that still made use of the approximations from reference [9] to avoid the null-vector problem. In our study we therefore considered independent amplitudes for the two peaks around the kink-antikink centers for the collective coordinate system without any further approximation. The ϕ^6 model does not contain an internal shape mode. Nevertheless the PDE produce resonance type solutions for the kink-

antikink interaction. We have therefore investigated the hypothesis according to which the collective coordinate ansätze allow a shape type mode to be excited. In this scenario we have then compared the numerical solutions of the resulting ODE with those of the full PDE.

From the approximation with only two collective coordinates the null-vector problem is obvious from the ansätze. In the case with three such coordinates the problem is generally not present. However, it emerges for configurations in which the amplitudes of the shape mode are zero in the infinite past. Unfortunately this applies to the kink-antikink interaction in both the ϕ^4 and ϕ^6 models. We circumvented this obstacle by adopting modified ansätze for the kink-antikink configurations in the collective coordinate approach. This adds short range repulsions to the kink-antikink potential and yields solutions with one or more bounces or traps.

We also found from our results that the results from the ODE system agree well with those from the PDE system to some extent for large initial velocities, but disagree for specific low initial velocities. Apart from these (dis)agreements the ODE system predicts larger critical velocities than the full PDE system. We may speculate that this is caused by the additional (fast moving) fluctuations that are included only in the PDE scenario. They can dispense energy quickly to the kink and antikink which then have sufficient energy to separate already at a lower relative velocity compared to the ODE case in which these fluctuations are omitted.

Furthermore, we found that using the initial condition $A(0) = B(0) \neq 0$ in solving the Euler-Lagrange equations for $X(t)$, $A(t)$ and $B(t)$ results in $A(t) \neq B(t)$ at all times so that the singularity emerging from the null-vector problem is avoided. This suggests that the three component approach can indeed be a remedy of this problem. We have also seen that a small modification of the kink-antikink configuration avoids this problem.

Our results support those of reference [23]. The collective coordinate approach cannot be used to establish that the internal shape mode should be responsible for the existence of multiple bounces in the kink-antikink collision. We furthermore conclude that the good argument between the ODE and PDE solutions in the ϕ^4 model observed in previous studies is due to the many approximations. Our exhaustive study that avoids such approximations finds significant deviation between the two approaches.

Appendices

Appendix A

The Kink-Antikink Collective Coordinates

In sections 3.1, 5.1 and 5.2 we have introduced an interaction ansätze for the kink-antikink with a separation $2X(t)$ together with two independent amplitudes $A(t)$ and $B(t)$. The ansatz functions (equation (3.1.1) as well as equation (5.1.1)) reduce the PDE to simple ODEs with three degrees of freedom $(X(t), A(t), B(t))$. Here, we list the integral representations for coefficient function within the ODE.

A.1 Collective coordinates of the Kink-Antikink Configuration in the ϕ^4 Theory

We substituted the ansatz function (equation (3.1.1)) into the Lagrangian density (2.1.1) and by integrating over all space, from $-\infty$ to ∞, we have equation (3.1.3). The coefficient functions are given as $\left(\text{we define} \quad \chi_1^{0\prime}(\xi) = \dfrac{\mathrm{d}\chi_1^0(\xi)}{\mathrm{d}x} \quad \text{and} \quad \phi_K'(\xi) = \dfrac{\mathrm{d}\phi_K(\xi)}{\mathrm{d}x}\right)$:

$$
\begin{aligned}
a_1 &= \frac{1}{2}\int_{-\infty}^{\infty} \left[\phi_K'(\xi_+) + \phi_K'(\xi_-)\right]^2 \,\mathrm{d}x \\
a_2 &= \frac{1}{2}\frac{1}{1-v^2}\int_{-\infty}^{\infty} \left[\phi_K'(\xi_+) - \phi_K'(\xi_-)\right]^2 \,\mathrm{d}x + \frac{1}{2}\int_{-\infty}^{\infty} \left[\phi_0^2(x, X(t)) - 1\right]^2 \,\mathrm{d}x \\
a_3 &= \frac{3}{4}\int_{-\infty}^{\infty} (\chi_1^0(\xi_-))^2 \,\mathrm{d}x \\
a_4 &= \frac{3}{4}\frac{1}{1-v^2}\int_{-\infty}^{\infty} (\chi_1^{0\prime}(\xi_-))^2 \,\mathrm{d}x + \frac{3}{4}\int_{-\infty}^{\infty} (\chi_1^0(\xi_-))^2 \left[6\phi_0^2(x, X(t)) - 2\right] \,\mathrm{d}x \\
a_5 &= 2\sqrt{\frac{3}{2}}\frac{1}{1-v^2}\int_{-\infty}^{\infty} \left[\phi_K(\xi_+)\left\{\phi_K^2(\xi_+) - 1\right\} - \phi_K(\xi_-)\left\{\phi_K^2(\xi_-) - 1\right\}\right] \chi_1^0(\xi_-) \,\mathrm{d}x \\
&\quad - 2\sqrt{\frac{3}{2}}\int_{-\infty}^{\infty} \phi_0(x, X(t)) \left[\phi_0^2(x, X(t)) - 1\right] \chi_1^0(\xi_-) \,\mathrm{d}x
\end{aligned}
$$

$$a_6 = 2\sqrt{\frac{3}{2}}\int_{-\infty}^{\infty}\left[\phi_K(\xi_+)\left\{\phi_k^2(\xi_+)-1\right\}+\phi_K(\xi_-)\left\{\phi_k^2(\xi_-)-1\right\}\right]\chi_1^0(\xi_-)\,\mathrm{d}x$$

$$a_7 = \sqrt{\frac{3}{2}}\int_{-\infty}^{\infty}\left[\phi_K'(\xi_+)+\phi_K'(\xi_-)\right]\chi_1^0(\xi_-)\,\mathrm{d}x$$

$$a_8 = \frac{3}{4}\int_{-\infty}^{\infty}(\chi_1^{0'}(\xi_-))^2\,\mathrm{d}x$$

$$a_9 = -\frac{3}{2}\int_{-\infty}^{\infty}\chi_1^{0'}(\xi_-)\chi_1^0(\xi_-)\,\mathrm{d}x$$

$$a_{10} = 3\sqrt{\frac{3}{2}}\int_{-\infty}^{\infty}\phi_0(x,X(t))(\chi_1^0(\xi_-))^3\,\mathrm{d}x$$

$$a_{11} = \frac{9}{8}\int_{-\infty}^{\infty}(\chi_1^0(\xi_-))^4\,\mathrm{d}x$$

$$b_3 = a_3 = \frac{3}{4}\int_{-\infty}^{\infty}(\chi_1^0(\xi_+))^2\,\mathrm{d}x$$

$$b_4 = a_4 = \frac{3}{4}\frac{1}{1-v^2}\int_{-\infty}^{\infty}(\chi_1^{0'}(\xi_+))^2\,\mathrm{d}x+\frac{3}{4}\int_{-\infty}^{\infty}(\chi_1^0(\xi_+))^2\left[6\phi_0^2(x,X(t))-2\right]\,\mathrm{d}x$$

$$b_5 = -a_5 = 2\sqrt{\frac{3}{2}}\frac{1}{1-v^2}\int_{-\infty}^{\infty}\left[\phi_K(\xi_+)\left\{\phi_k^2(\xi_+)-1\right\}-\phi_K(\xi_-)\left\{\phi_k^2(\xi_-)-1\right\}\right]\chi_1^0(\xi_+)\,\mathrm{d}x$$
$$-2\sqrt{\frac{3}{2}}\int_{-\infty}^{\infty}\phi_0(x,X(t))\left[\phi_0^2(x,X(t))-1\right]\chi_1^0(\xi_+)\,\mathrm{d}x$$

$$b_6 = -a_6 = -2\sqrt{\frac{3}{2}}\int_{-\infty}^{\infty}\left[\phi_K(\xi_+)\left\{\phi_k^2(\xi_+)-1\right\}+\phi_K(\xi_-)\left\{\phi_k^2(\xi_-)-1\right\}\right]\chi_1^0(\xi_+)\,\mathrm{d}x$$

$$b_7 = -a_7 = \sqrt{\frac{3}{2}}\int_{-\infty}^{\infty}\left[\phi_K'(\xi_+)+\phi_K'(\xi_-)\right]\chi_1^0(\xi_+)\,\mathrm{d}x$$

$$b_8 = a_8 = \frac{3}{4}\int_{-\infty}^{\infty}(\chi_1^{0'}(\xi_+))^2\,\mathrm{d}x$$

$$b_9 = a_9 = \frac{3}{2}\int_{-\infty}^{\infty}\chi_1^{0'}(\xi_+)\chi_1^0(\xi_+)\,\mathrm{d}x$$

$$b_{10} = 3\sqrt{\frac{3}{2}}\int_{-\infty}^{\infty}\phi_0(x,X(t))(\chi_1^0(\xi_+))^3\,\mathrm{d}x$$

$$b_{11} = \frac{9}{8}\int_{-\infty}^{\infty}(\chi_1^0(\xi_+))^4\,\mathrm{d}x$$

$$d_1 = \frac{3}{2}\int_{-\infty}^{\infty}\chi_1^0(\xi_+)\chi_1^0(\xi_-)\,\mathrm{d}x$$

$$d_2 = -\frac{3}{2}\int_{-\infty}^{\infty}\chi_1^{0'}(\xi_+)\chi_1^{0'}(\xi_-)\,\mathrm{d}x$$

$$d_3 = \frac{3}{2}\int_{-\infty}^{\infty}\chi_1^{0'}(\xi_+)\chi_1^0(\xi_-)\,\mathrm{d}x$$

$$d_4 = -d_3 = -\frac{3}{2}\int_{-\infty}^{\infty} \chi_1^{0\prime}(\xi_-)\chi_1^0(\xi_+)\,\mathrm{d}x$$

$$d_5 = \frac{3}{2}\frac{1}{1-v^2}\int_{-\infty}^{\infty} \chi_1^{0\prime}(\xi_+)\chi_1^{0\prime}(\xi_-)\,\mathrm{d}x + \frac{3}{2}\int_{-\infty}^{\infty}\left[6\phi_0^2(x,X(t))-2\right]\chi_1^0(\xi_+)\chi_1^0(\xi_-)\,\mathrm{d}x$$

$$d_6 = \frac{27}{4}\int_{-\infty}^{\infty}(\chi_1^0(\xi_+))^2(\chi_1^0(\xi_-))^2\,\mathrm{d}x$$

$$d_7 = 9\sqrt{\frac{3}{2}}\int_{-\infty}^{\infty}(\chi_1^0(\xi_-))^2\chi_1^0(\xi_+)\,\mathrm{d}x$$

$$d_8 = 9\sqrt{\frac{3}{2}}\int_{-\infty}^{\infty}\chi_1^0(\xi_-)(\chi_1^0(\xi_+))^2\,\mathrm{d}x$$

$$d_9 = \frac{9}{2}\int_{-\infty}^{\infty}(\chi_1^0(\xi_-))^3\chi_1^0(\xi_+)\,\mathrm{d}x$$

$$d_{10} = \frac{9}{2}\int_{-\infty}^{\infty}\chi_1^0(\xi_-)(\chi_1^0(\xi_+))^3\,\mathrm{d}x$$

A.2 Collective Coordinates of the Kink - Antikink configuration in the ϕ^6 Theory

As before we substituted the ansatz function equation (5.1.1) into the Lagrangian density (4.1.3) and by integrating over all space, from $-\infty$ to ∞, we have equation (5.1.3). The coefficient functions are given as $\left(\text{we define} \quad \chi_1^{0\prime}(\xi) = \frac{\mathrm{d}\chi_1^0(\xi)}{\mathrm{d}x} \quad \text{and} \quad \phi_K'(\xi) = \frac{\mathrm{d}\phi_K(\xi)}{\mathrm{d}x}\right)$:

$$
\begin{aligned}
a_1 &= \frac{1}{2}\int_{-\infty}^{\infty} \left[\phi_K'(-\xi_+) + \phi_K'(\xi_-)\right]^2 \,\mathrm{d}x \\
a_2 &= \frac{1}{2}\frac{1}{1-v^2}\int_{-\infty}^{\infty} \left[\phi_K'(-\xi_+) - \phi_K'(\xi_-)\right]^2 \,\mathrm{d}x + \frac{1}{2}\int_{-\infty}^{\infty} \phi_0(x,X(t))^2\left[\phi_0^2(x,X(t)) - 1\right]^2 \,\mathrm{d}x \\
a_3 &= \frac{3}{4}\int_{-\infty}^{\infty} (\chi_1^0(\xi_-))^2 \,\mathrm{d}x \\
a_4 &= \frac{3}{4}\frac{1}{1-v^2}\int_{-\infty}^{\infty} (\chi_1^{0\prime}(\xi_-))^2 \,\mathrm{d}x + \frac{3}{4}\int_{-\infty}^{\infty} (\chi_1^0(\xi_-))^2\left[15\phi_0^4(x,X(t)) - 12\phi_0^2(x,X(t)) + 1\right] \,\mathrm{d}x \\
a_5 &= \sqrt{\frac{3}{2}}\frac{1}{1-v^2}\int_{-\infty}^{\infty} \left\{3\phi_K^5(\xi_-) - 4\phi_k^3(\xi_-) + \phi_K(\xi_-)\right\}\chi_1^0(\xi_-)\,\mathrm{d}x \\
&\quad + \sqrt{\frac{3}{2}}\frac{1}{1-v^2}\int_{-\infty}^{\infty} \left\{3\phi_K^5(-\xi_+) - 4\phi_k^3(-\xi_+) + \phi_K(-\xi_+)\right\}\chi_1^0(\xi_-)\,\mathrm{d}x \\
&\quad - \sqrt{\frac{3}{2}}\int_{-\infty}^{\infty} \left[3\phi_0^5(x,X(t)) - 4\phi_0^3(x,X(t)) + \phi_0(x,X(t))\right]\chi_1^0(\xi_-)\,\mathrm{d}x \\
a_6 &= \sqrt{\frac{3}{2}}\int_{-\infty}^{\infty} \left\{3\phi_K^5(-\xi_+) - 4\phi_k^3(-\xi_+) + \phi_K(-\xi_+)\right\}\chi_1^0(\xi_-)\,\mathrm{d}x \\
&\quad - \sqrt{\frac{3}{2}}\int_{-\infty}^{\infty} \left\{3\phi_K^5(\xi_-) - 4\phi_k^3(\xi_-) + \phi_K(\xi_-)\right\}\chi_1^0(\xi_-)\,\mathrm{d}x \\
a_7 &= -\sqrt{\frac{3}{2}}\int_{-\infty}^{\infty} \left[\phi_K'(-\xi_+) + \phi_K'(\xi_-)\right]\chi_1^0(\xi_-)\,\mathrm{d}x \\
a_8 &= \frac{3}{4}\int_{-\infty}^{\infty} (\chi_1^{0\prime}(\xi_-))^2 \,\mathrm{d}x \\
a_9 &= -\frac{3}{2}\int_{-\infty}^{\infty} \chi_1^{0\prime}(\xi_-)\chi_1^0(\xi_-)\,\mathrm{d}x \\
a_{10} &= \sqrt{\frac{3}{2}}\int_{-\infty}^{\infty} \left\{15\phi_0^3(x,X(t)) - 6\phi_0(x,X(t))\right\}(\chi_1^0(\xi_-))^3 \,\mathrm{d}x \\
a_{11} &= \frac{9}{8}\int_{-\infty}^{\infty} \left\{15\phi_0^2(x,X(t)) - 2\right\}(\chi_1^0(\xi_-))^4 \,\mathrm{d}x, \\
a_{12} &= \frac{27}{4}\sqrt{\frac{3}{2}}\int_{-\infty}^{\infty} (\chi_1^0(\xi_-))^5\phi_0(x,X(t))\,\mathrm{d}x \\
a_{13} &= \frac{27}{16}\int_{-\infty}^{\infty} (\chi_1^0(\xi_-))^6 \,\mathrm{d}x
\end{aligned}
$$

$$b_3 = a_3 = \frac{3}{4}\int_{-\infty}^{\infty} (\chi_1^0(\xi_+))^2 \,\mathrm{d}x$$

$$b_4 = a_4 = \frac{3}{4}\frac{1}{1-v^2}\int_{-\infty}^{\infty} (\chi_1^{0'}(\xi_+))^2 \,\mathrm{d}x + \frac{3}{4}\int_{-\infty}^{\infty} (\chi_1^0(\xi_+))^2 \left[15\phi_0^4(x,X(t)) - 12\phi_0^2(x,X(t)) + 1\right] \,\mathrm{d}x$$

$$\begin{aligned} b_5 = -a_5 &= \sqrt{\frac{3}{2}}\frac{1}{1-v^2}\int_{-\infty}^{\infty} \left\{3\phi_K^5(-\xi_+) - 4\phi_k^3(-\xi_+) + \phi_K(-\xi_+)\right\} \chi_1^0(\xi_+) \,\mathrm{d}x \\ &+ \sqrt{\frac{3}{2}}\frac{1}{1-v^2}\int_{-\infty}^{\infty} \left\{3\phi_K^5(\xi_-) - 4\phi_k^3(\xi_-) + \phi_K(\xi_-)\right\} \chi_1^0(\xi_+) \,\mathrm{d}x \\ &- \sqrt{\frac{3}{2}}\int_{-\infty}^{\infty} \left[3\phi_0^5(x,X(t)) - 4\phi_0^3(x,X(t)) + \phi_0(x,X(t))\right] \chi_1^0(\xi_+) \,\mathrm{d}x \end{aligned}$$

$$\begin{aligned} b_6 = -a_6 &= -\sqrt{\frac{3}{2}}\int_{-\infty}^{\infty} \left\{3\phi_K^5(-\xi_+) - 4\phi_k^3(-\xi_+) + \phi_K(-\xi_+)\right\} \chi_1^0(\xi_+) \,\mathrm{d}x \\ &+ \sqrt{\frac{3}{2}}\int_{-\infty}^{\infty} \left\{3\phi_K^5(\xi_-) - 4\phi_k^3(\xi_-) + \phi_K(\xi_-)\right\} \chi_1^0(\xi_+) \,\mathrm{d}x \end{aligned}$$

$$b_7 = -a_7 = -\sqrt{\frac{3}{2}}\int_{-\infty}^{\infty} \left[\phi_K'(-\xi_+) + \phi_K'(\xi_-)\right] \chi_1^0(\xi_+) \,\mathrm{d}x$$

$$b_8 = a_8 = \frac{3}{4}\int_{-\infty}^{\infty} (\chi_1^{0'}(\xi_+))^2 \,\mathrm{d}x$$

$$b_9 = a_9 = \frac{3}{2}\int_{-\infty}^{\infty} \chi_1^{0'}(\xi_+)\chi_1^0(\xi_+) \,\mathrm{d}x$$

$$b_{10} = \sqrt{\frac{3}{2}}\int_{-\infty}^{\infty} \left\{15\phi_0^3(x,X(t)) - 6\phi_0(x,X(t))\right\} (\chi_1^0(\xi_+))^3 \,\mathrm{d}x$$

$$b_{11} = \frac{9}{8}\int_{-\infty}^{\infty} \left\{15\phi_0^2(x,X(t)) - 2\right\} (\chi_1^0(\xi_+))^4 \,\mathrm{d}x,$$

$$b_{12} = \frac{27}{4}\sqrt{\frac{3}{2}}\int_{-\infty}^{\infty} (\chi_1^0(\xi_+))^5 \phi_0(x,X(t)) \,\mathrm{d}x$$

$$b_{13} = \frac{27}{16}\int_{-\infty}^{\infty} (\chi_1^0(\xi_+))^6 \,\mathrm{d}x$$

$$d_1 = \frac{3}{2}\int_{-\infty}^{\infty} \chi_1^0(\xi_+)\chi_1^0(\xi_-) \,\mathrm{d}x$$

$$d_2 = -\frac{3}{2}\int_{-\infty}^{\infty} \chi_1^{0'}(\xi_+)\chi_1^{0'}(\xi_-) \,\mathrm{d}x$$

$$d_3 = \frac{3}{2}\int_{-\infty}^{\infty} \chi_1^{0'}(\xi_+)\chi_1^0(\xi_-) \,\mathrm{d}x$$

$$d_4 = -d_3 = -\frac{3}{2}\int_{-\infty}^{\infty} \chi_1^{0'}(\xi_-)\chi_1^0(\xi_+) \,\mathrm{d}x$$

$$\begin{aligned} d_5 &= \frac{3}{2}\frac{1}{1-v^2}\int_{-\infty}^{\infty} \chi_1^{0'}(\xi_+)\chi_1^{0'}(\xi_-) \,\mathrm{d}x \\ &+ \frac{3}{2}\int_{-\infty}^{\infty} \left[15\phi_0^4(x,X(t)) - 12\phi_0^2(x,X(t)) + 1\right] \chi_1^0(\xi_+)\chi_1^0(\xi_-) \,\mathrm{d}x \end{aligned}$$

$$d_6 = \frac{27}{4}\int_{-\infty}^{\infty}(\chi_1^0(\xi_+))^2(\chi_1^0(\xi_-))^2\left[15\phi_0^2(x,X(t))-2\right]\,\mathrm{d}x$$

$$d_7 = 3\sqrt{\frac{3}{2}}\int_{-\infty}^{\infty}(\chi_1^0(\xi_-))^2\chi_1^0(\xi_+)\left[15\phi_0^3(x,X(t))-6\phi_0(x,X(t))\right]\,\mathrm{d}x$$

$$d_8 = 3\sqrt{\frac{3}{2}}\int_{-\infty}^{\infty}\chi_1^0(\xi_-)(\chi_1^0(\xi_+))^2\left[15\phi_0^3(x,X(t))-6\phi_0(x,X(t))\right]\,\mathrm{d}x$$

$$d_9 = \frac{9}{2}\int_{-\infty}^{\infty}(\chi_1^0(\xi_-))^3\chi_1^0(\xi_+)\left[15\phi_0^2(x,X(t))-2\right]\,\mathrm{d}x$$

$$d_{10} = \frac{9}{2}\int_{-\infty}^{\infty}\chi_1^0(\xi_-)(\chi_1^0(\xi_+))^3\left[15\phi_0^2(x,X(t))-2\right]\,\mathrm{d}x$$

$$d_{11} = \frac{135}{4}\sqrt{\frac{3}{2}}\int_{-\infty}^{\infty}\phi_0(x,X(t))(\chi_1^0(\xi_-))^4\chi_1^0(\xi_+)\,\mathrm{d}x$$

$$d_{12} = \frac{135}{2}\sqrt{\frac{3}{2}}\int_{-\infty}^{\infty}\phi_0(x,X(t))(\chi_1^0(\xi_-))^3(\chi_1^0(\xi_+))^2\,\mathrm{d}x$$

$$d_{13} = \frac{135}{2}\sqrt{\frac{3}{2}}\int_{-\infty}^{\infty}\phi_0(x,X(t))(\chi_1^0(\xi_-))^2(\chi_1^0(\xi_+))^3\,\mathrm{d}x$$

$$d_{14} = \frac{135}{4}\sqrt{\frac{3}{2}}\int_{-\infty}^{\infty}\phi_0(x,X(t))\chi_1^0(\xi_-)(\chi_1^0(\xi_+))^4\,\mathrm{d}x$$

$$d_{15} = \frac{81}{8}\int_{-\infty}^{\infty}(\chi_1^0(\xi_-))^5\chi_1^0(\xi_+)\,\mathrm{d}x$$

$$d_{16} = \frac{405}{16}\int_{-\infty}^{\infty}(\chi_1^0(\xi_-))^4(\chi_1^0(\xi_+))^2\,\mathrm{d}x$$

$$d_{17} = \frac{135}{4}\int_{-\infty}^{\infty}(\chi_1^0(\xi_-))^3(\chi_1^0(\xi_+))^3\,\mathrm{d}x$$

$$d_{18} = \frac{405}{16}\int_{-\infty}^{\infty}(\chi_1^0(\xi_-))^2(\chi_1^0(\xi_+))^4\,\mathrm{d}x$$

$$d_{19} = \frac{81}{8}\int_{-\infty}^{\infty}\chi_1^0(\xi_-)(\chi_1^0(\xi_+))^5\,\mathrm{d}x$$

A.3 Collective Coordinates of the Antikink - kink configuration in the ϕ^6 Theory

The coefficient functions obtained after substituted the configuration function (5.2.1) into the Lagrangian density (4.1.3) and integrating over all space, from $-\infty$ to ∞, are given as follows $\left(\text{we define} \quad \chi_1^{0'}(\xi) = \frac{\mathrm{d}\chi_1^0(\xi)}{\mathrm{d}x} \quad \text{and} \quad \phi_K'(\xi) = \frac{\mathrm{d}\phi_K(\xi)}{\mathrm{d}x}\right)$:

$$
\begin{aligned}
a_1 &= \frac{1}{2}\int_{-\infty}^{\infty} \left[\phi_K'(\xi_+) + \phi_K'(-\xi_-)\right]^2 \,\mathrm{d}x \\
a_2 &= \frac{1}{2}\frac{1}{1-v^2}\int_{-\infty}^{\infty} \left[\phi_K'(-\xi_-) - \phi_K'(\xi_+)\right]^2 \,\mathrm{d}x + \frac{1}{2}\int_{-\infty}^{\infty} \phi_0(x,X(t))^2\left[\phi_0^2(x,X(t)) - 1\right]^2 \,\mathrm{d}x \\
a_3 &= \frac{3}{4}\int_{-\infty}^{\infty} (\chi_1^0(\xi_-))^2 \,\mathrm{d}x \\
a_4 &= \frac{3}{4}\frac{1}{1-v^2}\int_{-\infty}^{\infty} (\chi_1^{0'}(\xi_-))^2 \,\mathrm{d}x + \frac{3}{4}\int_{-\infty}^{\infty} (\chi_1^0(\xi_-))^2\left[15\phi_0^4(x,X(t)) - 12\phi_0^2(x,X(t)) + 1\right] \,\mathrm{d}x \\
a_5 &= -\sqrt{\frac{3}{2}}\frac{1}{1-v^2}\int_{-\infty}^{\infty} \left\{3\phi_K^5(-\xi_-) - 4\phi_k^3(-\xi_-) + \phi_K(-\xi_-)\right\}\chi_1^0(\xi_-)\,\mathrm{d}x \\
&\quad - \sqrt{\frac{3}{2}}\frac{1}{1-v^2}\int_{-\infty}^{\infty} \left\{3\phi_K^5(\xi_+) - 4\phi_k^3(\xi_+) + \phi_K(\xi_+)\right\}\chi_1^0(\xi_-)\,\mathrm{d}x \\
&\quad - \sqrt{\frac{3}{2}}\int_{-\infty}^{\infty} \left[3\phi_0^5(x,X(t)) - 4\phi_0^3(x,X(t)) + \phi_0(x,X(t))\right]\chi_1^0(\xi_-)\,\mathrm{d}x \\
a_6 &= -\sqrt{\frac{3}{2}}\int_{-\infty}^{\infty} \left\{3\phi_K^5(\xi_+) - 4\phi_k^3(\xi_+) + \phi_K(\xi_+)\right\}\chi_1^0(\xi_-)\,\mathrm{d}x \\
&\quad + \sqrt{\frac{3}{2}}\int_{-\infty}^{\infty} \left\{3\phi_K^5(-\xi_-) - 4\phi_k^3(-\xi_-) + \phi_K(-\xi_-)\right\}\chi_1^0(\xi_-)\,\mathrm{d}x \\
a_7 &= -\sqrt{\frac{3}{2}}\int_{-\infty}^{\infty} \left[\phi_K'(\xi_+) + \phi_K'(-\xi_-)\right]\chi_1^0(\xi_-)\,\mathrm{d}x \\
a_8 &= \frac{3}{4}\int_{-\infty}^{\infty} (\chi_1^{0'}(\xi_-))^2 \,\mathrm{d}x \\
a_9 &= -\frac{3}{2}\int_{-\infty}^{\infty} \chi_1^{0'}(\xi_-)\chi_1^0(\xi_-)\,\mathrm{d}x \\
a_{10} &= \sqrt{\frac{3}{2}}\int_{-\infty}^{\infty} \left\{15\phi_0^3(x,X(t)) - 6\phi_0(x,X(t))\right\}(\chi_1^0(\xi_-))^3 \,\mathrm{d}x \\
a_{11} &= \frac{9}{8}\int_{-\infty}^{\infty} \left\{15\phi_0^3(x,X(t)) - 2\right\}(\chi_1^0(\xi_-))^4 \,\mathrm{d}x, \\
a_{12} &= \frac{27}{4}\sqrt{\frac{3}{2}}\int_{-\infty}^{\infty} (\chi_1^0(\xi_-))^5\phi_0(x,X(t))\,\mathrm{d}x \\
a_{13} &= \frac{27}{16}\int_{-\infty}^{\infty} (\chi_1^0(\xi_-))^6 \,\mathrm{d}x,
\end{aligned}
$$

$$b_3 = a_3 = \frac{3}{4}\int_{-\infty}^{\infty} (\chi_1^0(\xi_+))^2 \,\mathrm{d}x$$

$$b_4 = a_4 = \frac{3}{4}\frac{1}{1-v^2}\int_{-\infty}^{\infty} (\chi_1^{0'}(\xi_+))^2 \,\mathrm{d}x + \frac{3}{4}\int_{-\infty}^{\infty} (\chi_1^0(\xi_+))^2 \left[15\phi_0^4(x,X(t)) - 12\phi_0^2(x,X(t)) + 1\right] \,\mathrm{d}x$$

$$b_5 = -a_5 = -\sqrt{\frac{3}{2}}\frac{1}{1-v^2}\int_{-\infty}^{\infty} \left\{3\phi_K^5(-\xi_-) - 4\phi_k^3(-\xi_-) + \phi_K(-\xi_-)\right\} \chi_1^0(\xi_+) \,\mathrm{d}x$$
$$- \sqrt{\frac{3}{2}}\frac{1}{1-v^2}\int_{-\infty}^{\infty} \left\{3\phi_K^5(\xi_+) - 4\phi_k^3(\xi_+) + \phi_K(\xi_+)\right\} \chi_1^0(\xi_+) \,\mathrm{d}x$$
$$- \sqrt{\frac{3}{2}}\int_{-\infty}^{\infty} \left[3\phi_0^5(x,X(t)) - 4\phi_0^3(x,X(t)) + \phi_0(x,X(t))\right] \chi_1^0(\xi_+) \,\mathrm{d}x$$

$$b_6 = -a_6 = \sqrt{\frac{3}{2}}\int_{-\infty}^{\infty} \left\{3\phi_K^5(\xi_+) - 4\phi_k^3(\xi_+) + \phi_K(\xi_+)\right\} \chi_1^0(\xi_+) \,\mathrm{d}x$$
$$- \sqrt{\frac{3}{2}}\int_{-\infty}^{\infty} \left\{3\phi_K^5(-\xi_-) - 4\phi_k^3(-\xi_-) + \phi_K(-\xi_-)\right\} \chi_1^0(\xi_+) \,\mathrm{d}x$$

$$b_7 = -a_7 = -\sqrt{\frac{3}{2}}\int_{-\infty}^{\infty} \left[\phi_K'(\xi_+) + \phi_K'(-\xi_-)\right] \chi_1^0(\xi_+) \,\mathrm{d}x$$

$$b_8 = a_8 = \frac{3}{4}\int_{-\infty}^{\infty} (\chi_1^{0'}(\xi_+))^2 \,\mathrm{d}x$$

$$b_9 = a_9 = \frac{3}{2}\int_{-\infty}^{\infty} \chi_1^{0'}(\xi_+)\chi_1^0(\xi_+) \,\mathrm{d}x$$

$$b_{10} = \sqrt{\frac{3}{2}}\int_{-\infty}^{\infty} \left\{15\phi_0^3(x,X(t)) - 6\phi_0(x,X(t))\right\} (\chi_1^0(\xi_+))^3 \,\mathrm{d}x$$

$$b_{11} = \frac{9}{8}\int_{-\infty}^{\infty} \left\{15\phi_0^2(x,X(t)) - 2\right\} (\chi_1^0(\xi_+))^4 \,\mathrm{d}x,$$

$$b_{12} = \frac{27}{4}\sqrt{\frac{3}{2}}\int_{-\infty}^{\infty} (\chi_1^0(\xi_+))^5 \phi_0(x,X(t)) \,\mathrm{d}x$$

$$b_{13} = \frac{27}{16}\int_{-\infty}^{\infty} (\chi_1^0(\xi_+))^6 \,\mathrm{d}x,$$

$$d_1 = \frac{3}{2}\int_{-\infty}^{\infty} \chi_1^0(\xi_-)\chi_1^0(\xi_+) \,\mathrm{d}x$$

$$d_2 = -\frac{3}{2}\int_{-\infty}^{\infty} \chi_1^{0'}(\xi_+)\chi_1^{0'}(\xi_-) \,\mathrm{d}x$$

$$d_3 = \frac{3}{2}\int_{-\infty}^{\infty} \chi_1^{0'}(\xi_+)\chi_1^0(\xi_-) \,\mathrm{d}x$$

$$d_4 = -d_3 = -\frac{3}{2}\int_{-\infty}^{\infty} \chi_1^{0'}(\xi_-)\chi_1^0(\xi_+) \,\mathrm{d}x$$

$$d_5 = \frac{3}{2}\frac{1}{1-v^2}\int_{-\infty}^{\infty} \chi_1^{0'}(\xi_+)\chi_1^{0'}(\xi_-) \,\mathrm{d}x$$
$$+ \frac{3}{2}\int_{-\infty}^{\infty} \left[15\phi_0^4(x,X(t)) - 12\phi_0^2(x,X(t)) + 1\right] \chi_1^0(\xi_+)\chi_1^0(\xi_-) \,\mathrm{d}x$$

$$d_6 = \frac{27}{4}\int_{-\infty}^{\infty}(\chi_1^0(\xi_+))^2(\chi_1^0(\xi_-))^2\left[15\phi_0^2(x,X(t))-2\right]\,\mathrm{d}x$$

$$d_7 = 3\sqrt{\frac{3}{2}}\int_{-\infty}^{\infty}(\chi_1^0(\xi_-))^2\chi_1^0(\xi_+)\left[15\phi_0^3(x,X(t))-6\phi_0(x,X(t))\right]\,\mathrm{d}x$$

$$d_8 = 3\sqrt{\frac{3}{2}}\int_{-\infty}^{\infty}\chi_1^0(\xi_-)(\chi_1^0(\xi_+))^2\left[15\phi_0^3(x,X(t))-6\phi_0(x,X(t))\right]\,\mathrm{d}x$$

$$d_9 = \frac{9}{2}\int_{-\infty}^{\infty}(\chi_1^0(\xi_-))^3\chi_1^0(\xi_+)\left[15\phi_0^2(x,X(t))-2\right]\,\mathrm{d}x$$

$$d_{10} = \frac{9}{2}\int_{-\infty}^{\infty}\chi_1^0(\xi_-)(\chi_1^0(\xi_+))^3\left[15\phi_0^2(x,X(t))-2\right]\,\mathrm{d}x$$

$$d_{11} = \frac{135}{4}\sqrt{\frac{3}{2}}\int_{-\infty}^{\infty}\phi_0(x,X(t))(\chi_1^0(\xi_-))^4\chi_1^0(\xi_+)\,\mathrm{d}x$$

$$d_{12} = \frac{135}{2}\sqrt{\frac{3}{2}}\int_{-\infty}^{\infty}\phi_0(x,X(t))(\chi_1^0(\xi_-))^3(\chi_1^0(\xi_+))^2\,\mathrm{d}x$$

$$d_{13} = \frac{135}{2}\sqrt{\frac{3}{2}}\int_{-\infty}^{\infty}\phi_0(x,X(t))(\chi_1^0(\xi_-))^2(\chi_1^0(\xi_+))^3\,\mathrm{d}x$$

$$d_{14} = \frac{135}{4}\sqrt{\frac{3}{2}}\int_{-\infty}^{\infty}\phi_0(x,X(t))\chi_1^0(\xi_-)(\chi_1^0(\xi_+))^4\,\mathrm{d}x$$

$$d_{15} = \frac{81}{8}\int_{-\infty}^{\infty}(\chi_1^0(\xi_-))^5\chi_1^0(\xi_+)\,\mathrm{d}x$$

$$d_{16} = \frac{405}{16}\int_{-\infty}^{\infty}(\chi_1^0(\xi_-))^4(\chi_1^0(\xi_+))^2\,\mathrm{d}x$$

$$d_{17} = \frac{135}{4}\int_{-\infty}^{\infty}(\chi_1^0(\xi_-))^3(\chi_1^0(\xi_+))^3\,\mathrm{d}x$$

$$d_{18} = \frac{405}{16}\int_{-\infty}^{\infty}(\chi_1^0(\xi_-))^2(\chi_1^0(\xi_+))^4\,\mathrm{d}x$$

$$d_{19} = \frac{81}{8}\int_{-\infty}^{\infty}\chi_1^0(\xi_-)(\chi_1^0(\xi_+))^5\,\mathrm{d}x$$

Appendix B

Numerical Algorithms

Here, we discuss the algorithms used in solving both the PDE and ODE equations in both models.

B.1 PDE Simulations

We follow the algorithm used by [9] and [47] to solve the dynamical equation pertaining to colliding kink-antikink pairs of equation (2.2.1) and equation (4.2.1) respectively.

The scalar field is defined by $\phi_n(t) = \phi(x_n, t)$ for $n = 1, 2, \cdots, n_x$ on a grid with n_x nodes, where the location of the nth point on the grid is given by

$$x_n = x_{min} + (x_{max} - x_{min})\frac{n-1}{n_x - 1}. \tag{B.1.1}$$

In reference [9], the authors choose a large grid in a such a way that radiation emitted during the collision does not have time to propagate back into the grid after reaching the boundaries. Accordingly we take the left and right grid boundaries at $x_{min} = -100$ and $x_{max} = 100$. For a better computational accuracy we discretized the grid with quite a large number of nodes ($n_x = 8001$).

We use a fourth-order center difference scheme to approximate the first and second spatial derivatives [9]:

$$\begin{aligned} \frac{\partial \phi_n}{\partial x} &= \frac{1}{12h}\left(\phi_{n-2} - 8\phi_{n-1} + 8\phi_{n+1} - \phi_{n+2}\right) = \phi_n', \\ \frac{\partial^2 \phi_n}{\partial x^2} &= \frac{1}{12h^2}\left(-\phi_{n-2} + 16\phi_{n-1} - 30\phi_n + 16\phi_{n+1} - \phi_{n+2}\right) = \phi_n'', \end{aligned} \tag{B.1.2}$$

where $h = x_2 - x_1$. This leads to a set of n_x coupled second-order ordinary differential equations (ODE's) for the ϕ_n:

$$\frac{\mathrm{d}^2 \phi_n}{\mathrm{d}t^2} = \phi_n'' - \phi_n^3 + \phi_n. \tag{B.1.3}$$

The ordinary differential equations (B.1.3) are solved using a fourth-order Runge-Kutta scheme in time (with errors that scale as $(\Delta t)^4$ and $(\Delta x)^4$). Here, the time axis is defined as

$$t_k = t_{min} + \Delta t, \tag{B.1.4}$$

where $k = 1, 2, \cdots, n_t$ with $t_{min} = t_1$ and $t_{max} = t_{n_t}$. We have defined Δt via the adaptive step size control [48]. This ensures that the integration over time is done with good accuracy.

B.2 ODE Simulations

Here we sketch the numerical solution of the ordinary the ordinary differential equations (3.1.7) and (5.1.7) in both the ϕ^4 and ϕ^6 theories, respectively. We compute the coefficients functions $a_1, \cdots, d_{19}$ as well as their derivative with respect to the position of the antikink $X(t)$, for discretized values

$$X_n = X_{min} + (X_{max} - X_{min})\frac{n-1}{n_x - 1}, \tag{B.2.1}$$

where $n = 1, 2, \cdots, n_x$, on a grid with n_x nodes. We choose the left grid at $X_{max} = 10$ and the right grid at $X_{max} = 10.1234$. As before, for greater computational accuracy, we have discretized the grid with a large number of nodes ($n_x = 12001$).

To compute the integrals over the coordinate space x, we use the Bode algorithm which combines the function values of four equidistant subintervals defined by five points, $x_i = x_1 + h(i-1)$, with $i = 1, \cdots, 5$. Let $f(x, X_n)$ be any of the integrands in $a_1, \cdots, d_{19}$. Then

$$\int_{x_1}^{x_5} f(x, X_n)\,\mathrm{d}x = \frac{h}{45}\left(14f(x_1) + 64f(x_2) + 24f(x_3) + 64f(x_4) + 14f(x_5)\right), \tag{B.2.2}$$

where $h = x_2 - x_1$. We repeat that for $x_0, \cdots, x_n$ with

$$x_n = x_{min} + (x_{max} - x_{min})\frac{n-1}{n_x - 1}, \tag{B.2.3}$$

$n = 1, 2, \cdots, n_x$, with the left and right grid boundaries of x given as $x_{upper} = 28$ and $x_{lower} = -28$ respectively. This gives an n_x- dimensional array along the $X-$ axis. We then use a Laguerre interpolation to get the coefficient function at precisely the value of X from this array as required from the ODE. The ODE are then solved using a fourth-order Runge-Kutta scheme in time with adaptive size control [48]. This ensures that the integration over time is done with good accuracy.

Bibliography

[1] Russell, J.S.: Report of the 7th Meeting of the British Association for the Advancement of Science. 1838.

[2] Korteweg, D.J. and De Vries, G.: On the change of form of long waves advancing in a rectangular canal, and on a new type of long stationary waves. *Philos. Mag. Ser*, vol. 39, no. 240, p. 422, 1895.

[3] Zabusky, N.J. and Kruskal, M.D.: Interaction of solitons in a collisionless plasma and the recurrence of initial states. *Phys. Rev. Lett.*, vol. 15, no. 6, p. 240, 1965.

[4] Rajaraman, R.: *Instantons and solitons.* Amsterdam: North Holland, 1982.

[5] Scott, A.C.: *Nonlinear Science: Emergence and Dynamics of Coherent Structure.* Oxford: Oxford University Press, 1999.

[6] Sánchez, A. and Bishop, A.: Collective coordinates and length-scale competition in spatially inhomogeneous soliton-bearing equations. *SIAM Rev.*, vol. 40, no. 3, pp. 579–615, 1998.

[7] Vachaspati, T.: *Kinks and domain walls: an introduction to classical and quantum solitons.* Cambridge: Cambridge University Press, 2006.

[8] Vilenkin, A. and Shellard, E.P.S.: *Cosmic strings and other topological defects.* Cambridge: Cambridge University Press, 2000.

[9] Anninos, P., Oliveira, S. and Matzner, R.A.: Fractal structure in the scalar $\lambda(\varphi^2 - 1)^2$ theory. *Phys. Rev. D*, vol. 44, no. 4, p. 1147, 1991.

[10] Bishop, A., Krumhansl, J. and Trullinger, S.: *Solitons in condensed matter: a paradigm.* Berlin: Springer Verlag, 1980.

[11] Ivanov, B., Kichizhiev, A. and Mitsai, Y.N.: Nonlinear dynamics and relaxation of strongly anisotropic ferromagnets. *Sov. Phys. JETP*, vol. 75, no. 2, p. 329, 1992.

[12] Bishop, A., Krumhansl, J. and Trullinger, S.: Solitons in condensed matter: a paradigm. *Physica D*, vol. 1, no. 1, p. 1, 1980.

[13] Witten, E.: Baryons in the 1/N expansion. *Nucl. Phys. B*, vol. 160, no. 1, p. 57, 1979.

[14] Weigel, H.: *Chiral soliton models for baryons*, vol. 743. Berlin: Springer Verlag, 2008.

[15] Campbell, D.K. and Peyrard, M.: Solitary wave collisions revisited. *Physica D*, vol. 18, no. 1, p. 47, 1986.

[16] Barashenkov, I. and Oxtoby, O.: Wobbling kinks in ϕ 4 theory. *Phys. Rev. E*, vol. 80, no. 2, p. 026608, 2009.

[17] Dorey, P., Mersh, K., Romanczukiewicz, T. and Shnir, Y.: Kink-antikink collisions in the ϕ^6 model. *Phys. Rev. Lett.*, vol. 107, no. 9, p. 091602, 2011.

[18] Sugiyama, T.: Kink-antikink collisions in the two-dimensional φ^4 model. *Prog. Theor. Phys.*, vol. 61, no. 5, p. 1550, 1979.

[19] Belova, T. and Kudryavtsev, A.: Quasi-periodic orbits in the scalar classical $\lambda\phi^4$ field theory. *Physica D*, vol. 32, no. 1, p. 18, 1988.

[20] Goodman, R.H. and Haberman, R.: Chaotic scattering and the n-bounce resonance in solitary-wave interactions. *Phys. Rev. Lett.*, vol. 98, no. 10, p. 104103, 2007.

[21] Kudryavtsev, A.: Soliton like solutions for a Higgs scalar field. *Pisma Zh. Eksp. Teor. Fiz.*, vol. 22, p. 178, 1975.

[22] Goodman, R.H. and Haberman, R.: Kink-antikink collisions in the ϕ^4 equation: The n-bounce resonance and the separatrix map. *SIAM J. App. Dyn. Sys.*, vol. 4, no. 4, p. 1195, 2005.

[23] Weigel, H.: Kink–antikink scattering in ϕ^4 and ϕ^6 models. *J. Phys: Conference Series*, vol. 482, p. 012045, 2014.

[24] Caputo, J. and Flytzanis, N.: Kink-antikink collisions in Sine-G and φ^4 models: Problems in the variational approach. *Phys. Rev. A*, vol. 44, no. 10, p. 6219, 1991.

[25] Ablowitz, M.J. and Clarkson, P.A.: *Solitons, nonlinear evolution equations and inverse scattering*, vol. 149. Cambridge: Cambridge University Press, 1991.

[26] Quintero, N.R., Sánchez, A. and Mertens, F.G.: Anomalous resonance phenomena of solitary waves with internal modes. *Phys. Rev. Lett*, vol. 84, no. 5, p. 871, 2000.

[27] Morales-Molina, L., Quintero, N.R., Mertens, F.G. and Sánchez, A.: Internal mode mechanism for collective energy transport in extended systems. *Phys. Rev. Lett*, vol. 91, no. 23, p. 234102, 2003.

[28] Moshir, M.: Soliton-antisoliton scattering and capture in $\lambda\varphi^4$ theory. *Nucl. Phys. B*, vol. 185, no. 2, p. 318, 1981.

[29] Romanczukiewicz, T. and Shnir, Y.: Oscillon resonances and creation of kinks in particle collisions. *Phys. Rev. Lett.*, vol. 105, no. 8, p. 081601, 2010.

[30] Adkins, G., Nappi, C. and Witten, E.: Static properties of nucleons in the skyrme model. *Nucl. Phys. B*, vol. 228, p. 552, 1983.

[31] Skyrme, T.H.R.: A non-linear field theory. *The Royal Society*, vol. 260, no. 1300, p. 127, 1961.

[32] Braaten, E., Tse, S.-M. and Willcox, C.: Electroweak form factors of the skyrmion. *Physical Rev. D*, vol. 34, no. 5, p. 1482, 1986.

[33] Campbell, D.K., Schonfeld, J.F. and Wingate, C.A.: Resonance structure in kink-antikink interactions in φ^4 theory. *Physica D*, vol. 9, no. 1, p. 1, 1983.

[34] Manton, N. and Sutcliffe, P.: *Topological solitons*. Cambridge: Cambridge University Press, 2004.

[35] Shellard, E. and Vilenkin, A.: *Cosmic strings and other topological defects*. Cambridge: Cambridge University Press, 1994.

[36] Weinberg, E.J.: *Classical solutions in quantum field theory: Solitons and Instantons in High Energy Physics*. Cambridge: Cambridge University Press, 2012.

[37] Morse, P.M. and Feshbach, H.: *Methods of theoretical physics*. New York: McGraw-Hill, 1953.

[38] Drazin, P.G. and Johnson, R.S.: *Solitons: an introduction*, vol. 2. Cambridge: Cambridge University Press, 1989.

[39] Schwabl, F.: *Quantum Mechanics*. Berlin: Springer Verlag, 2007.

[40] Jeyadev, S. and Schrieffer, J.: Collective coordinate description of soliton dynamics in trans-polyacetylene-like systems. *Syn. Metals*, vol. 9, no. 4, p. 451, 1984.

[41] Goatham, S.W.: ϕ^6 kink scattering. *arXiv preprint arXiv:1209.3055*, 2012.

[42] Hoseinmardy, S. and Riazi, N.: Inelastic collision of kinks and antikinks in the ϕ^6 system. *Int. J. Mod. Phys. A*, vol. 25, no. 16, p. 3261, 2010.

[43] Lohe, M.: Soliton structures in $p(\varphi)_2$. *Phys. Rev. D*, vol. 20, no. 12, p. 3120, 1979.

[44] Barashenkov, I. and Makhankov, V.: Soliton-like "bubbles" in a system of interacting bosons. *Phys. Lett. A*, vol. 128, no. 1, p. 52, 1988.

[45] Barashenkov, I.V. and Panova, E.Y.: Stability and evolution of the quiescent and travelling solitonic bubbles. *Physica D*, vol. 69, no. 1, p. 114, 1993.

[46] Barashenkov, I., Gocheva, A., Makhankov, V. and Puzynin, I.: Stability of the soliton-like "bubbles". *Physica D*, vol. 34, no. 1, p. 240, 1989.

[47] Abdelhady, A.M.H.H: *Scattering in soliton models and crossing symmetry*. Master's thesis, Stellenbosch: Stellenbosch University, 2012.

[48] Press, W.H., Teukolsky, S.A., Vetterling, W.T. and Flannery, B.P.: *Numerical recipes in Fortran 77 and Fortran 90*. Cambridge: Cambridge University Press, 1996.